VII

Shaping up to stress in the Apennines

Italy's Apennine mountain chain is a tectonically active area where the rocks are subject to high stresses. This stress regime exerts a major influence over drilling programs and production management of oil fields. This article shows how engineers in Italy have pioneered a method of deducing the orientation and magnitude of the principal stress regimes through analysis of borehole topography in deviated wells. The article also highlights how equipment such as the UBI* Ultrasonic Borehole Imager tool has been used to identify features such as breakouts and induced fractures

La catena appenninica italiana è un'area tettonicamente attiva, dove le rocce sono sottoposte a notevoli sforzi, i cui effetti si ripercuotono in maniera considerevole su programmi di perforazione e sulla gestione della produzione di campi petroliferi. Questo articolo spiega come i tecnici italiani abbiano introdotto un metodo che consente di delineare l'orientamento e la grandezza degli sforzi principali analizzando la topografia del foro in pozzi deviati; l'articolo illustra quindi come lo strumento UBI* (Ultrasonic Borehole Imager), sia in grado di individuare caratteristiche quali "break outs" (orientamento prevalente di fratturazione della roccia) e fratture indotte

Agip
M Cesaro
M Gonfalini

Schlumberger
P Cheung
A Etchecopar

Stress modifications caused by drilling can lead to borehole stability problems. Likewise, production engineers need a clear understanding of the tectonic forces at work before setting a well plan, assessing fracture efficiency and formulating injection/production optimization schemes. In vertical wells, the vertical stress has no influence on the breakout orientation, so the minimum horizontal stress direction is the only parameter that can be determined directly from breakout analysis. In deviated wells, breakouts depend on the three main stresses – vertical (σ_v), maximum horizontal (σ_H) and minimum horizontal (σ_h).

Until now, little effort has been made to estimate in-situ stress by direct analysis of breakouts and of other stress-induced features in deviated wells. Part of the reason for this is the difficulty of distinguishing stress-induced from drilling-induced microstructures. A relatively new technique, ultrasonic scanning of the borehole wall, is now providing the opportunity to identify the exact nature and origin of borehole damage.

Detecting borehole damage in deviated wells

Stress-induced features are breakouts, induced fractures and slips at pre-existing planes; drilling-induced ones are keyseat and reaming effects. The overall state of stress must be computed from stress-induced features only, so drilling damage, which can cause oriented enlargement of the borehole, must be clearly identified to be ignored during this computation. For example, in the key well studied, 80% of the ovalization is due to drilling damage.

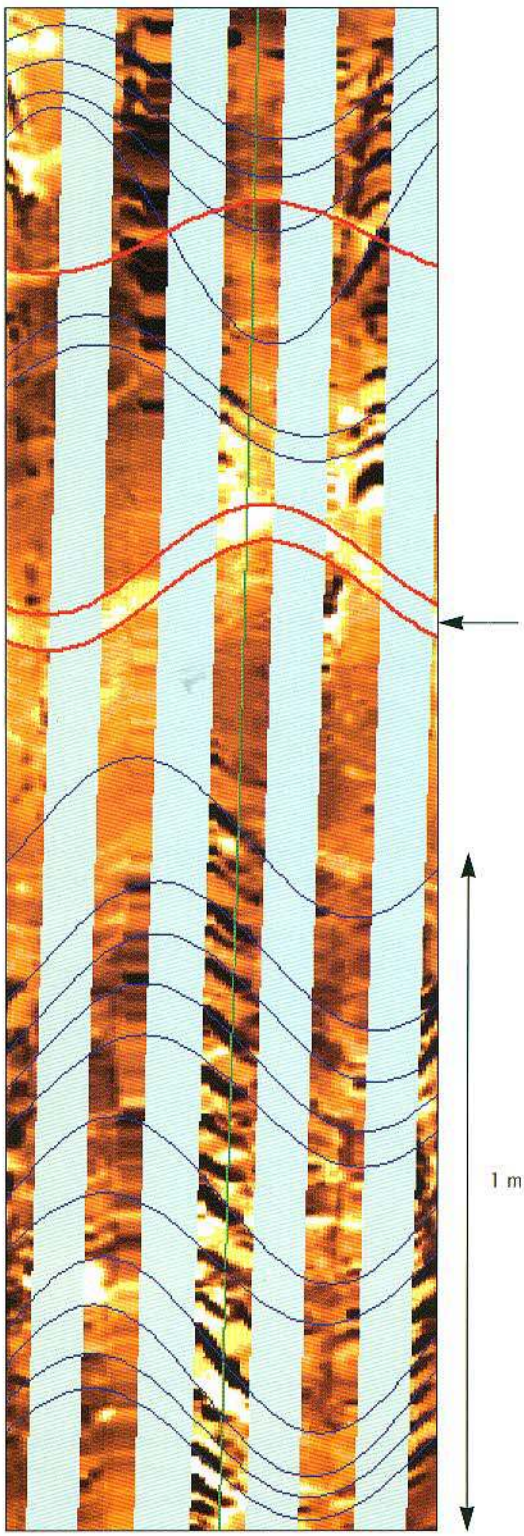

Figure 7.1 *Induced fractures on Formation MicroScanner* image. (Blue features are induced (tensile) fractures; red features are layering.) Note the symmetry relative to the well, and the change in the orientation at the layer indicated by an arrow*

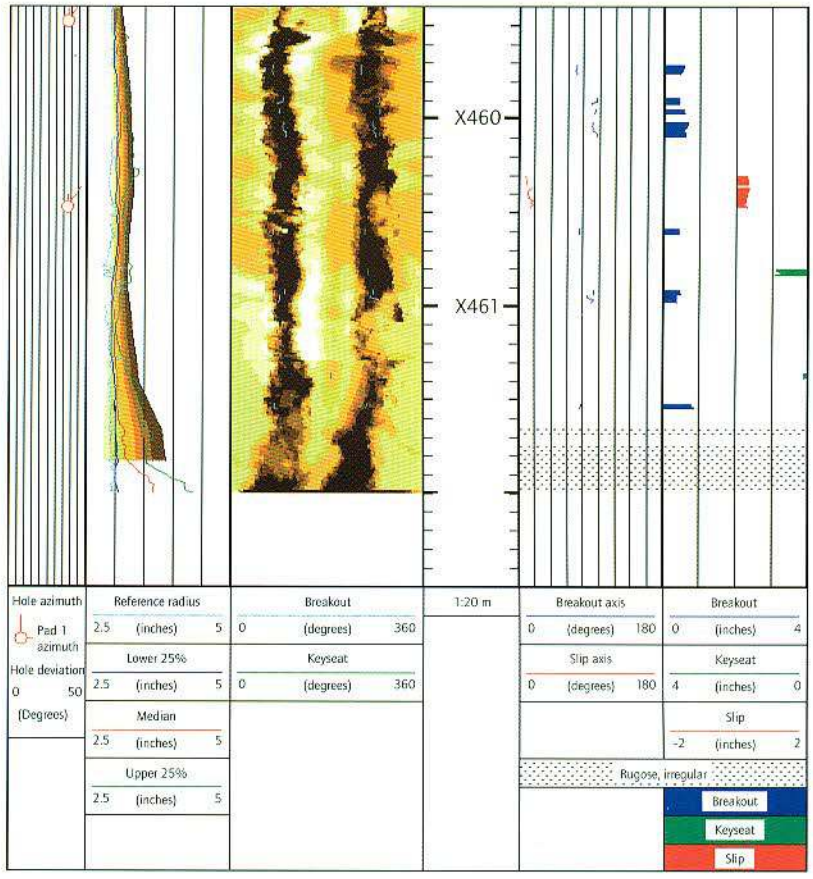

Figure 7.2 *Computer generated Hole Shape Analysis results; example of a zone affected by breakout. Track 3 from left presents the borehole radius as an image. The left edge is the top of the hole. The value of the radius corresponding to each color is indicated in track 2, which also gives the median, the upper and the lower 25-percentile radius values. Tracks 4, 5 and 1 give, respectively, the orientation of the damage relative to top of hole, the extent of the feature relative to the hole size, and the well deviation*

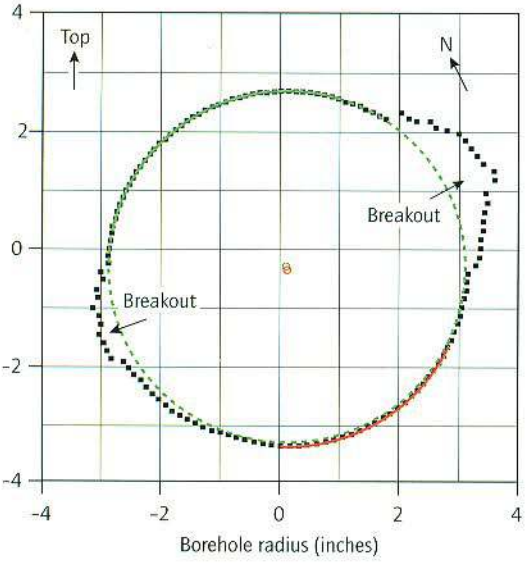

Figure 7.3a *Borehole cross section showing a breakout. The dots are data points. The solid lines represent the parts of the borehole wall that have a constant curvature. The broken lines are the continuation of the largest solid arcs*

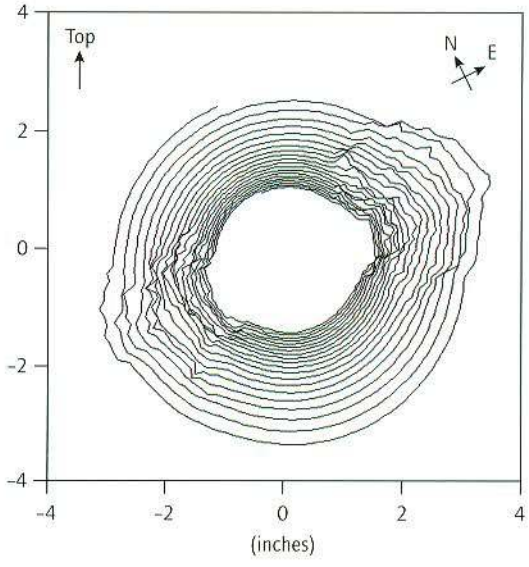

Figure 7.3b *Perspective view of a breakout*

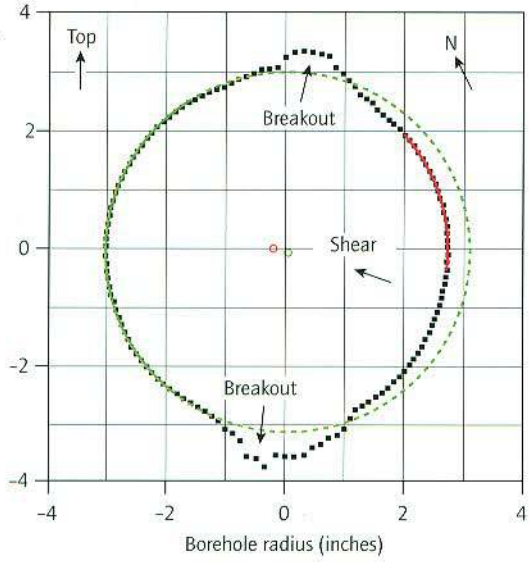

Figure 7.4 *Borehole cross section showing a breakout with closure (1.5 cm) (see caption to Figure 7.3a for notation)*

The key well chosen for this study shows a constant deviation of about 38°, but its azimuth varies from 30 to 90°N. In order to understand the local stress regimes around the well, a UBI Ultrasonic Borehole Imager tool was run from X475 to X165 m (total logging interval). The UBI amplitude and transit time images were analysed; the resulting log clearly reveals two main zones: one above X190m, in which large caves dominate and the borehole shape is lost; and another just below this depth, which contains typical stress and drilling induced microstructures.

Induced fractures are easily detected on UBI or FMI* Fullbore Formation MicroImager and Formation MicroScanner images because they are symmetrical relative to the borehole wall. Figure 7.1 shows numerous induced (tensile) fractures in this well, which have an average strike of 155°N. To determine the nature, geometry and orientation of other types of damage, an analysis of the borehole curvature must be performed at each level, based on sonic transit time data. This analysis is carried out using either the HOSANA (Hole Shape Analysis) software or an interactive program, HSView, which allows users to examine a particular level or a perspective view of a short well section.

The curvature analysis is performed in three steps:

- at each level and at each azimuth, the radius and center of curvature are computed in a sliding window approximately 40° wide
- if consecutive curvature computations match, the corresponding angular zones are merged into a single arc whose center is computed

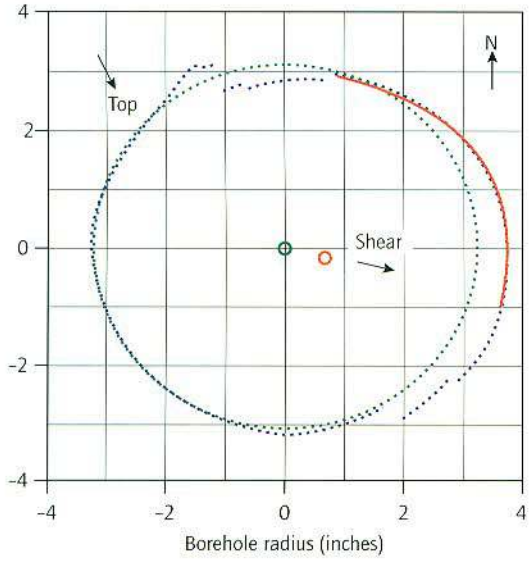

Figure 7.5a *Borehole cross section showing a shear at a pre-existing fracture (see caption to Figure 7.3a for notation)*

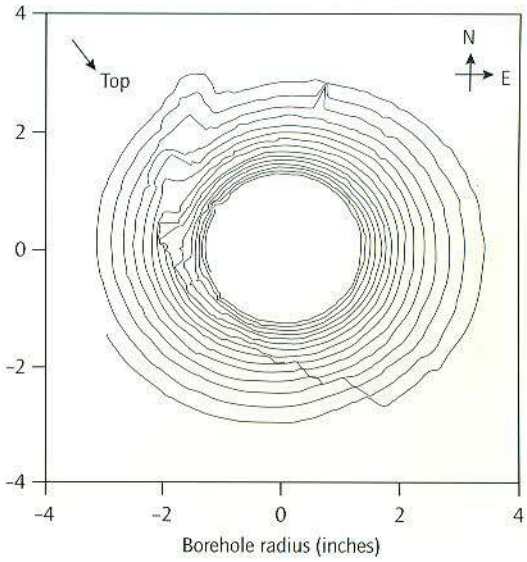

Figure 7.5b *Perspective view of a shear at a pre-existing fracture*

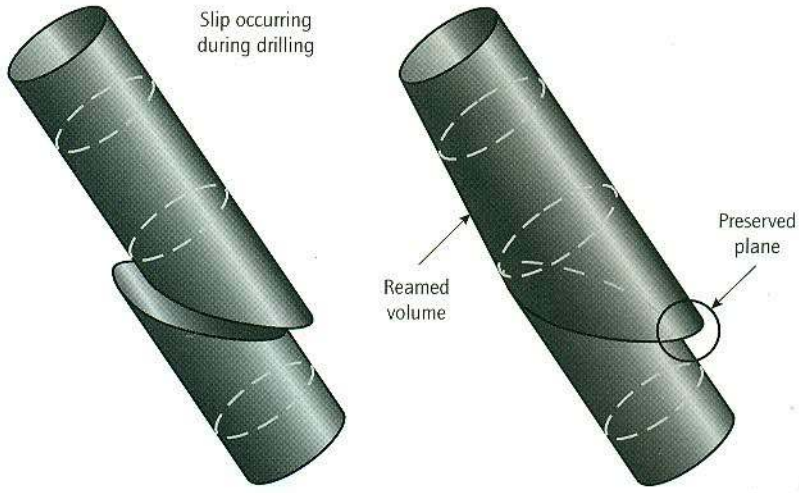

Figure 7.6 *Theoretical sketch of a shear at a pre-existing fracture followed by a reaming. Note the asymmetric enlargement of the borehole relative to the shear plane depth*

- according to the distribution of the arcs and their centers, the borehole damage is automatically identified as breakouts, shearing at the borehole wall, keyseat or reaming

Breakouts are highlighted when two undeformed arcs (ie, whose radii are close to the radius of the bit) are separated by two damaged zones 180° apart (Figures 7.2 and 7.3). The average orientation and depth of the breakout are displayed. If the centers of the two arcs do not coincide, this is due to a closing movement in the direction of the main stress (Figure 7.4). The HOSANA and HSView outputs indicate 49 breakout zones or shortening incidences in the key well.

Shearing at the borehole wall (Figure 7.5a) is observed when two undeformed arcs are displaced relative to each other. Such movement corresponds to faulting on a pre-existing plane which can be either normal, reverse or strike-slip. The projection onto the shear plane of the vector joining the centers of the two arcs corresponds to the slip vector. To avoid confusing this with simple reaming, a plane crossing the level must be observed on the UBI image or in a perspective view

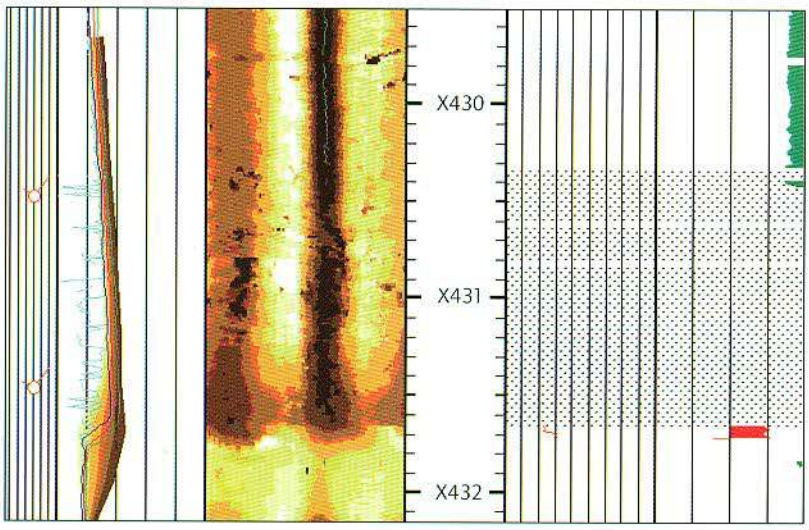

Figures 7.7a *Shear at pre-existing fracture and asymmetric reaming detected by the program* HOSANA *(see caption to Figure 7.2 for notation). Note the particular shape of the curves in the second track. There is a sudden enlargement of the well at the shear plane and a slow decrease of this enlargement over the 2 m above*

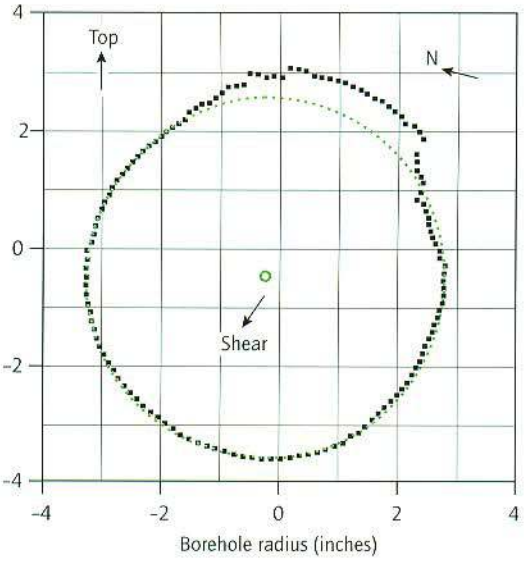

Figures 7.7b *Borehole cross section showing the single shear at a pre-existing fracture that has been measured in this well (14 others were detected, but unfortunately were not measurable due to reaming)*

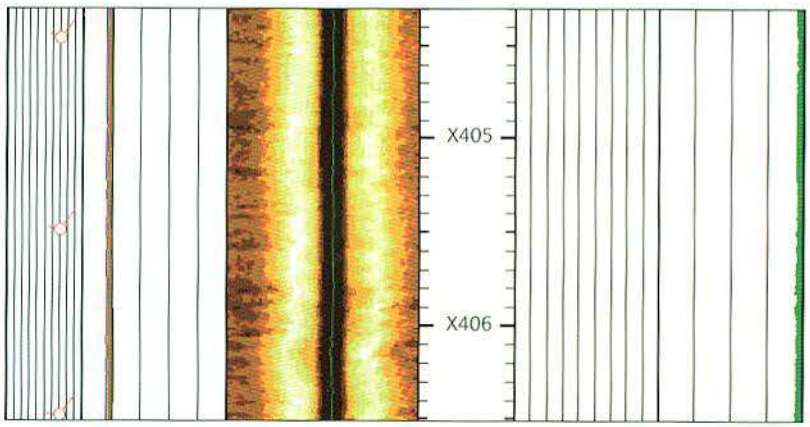

Figure 7.8a Zone of keyseating detected by the program HOSANA *(see caption to Figure 7.2 for notation)*

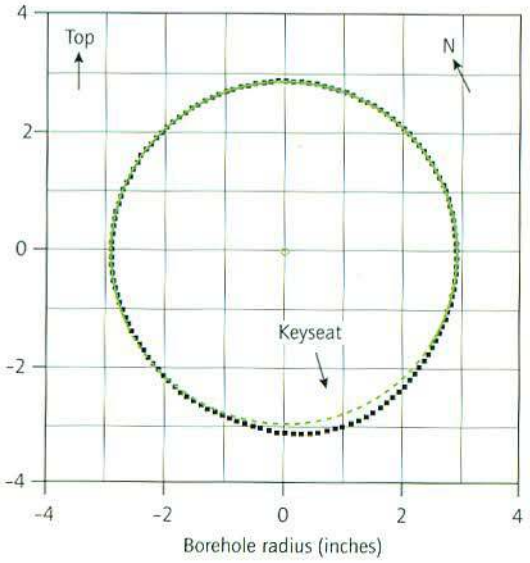

Figure 7.8b Borehole cross section showing a keyseat (see caption to Figure 7.3a for notation)

of this part of the well (Figure 7.5b). The obvious slip shown on Figure 7.5 does not come from the key well in which such slips occurred along pre-existing planes, but were masked by subsequent reaming and/or back-reaming (Figure 7.6). Such a reamed slip creates a sudden borehole enlargement at the slip plane itself, followed by a smooth decrease in the average hole radius. This can be observed over 30 m of the well where, in the uphole direction, there is a succession of 15 sudden borehole enlargements followed by a smooth decrease in the average radius, as shown on Figure 7.7a at X431.7 m. Unfortunately there is only one section (see Figure 7.7), where the reaming has preserved a zone large enough to enable measurement of both the slip plane and the slip vector.

Keyseat (Figure 7.8) is seen when a radius of curvature smaller than the bit size is detected at the bottom of the borehole.

Reaming (Figure 7.9) is detected when two arcs whose radii correspond to the bit size exhibit centers clearly separated, accompanied by an enlargement of the well.

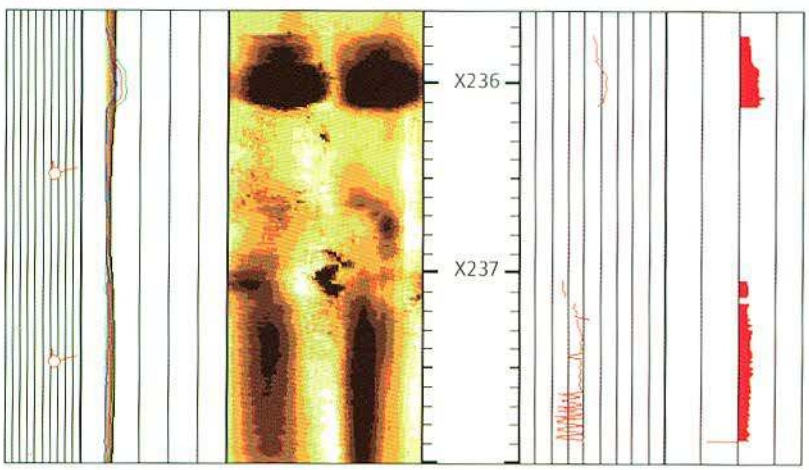

Figure 7.9a Zone of reaming detected by the program HOSANA *(see caption to Figure 7.2 for notation)*

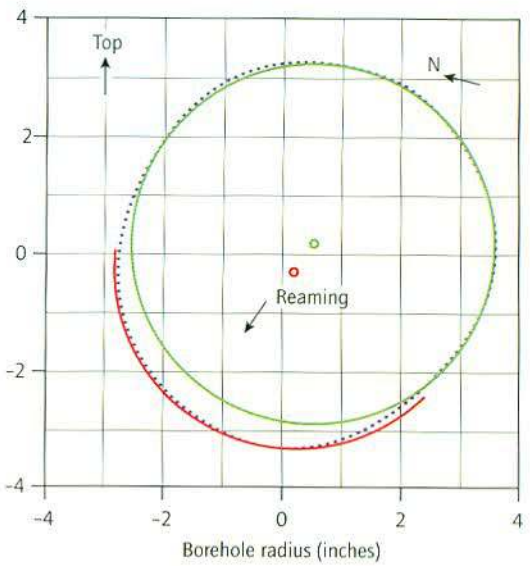

Figure 7.9b Borehole cross section showing a reaming (see caption to Figure 7.3a for notation)

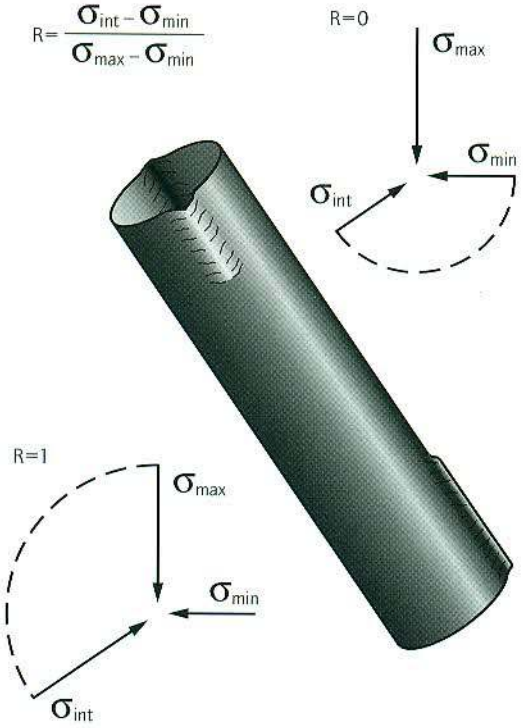

Figure 7.10 *Theoretical sketch showing the change in breakout orientation due just to the change in intermediate stress magnitude. At the top the intermediate stress is equal to the minimum; at the bottom it is equal to the maximum (here vertical)*

Relation of the stress-induced features to the stress axes

The three types of stress-induced microstructures described previously can be related to the full stress tensor which has three axes σ_v, σ_H, σ_h – respectively the vertical, maximum horizontal and minimum horizontal main stress. (In sedimentary basins, it is generally agreed that one of the principal axes is vertical.)

Induced tensile fractures

These form along planes perpendicular to the minimum stress. They are usually parallel to the borehole wall in vertical wells and en echelon in deviated wells as they are inclined relative to each of the principal axes.

Breakouts

A breakout appears where there is maximum tangential stress at the borehole wall. As a vertical well is parallel to σ_v, breakouts simply indicate the σ_h azimuth; a deviated well is oblique to the three main stresses which influence the maximum tangential stress. Studies have shown that for a given borehole orientation, breakout orientation (measured, say, relative to the top-of-hole and ignoring a small angle of less than 5° due to mud and formation fluid pressure), depends essentially on the following parameters (Figure 7.10):

1. the direction of the minimum horizontal stress (σ_h)
2. the stress regime – which principal stress (maximum, intermediate or minimum) is vertical
3. the ratio R of the stress magnitude, given by:

$$(\sigma_{int} - \sigma_{min}) / (\sigma_{max} - \sigma_{min})$$

2 and 3 can be combined into a single parameter Q in the range $0 <= Q < 3$ such that:

$0 <= Q < 1$ implies $\sigma_v > \sigma_H > \sigma_h$, $R = Q$

$1 <= Q < 2$ implies $\sigma_H > \sigma_v > \sigma_h$, $R = 2 - Q$

$2 <= Q < 3$ implies $\sigma_H > \sigma_h > \sigma_v$, $R = Q - 2$

The parameters σ_h and Q are the same as those constraining the slip direction of microfaults, or the geometry of the nodal planes of focal mechanisms.

Figure 7.11 *State of stress compatible with individual breakout measurements. On the crossplot σ_h and Q are respectively the x- and y-axes, and each point on it corresponds to a stress state. The Q axis is divided into three parts corresponding to the stress regime where σ_v is, respectively, the maximum, intermediate or minimum stress as indicated by the scale. The stress states which give a breakout direction to within ±5° from the first observation are marked by a '1' (well deviated by 38° towards N32), and for the second by a '2' (well deviated by 37° towards N71). The single state marked by '3' is compatible with both observations*

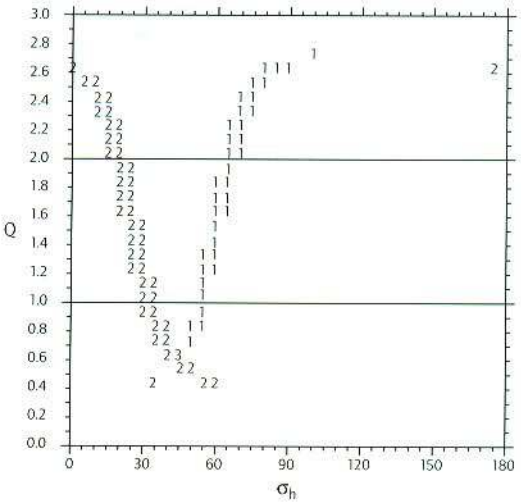

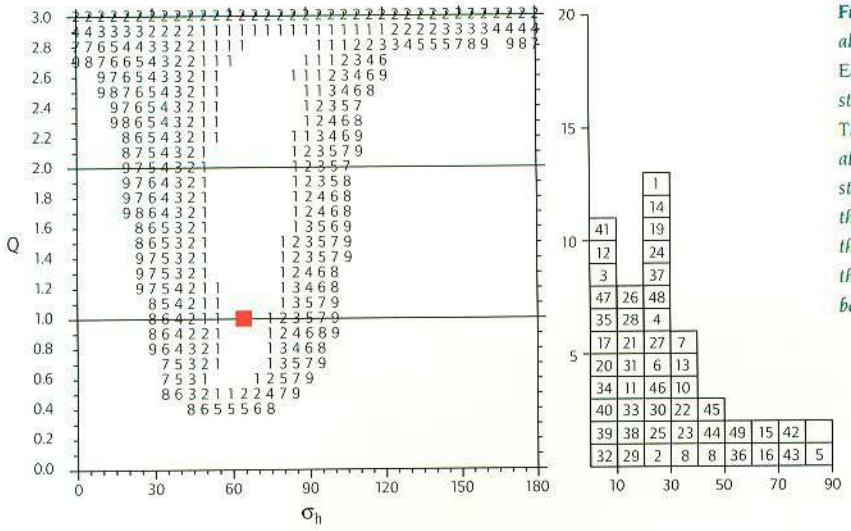

Figure 7.12 *Crossplot showing the mean absolute deviation to all data points as a function of the stress parameters σ_h and Q. Each point of the crossplot represents a stress state. The stress state giving the best fit to the data point is marked by a square. The digits 1, 2, ...9 mark the stress state where the mean absolute deviation is 10, 20, ...90% above the best-fit value. The stress states with no marking have an absolute deviation less than 10% in the area around the square and more than 100% in the other area. The histogram to the right of the crossplot shows the absolute deviation delta of the individual data points for the best-fit stress state. The mean absolute deviation is 35°*

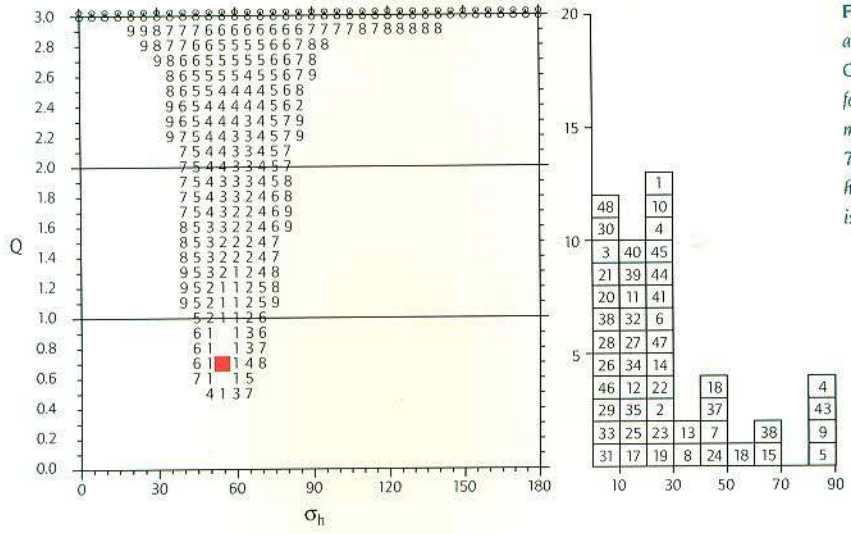

Figure 7.13 *Crossplot showing the trimmed (best 80%) mean absolute deviation as a function of the stress parameters σ_h and Q (see caption to Figure 7.12 for notation). The fit is computed for the best 80% of points at each stress state, ie, different points may be rejected at different stress states. Compared to Figure 7.12, a much more precise best-fit stress state is obtained. The histogram is also narrower. The trimmed mean absolute deviation is 17° for the best-fit state*

Shear movements at the borehole wall

Slip planes in rocks can be reactivated during or after drilling. Such planes normally lie at an oblique angle to the current stress axes, and if the fault is re-activated a relative displacement of two borehole sections may occur (Figure 7.5). In ideal cases, the UBI images may reveal the orientation of the fault plane and its shear vector.

The orientation of the shear vector depends on the natural state of stress but not on the well trajectory, as is the case for the breakout orientation. This means that a change in the well trajectory can greatly modify the amount of breakouts but not the occurrence of such slip at pre-existing planes.

Inversion methods for stress determination

A single breakout or fault movement cannot provide sufficient information to determine the complete set of stress parameters (Figure 7.11). Theoretically, the minimum number of features needed for an inversion is two. The number of available data points is much greater than this. The problem becomes overdetermined but many measurements may be erroneous and may have to be rejected. In Italy an inversion method has been developed which automatically sifts out incorrect data to enable accurate determination of the average stress.

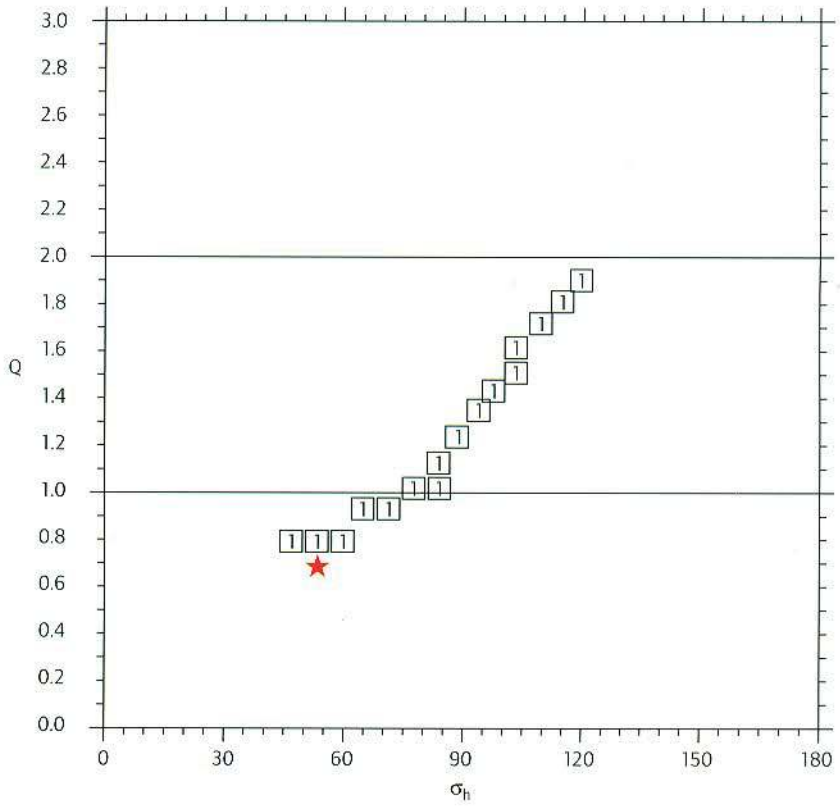

Figure 7.14 *Stress states compatible with shearing of the borehole at a pre-existing fracture (see caption to Figure 7.12 for notation). The star corresponds to the best fit stress state obtained from breakout analysis*

Principle and application in key well

If breakouts are observed at several borehole orientations (from the same well or from several neighboring wells), the observations can be inverted to give the main stress parameters. As they depend on the same parameters, the method for breakout inversion is very similar to the one proposed for the inversion of striation on microfaults by Etchecopar et al (1981).

In such an interpretation the unknowns are σ_h and Q. The solution lies in the analysis of breakout orientation data relative to the well, and the well orientation.

The analyst concentrates on determining the parameters which give the lowest value for the misfit M (M_{min}) which is defined as the sum of the individual angular misfits between actual and 'computed' breakouts. A 'computed' breakout should occur along the direction of maximum tangential stress at the borehole wall. Determination of the minimum misfit M_{min} value for all the data involves investigating a range of solutions using a plot of σ_h versus Q (Figure 7.12). A square indicates the solution corresponding to M_{min}. The numbers N around the best solution indicate, for the corresponding tensors, the misfit M_f as a function of M_{min}:

$$N = 10 * (Mf - M_{min}) / M_{min}$$

ie, 1 means the fit M_f is within 10% of the minimum fit M_{min} etc.

If $M_f > 2 * M_{min}$, N is not displayed.

Figure 7.12 shows the results of this method applied to complete set of breakouts in the key well. It is clear that this solution is badly constrained in azimuth and not at all in R. This is probably due to incorrect data (e.g. confusion between keyseat and breakout) and local stress deviations. Such incorrect data must be identified and rejected.

Automatic rejection of incorrect data

The minimization method is very sensitive to any misinterpretation of the borehole damage or to local changes in the stress orientation. So this method has been modified in order to reject an a priori percentage of data (usually 20%). Instead of minimizing

for the whole data set, the method minimizes for the best N%, where N is a chosen value (usually 80%). To determine the minimum misfit, each possible tensor is examined as follows:

- for each stress tensor solution, the misfit for each individual data point is computed
- the individual misfits are sorted in increasing order
- the total misfit M_f is taken to be the sum of the N% smallest individual misfits
- the best solution is the tensor for which M_f is minimum

Using these criteria, a second run was performed on 80% of the data. The new solution (Figure 7.13) is constrained in orientation (N150), but less in Q ($0.6<Q<0.9$). This Q range corresponds to $0.6<R<0.9$ with σ_v being σ_{max}. The variability of R probably reflects the changes in elastic properties of the different lithologies. However, it is clear that the maximum stress is vertical and that σ_H is much closer to σ_v than to σ_h. Using the misfit histogram associated with this solution (Figure 7.13), it is possible to locate zones where the orientation of the stress varies and these can often be confirmed by changes in the orientation of induced fractures (see Figure 7.1). The origin of these variations is an interesting problem but beyond the scope of this article.

Is this a reliable solution?

Two types of microstructures support this solution: tensile fractures oriented N150 as the maximum horizontal stress determined, and the single slip in which it has been possible to measure a pre-existing fracture. Figure 7.14 shows that the stress is compatible with both breakouts and the slip movement.

Engineers thrive on stress

Production engineers are keen to understand the state of stress and its deviation as these are key to determining the behavior of fractures (see Articles VI and VIII). In addition, the data are useful in analysing borehole stability.

The key well has both breakouts and slips at pre-existing fractures. Increasing the mud weight stabilizes the breakouts but also increases the risk of slip movements. Also, breakout occurrence depends on the tangential stress anisotropy at the borehole wall which does not affect slip movements. As this anisotropy depends on the borehole orientation, some drilling directions are safer than others at preventing breakouts.

Using stress information determined from breakouts and shear, stress components tangential to the borehole wall can be computed for all well orientations (Figure 7.15). It is possible to limit breakout extension by keeping the well in a direction where the tangential stresses are isotropic. In this case, the maximum tangential stress is also minimized. This implies that mud weight can be reduced. In so doing, the risks of hydraulic fracturing and slip along pre-existing fracture are also reduced.

Full understanding of the stress regime shown in this example will lead to a reduction in drilling costs, for example, due to reduced mud weight.

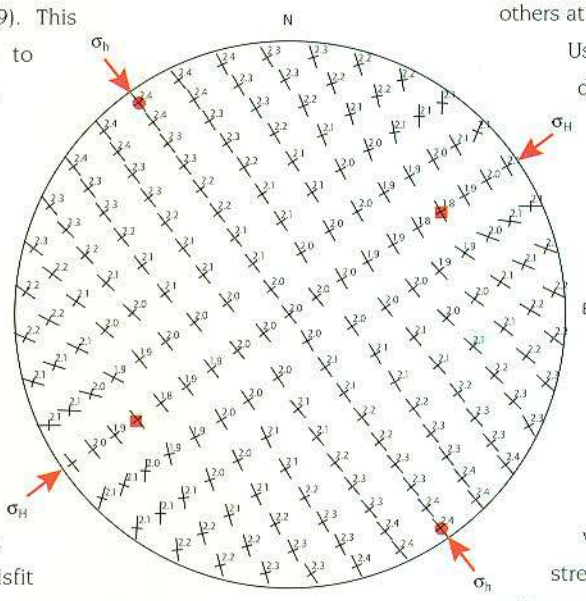

Figure 7.15 *Diagram (Schmidt projection) showing the tangential stress state at the borehole wall for different well deviations and azimuths. The center of the Schmidt plot corresponds to a vertical well. A point on the outer circle corresponds to a horizontal well. The crosses indicate the maximum and minimum tangential stresses and their orientation. The numbers correspond to the ratio between the maximum tangential stress and the vertical one (the ratio σ_H/σ_v is assumed to be 0.6, and the fluid pressure is not taken into account). The squares and circles indicate, respectively, the well orientation minimizing or maximizing the tangential stress at the borehole wall. When the maximum tangential stress is minimum it is also identical all around the borehole wall; this also indicates the direction where drilling is safer*

VIII

Enhancing the image of the southern Apennines

The 1980s saw the development of the first geological model of the deep structure of the southern Apennines, a move that paved the way for oil discovery in the Val d'Agri area. Since then there has been a drive to update the geological model as more data become available. Because production is coming mainly from fractures, the MDT* Modular Formation Dynamics Tester dual packer module, in combination with the UBI* Ultrasonic Borehole Imager and FMI* Fullbore Formation MicroImager tools, has been introduced to evaluate production from fractures, and the fluid type

Negli anni '80 è stato sviluppato il primo modello geologico della struttura profonda degli Appennini meridionali, aprendo così la strada alla scoperta dei giacimenti petroliferi in Val d'Agri. Dal quel momento la disponibilità di nuovi dati ha spinto in modo costante ad aggiornare questo modello geologico. Dal momento che la produzione deriva prevalentemente dalle fratture, è stato introdotto lo strumento MDT* (Modular Formation Dynamics Tester) con "dual packer" che, combinato con l'UBI* (Ultrasonic Borehole Imager) e l'FMI* (Fullbore Formation MicroImager), consente di valutare la produttività delle fratture ed il tipo di fluido

Agip
V Chelini
G Sartori

Enterprise
M Giorgioni
A Pelliccia

Schlumberger
G Ciammetti

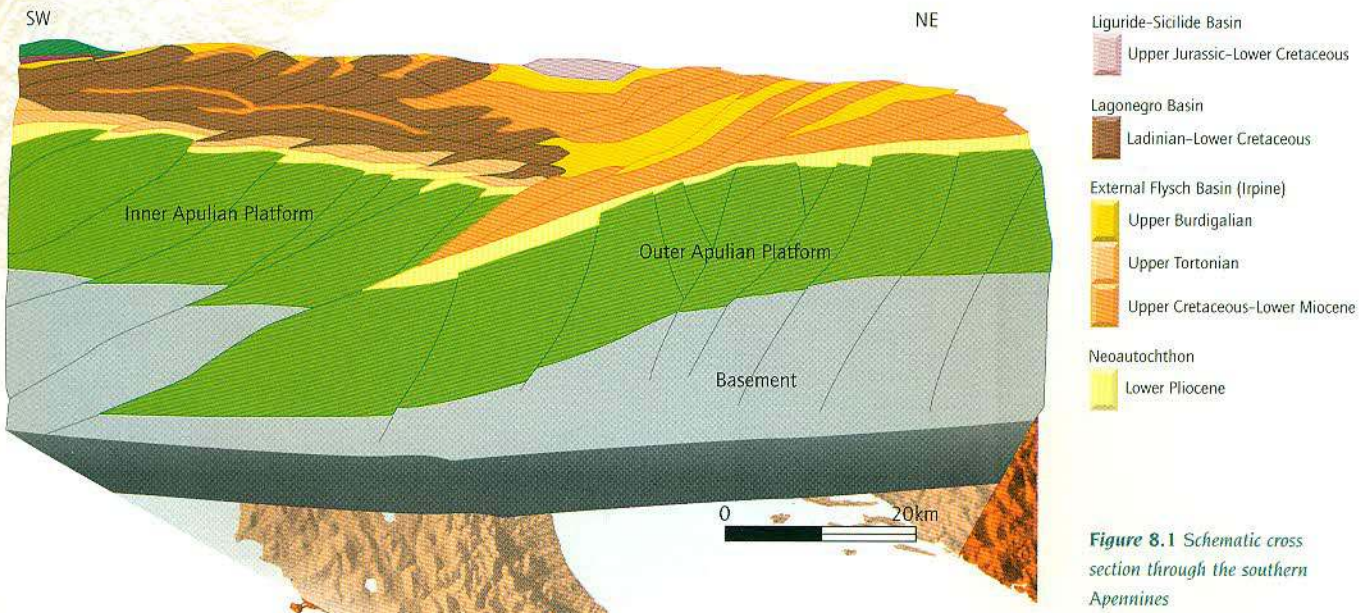

Figure 8.1 *Schematic cross section through the southern Apennines*

The southern Apennine region of Italy has been an important oil-producing area for the past 20 years. However, until recently, the region's geology was little understood.

Figure 8.1 shows a geological section across the fold-belt and foreland system. This runs from the innermost sector of the belt, through the Val d'Agri oil fields, to the almost undisturbed Apulian foreland. The Late Cretaceous paleogeography of the area was characterized by a system of alternating basin and carbonate platform environments. It is possible to unravel the sequence of tectonic thrust regimes from west to east. In the west is the Liguride–Sicilide Basin, followed by the Apennine Platform which transforms into the Lagonegro Basin and the Apulian Platform in the east.

Well and seismic data confirm this orogenic picture and indicate that most of the tectonic activity occurred towards the end of the Late Pliocene. In fact, the final closure of the ensialic shear-zone, which resulted in the subduction of over 100 km of continental crust from under the Lagonegro Basin, can be dated to the Early Pliocene.

Movements of the Inner Apulian rocks, which lie at the core of the belt, and the activation of a new ensialic shear-zone, can be dated to the Pliocene–Pleistocene.

The profile also clearly shows the stark contrast between the massive deep structures that lie at the core of the belt and faulted and strained nature of the Lagonegro, Liguride and Sicilide units.

By comparison, the basement of the Inner Apulian Platform is affected by the orogeny while the Outer Apulian Platform has suffered A-type subduction brought about by regional flexural folding and associated normal faulting. It is obvious that the outcropping nappe structures, created during the first

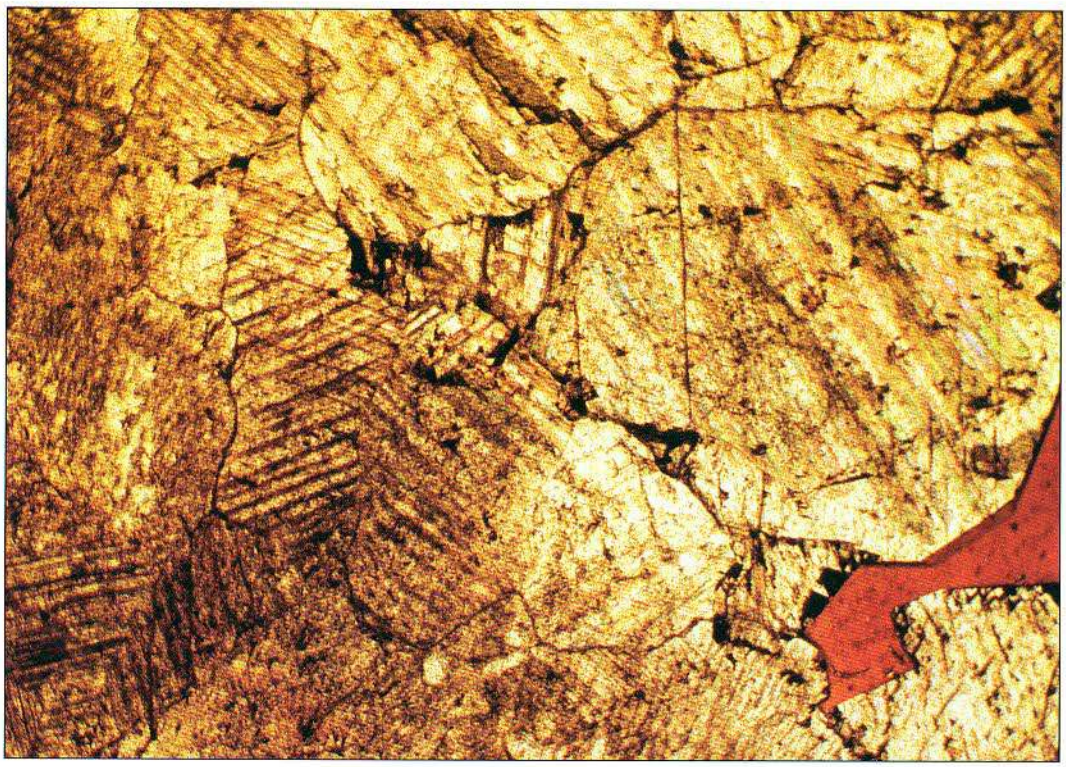

Figure **8.2** *Typical thin section display of oil-bearing (red) rock from the southern Apennines (Courtesy: Agip Laboratories PETR)*

compressional phase, are unrelated to the Apulian Platform structures.

The oil exploration target in the Val d'Agri is a carbonate sequence in the Inner Apulian Platform comprising both the reservoir and the source rock. Geochemical data indicate that a possible source rock of Turonian–Albian age lies within the Val d'Agri area (Figure 8.2).

Hydrocarbon generation and migration phases in the Inner Apulian Unit occurred relatively recently – within the past two million years. The geochemical model indicates that the hydrocarbon generation and migration were most prolific along the area of the present culmination of the Inner Apulian Unit and peaked shortly after the nappes were formed.

From the oil-exploration viewpoint, the axial zone of the belt, corresponding to the regional culmination of the Inner Apulian Platform, is the most promising area, especially considering the size of the structures.

Finding out about fractures

In such tight carbonates, where the production is linked to the fracture network, conventional logging alone is not sufficient. The low porosity results in a consistently high resistivity reading which contains little quantitative information. It is possible to determine qualitatively the presence of connected fractures and the extent of invasion by comparing the separation between deep and shallow laterologs (Figure 8.3).

Information provided by monopole sonic measurements is also of some help in these situations. However, a better picture of the formation can be gleaned from detailed analysis of the dipole sonic waveforms – such as the Stoneley wave – acquired using the DSI* Dipole Shear Sonic Imager tool.

In most reservoirs tools such as the CNL* Compensated Neutron Log and the Litho-Density* tool (LDT) are extremely useful as they highlight lithological changes. But in these fractured carbonates such variations are rare. The combined use of the APS (Accelerator Porosity Sonde) and PLATFORM EXPRESS* density data can give a reliable indication of porosity as the readings are less subject to borehole effects. In other situations this combination also gives information on lithology.

The NGS* Natural Gamma Ray Spectrometry tool is another measurement that has useful application in these carbonates. The quantity of organic material in a formation is proportional to the amount of uranium in the rock. The presence of shales can be deduced by measuring the amount of thorium and potassium in the formation.

Monitoring changes in the temperature gradients, which are often due to mud losses, is another way to deduce the location of open fractures.

A better way of finding fractures

For several years the FMI Fullbore Formation MicroImager tool has led the way in the investigation of a rock's sedimentological and structural elements. The tool provides a clear picture of the sedimentary and tectonic features seen along the borehole walls of wells in both clastic and carbonate formations.

In the tight carbonates described here the overriding priority is to determine the fracture type and distribution and identify changes in dip that could indicate faults. The FMI tool can be used to distinguish between the four main fracture types: conductive fractures, conductive microfractures, healed fractures and induced fractures.

The identification of induced fractures is particularly important as these are produced by the mechanical action of the drill bit and thus do not extend throughout the reservoir. They must not be confused with natural fractures. Induced fractures develop along the line of minimum horizontal stress and so give an insight into the regional compressive forces acting on the reservoir.

Such structural information helps to differentiate the open conductive fractures and microfractures from closed fractures. Normally, open fractures are oriented with their strike perpendicular to the direction of minimum compressive stress.

Using FMI images it is relatively easy to pinpoint the intervals with higher fracture density. However, it is more difficult to quantify the hydraulic fracture aperture, and attempts to do this using the excess current technique have so far met with little success.

The MDT Modular Formation Dynamics Tester tool gives an indication of the likely productivity of the interval between packers, but to do this it needs to be stationed in zones with high natural fracture density. In addition to the FMI images, the selection of such intervals can be deduced from caliper logs which reveal changes in borehole shape caused by regional stress. In bad hole sections, indicated by borehole caliper measurements, the MDT tool should not be set. Good pay zones are often revealed by the presence of fracture sets which have different azimuths as seen on the FMI image. Fracture continuity is also important in pay zones. Fracture events which are visible on images from all four of the FMI tool measurements could be assumed to have good continuity.

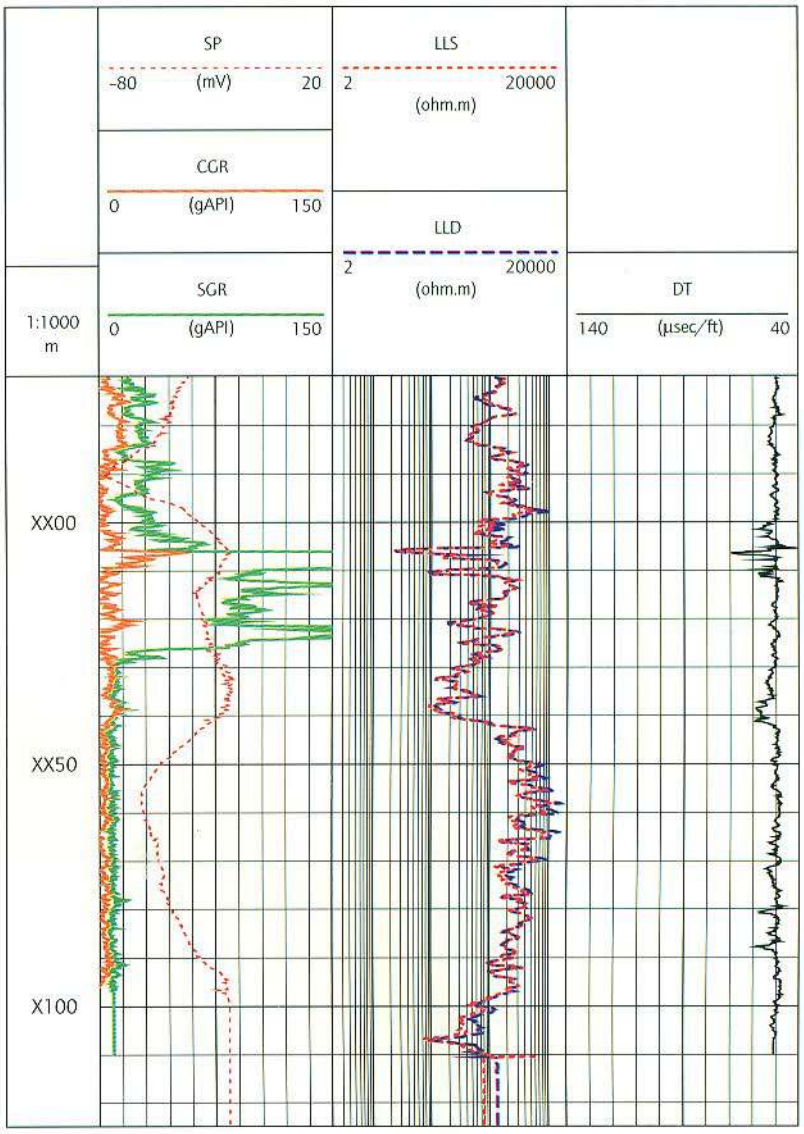

Figure 8.3 *Until recently, the only way of determining the presence of fractures or the extent of formation invasion was to compare the separation between the curves of the deep and shallow readings of the laterolog tool*

MDT tool description

The typical MDT tool string used for testing fractured reservoirs is shown in Figure 8.4. This is the only wireline tool presently available for fracture testing. It comprises a number of modules that can be combined to provide the required tool string configuration. Some of the modules are described below.

The dual packer module consists of two inflatable packers which can isolate about 1 m of the borehole. The ability to isolate the borehole allows pressure measurements and fluid samples to be taken when it is

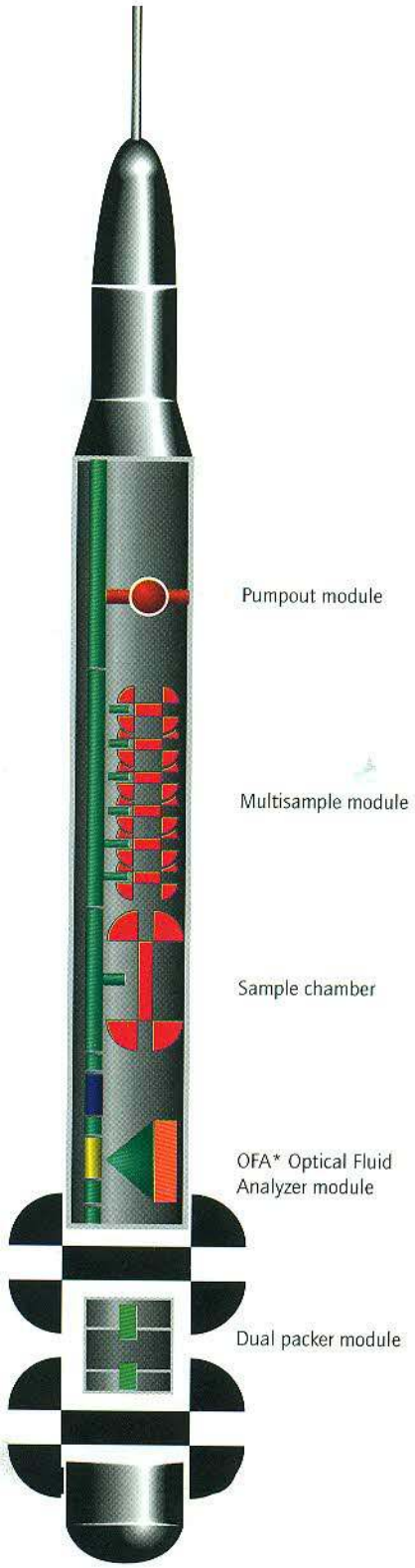

Figure 8.4 *Typical* MDT *tool string used in the testing of fractured reservoirs*

impractical to use the probe, such as in laminated, shaly, fractured, vuggy or low-permeability formations. The hole size and the distance between packers determine the maximum angle of dip at which a fracture can be tested without bypass problems.

The OFA* Optical Fluid Analyzer module uses optical technology to distinguish the presence of oil, water and gas in the flowline (Figure 8.5). Oil and water are identified using visible and near-infrared spectroscopy; gas is detected using reflection techniques.

The conventional sample chamber modules are available in three sizes: 1, 2 and 6 gallons.

The multisample module contains six 450-cc bottles for storing samples for subsequent pressure–volume–temperature (PVT) analysis. Each bottle is certified for transportation as a pressure vessel. Up to two modules can be added to the tool string, so 12 samples can be taken.

The pumpout module pumps reservoir fluid from the formation through the flowline and back to the borehole, thus allowing virgin fluid to be recovered or analysed. It is also used to inflate the packers and to pump fluids into the formation during special applications.

The single probe module contains the probe assembly, the pressure gauges and the resistivity cell.

A gamma ray sensor (for correlation) and an auxilliary measurement sonde (for head tension, mud temperature and mud resistivity measurements) are normally incorporated in the tool string.

Criteria for MDT measuring stations

The key parameter determining which intervals should be investigated is the presence of fractures, as identified on the FMI log. Special attention must be paid to the hole shape to avoid setting in bad hole, washout, breakout, etc, and to ensure a proper seal. In particular, fractures must not extend beyond the packer or bypass problems will arise. Figure 8.6 shows a section of interpreted FMI log with the dual packer module and caliper logs.

The FMI calipers are the primary means of determining borehole geometry, but in larger holes accuracy is limited by the relatively smaller pad size. In such cases, breakout, keyseats or other small anomalies in the borehole escape detection. Detailed information on the hole shape can be obtained from

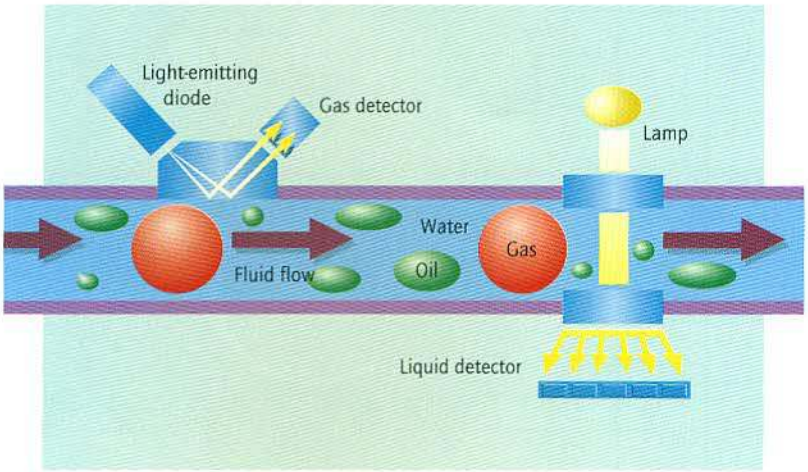

Figure 8.5 *The OFA Optical Fluid Analyzer module of the MDT tool contains an innovative detection system that can differentiate between oil, water and gas in the flowline*

the UBI Ultrasonic Borehole Imager tool. The 0.7-mm radial resolution of the UBI tool, and its ability to determine a hole cross section at any depth, help to identify the zones where setting problems might occur. Figure 8.7 shows a good hole, a bad hole and a breakout.

Pressure tests, sampling and fluid identification

Each test can be conducted with one or a combination of three different objectives:

- to measure pressure
- to take formation fluid samples
- to identify the formation fluid

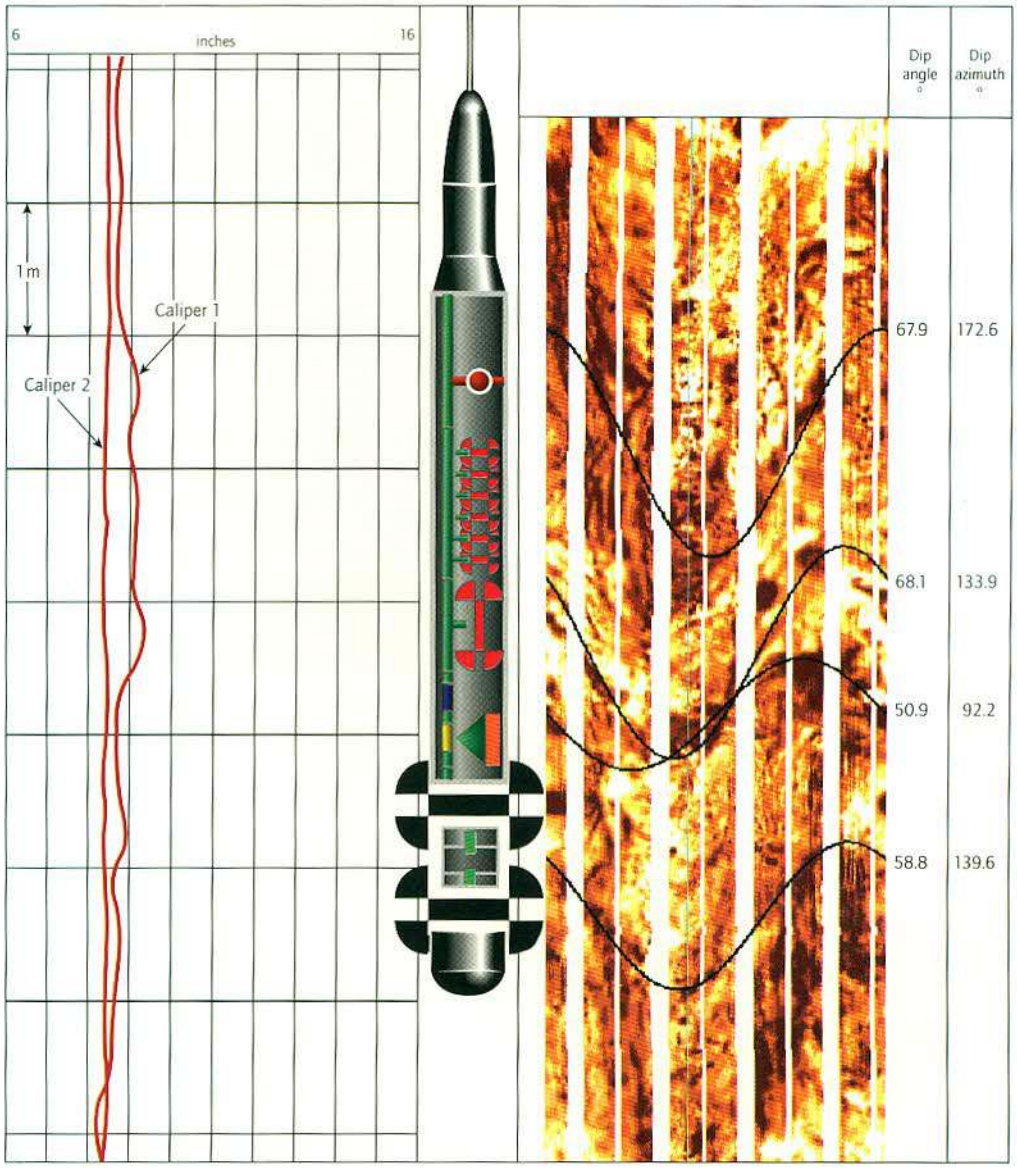

Figure 8.6 *The optimum testing interval for an* MDT *test can be selected by examination of* FMI *images and borehole shape information from caliper logs or* UBI *images*

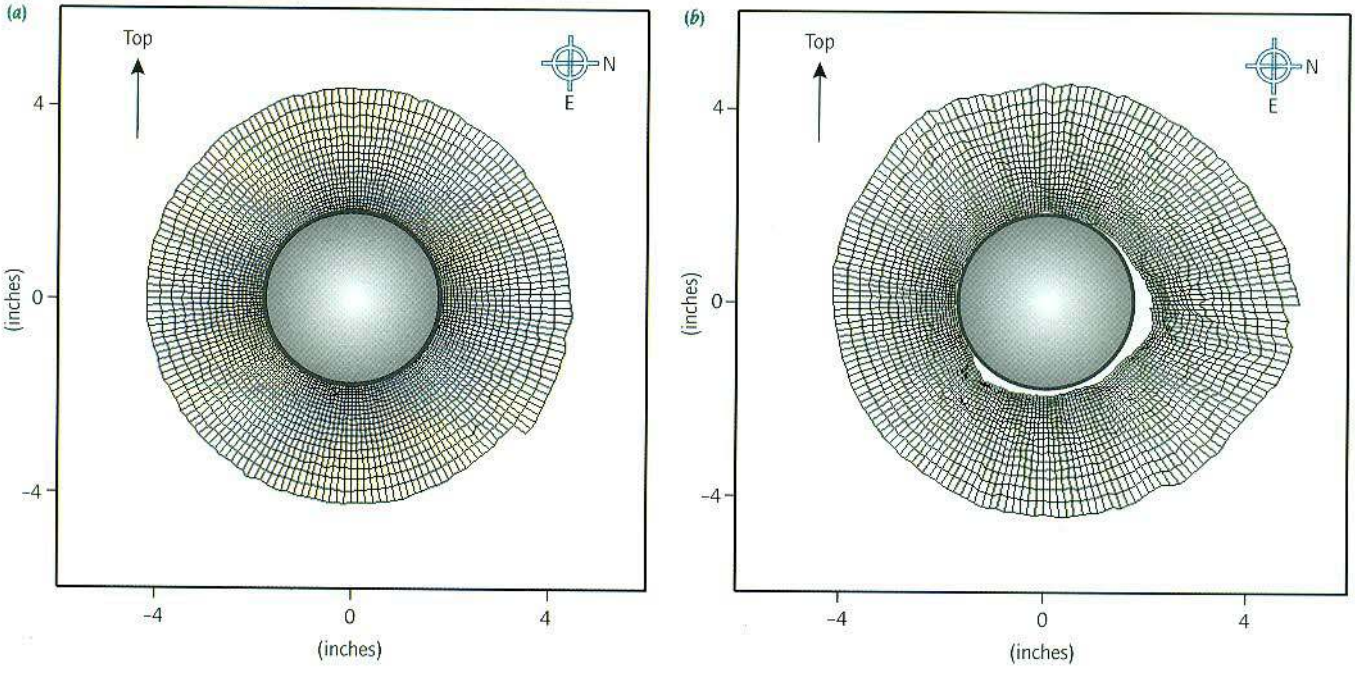

Figure 8.7 The good, the bad and the ugly. These UBI images show widely different hole conditions. There would be no problems setting packers in hole (a). But in hole (b) there may be sealing problems due to ovalization of the hole. In the worst case, (c), there will be packer sealing problems and probable packer damage due to the breakout

Figure 8.8 shows an example of a test where all three objectives have been achieved.

Packers are inflated by pumping mud from the borehole into the packers, to achieve a seal between the borehole and the formation.

A pressure drawdown is obtained by pumping out a certain amount of fluid from the sealed-off interval into the borehole. The pressure then builds up in the interval between the packers until it stabilizes sufficiently to give an accurate reading.

The cleanup period follows the pressure test and consists of pumping fluid from the packer interval back into the borehole. It is required either for fluid identification or to take a sample. The cleanup time depends on the extent of invasion: deeper invasions require longer cleanup times. Field experience shows that the minimum time before the first oil shows is the time needed to pump out the fluid volume between packers. In other cases the pumpout volume was over 200 liters and consequently longer times were needed.

The pumping duration also depends on the pump performance and formation permeability. Observed flow rate range is 1.4–2.5 m^3/day. Fluid properties are monitored in real time by the OFA Optical Fluid Analyzer module. The oil fraction is computed from the optical spectrum and displayed (middle diagram in Figure 8.8). Cleanup ends at 100% oil or at satisfactory oil:water ratio.

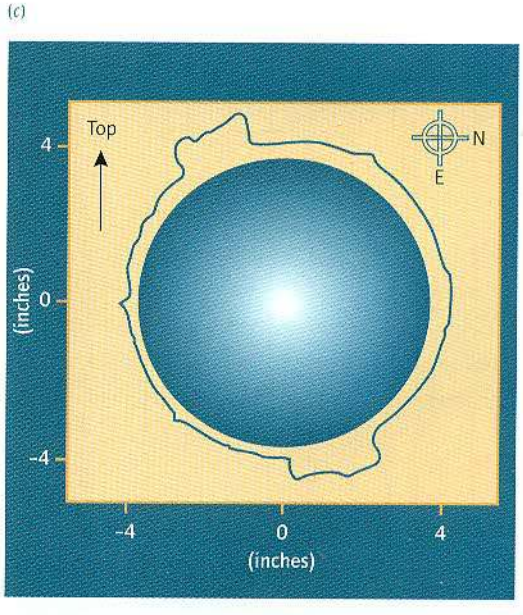

After the cleanup period one or more fluid samples can be taken as required.

At the end of the test the pressure is equalized, the packers are deflated and the tool can be moved to the next station.

Interpretation of MDT results

Gradients

To determine fluid gradients accurately, pressure data must be cleaned up to eliminate unrepresentative readings. In addition, special care must be given to

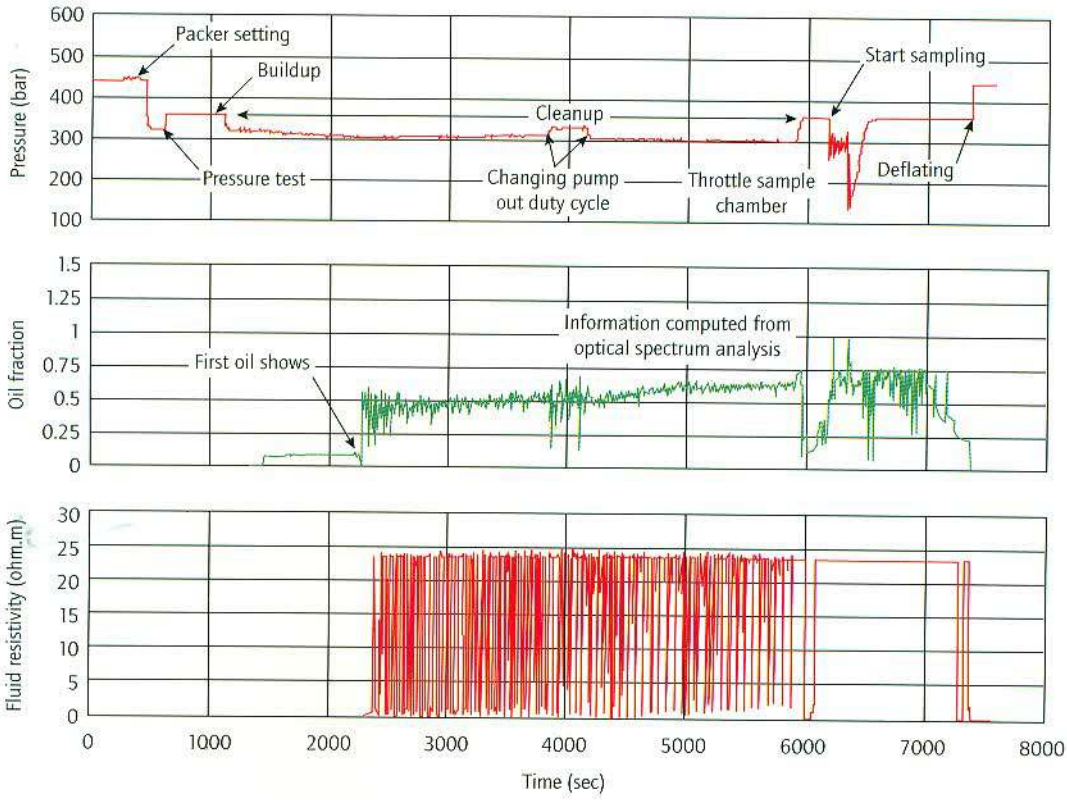

Figure 8.8 *This shows a testing sequence conducted with the* MDT *tool. The test was used to measure formation pressure, take formation fluid samples and identify the formation fluid*

the very low permeability points (less than 1 mD), which are often supercharged. Analysis of the cleaned data can then reveal fluids distribution.

Figure 8.9 shows fluid gradient measurements taken in Well A. Before the introduction of the dual packer module, point pressure measurements were not possible in such reservoirs. Also, openhole logs fail to provide useful information on the oil–water contact (OWC). This is why the regional OWC displayed in Figure 8.9 had to be extrapolated using production test results from a nearby field. The true OWC level was discovered to be 40 m shallower. Figure 8.10 shows the oil properties as a function of depth, as obtained from the MDT samples and production test.

Productivity and permeability from pressure analysis

Interpretation of the imaging logs does not shed any light on the fracture productivity.

Permeability values and skin factors for the testing interval between the two isolating packers can be obtained from the pressure analysis of the small-scale flow test. The fluid volumes are not as large as in a conventional well test and so analysis is limited to the near-wellbore region. However, field experience shows that the reservoir parameters determined by this method compare well with production tests.

Two techniques are available for the pressure analysis:

- standard well-test techniques in which information on drawdown, buildup and pumpout rates are used in interpretation. This technique can be conducted with any well-test software package

Figure 8.9 *The fluid gradient and oil–water contact* (OWC) *for the Well A*

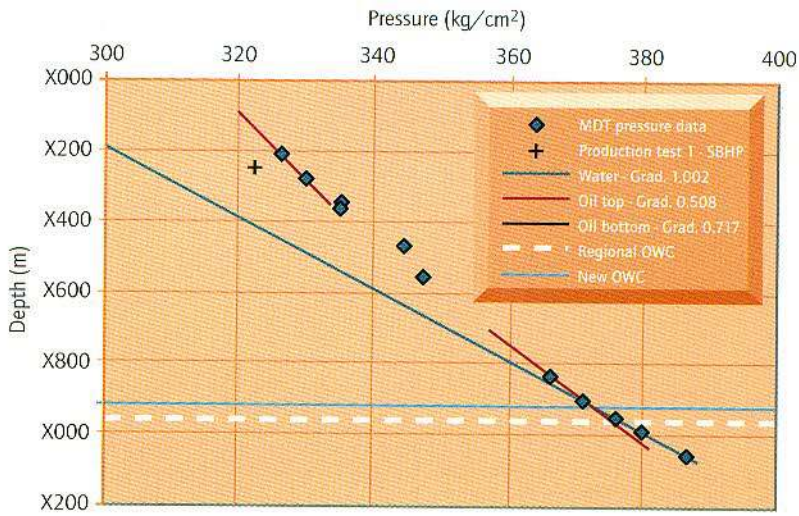

- simulation techniques using the Polaris* module of the GeoFrame* platform: the true pressure response is simulated for different values of permeability and skin until a match is achieved

These two techniques can also be used in tandem; for example, the parameters obtained from a well-test analysis can be used as a first guess input to a simulation. Most of the time these two techniques produce coherent results.

Figures 8.11, 8.12 and 8.13 (Time 1 column) show examples of pressure analysis for the set of fractures shown in Figure 8.6. The same fracture was tested again at a different time. The pressure analyses results for the second test (Time 2 column of Figures 8.11, 8.12 and 8.13) were very similar to those obtained in the first flow test.

Figure 8.10 *Oil properties as a function of depth obtained from* MDT *and production tests*

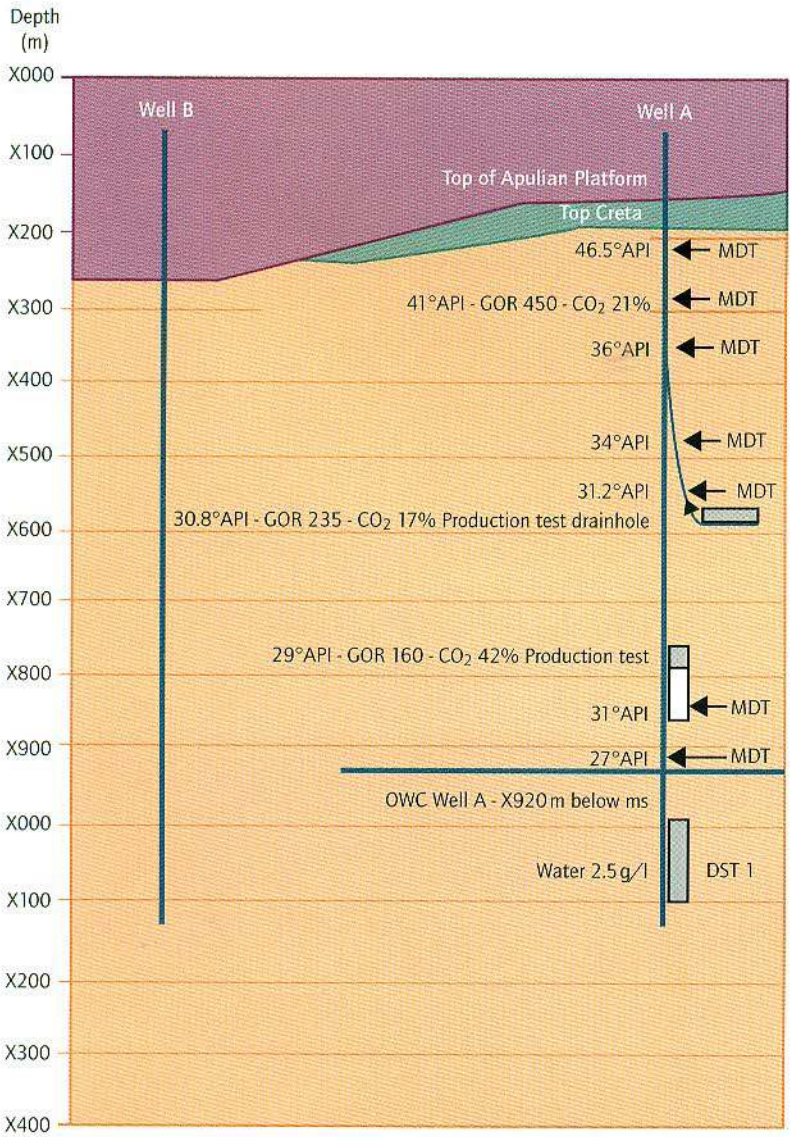

Integration brings enhancement

The use of the MDT tool, integrated with interpretation of imaging logs, brings benefits in terms of an enhanced reservoir description and production cost optimization (Figure 8.14).

Accurate fluid gradients obtained using point pressure measurements, previously impossible in a zero-porosity fractured reservoir, lead to a detailed analysis of fluid distribution – from gas condensate down to heavy oil and water. An understanding of oil properties and determination of the water table position were critical to completion design.

The estimation of permeability and skin values for the set of fractures isolated by the dual packer module brings us a major step forward in near-wellbore reservoir characterization. Until now it has been difficult to obtain detailed information on the fracture productivity. As a result some wells failed to produce as expected.

The MDT tool can also be used to determine the production capability of vuggy formations. Vuggy layers identified on the FMI log can be tested to determine the vugs' interconnectivity. Figure 8.15 shows a Formation MicroScanner* image of a vuggy zone. When the interval was isolated and tested with the MDT dual packer module it was found that the vugs were interconnected and would contribute to production. The pressure analysis gave a permeability of 450 mD.

From an economic viewpoint, information provided by the MDT tool is more complete and detailed than that obtained from a drillstem test (DST). An MDT survey is typically 40–70% cheaper than a DST. A cost comparison (including the expense of the rig) is shown in Figure 8.16. In this table all the MDT tools had to be run in tough logging conditions, thus requiring a longer rig time. The figures can be further improved when the tool is run with wireline cable.

Conclusion

The MDT measurement allows accurate prediction of production potential on a fracture-by-fracture basis. The capability of measuring oil parameters during the same trip in the well provides invaluable information for completion design and selective production.

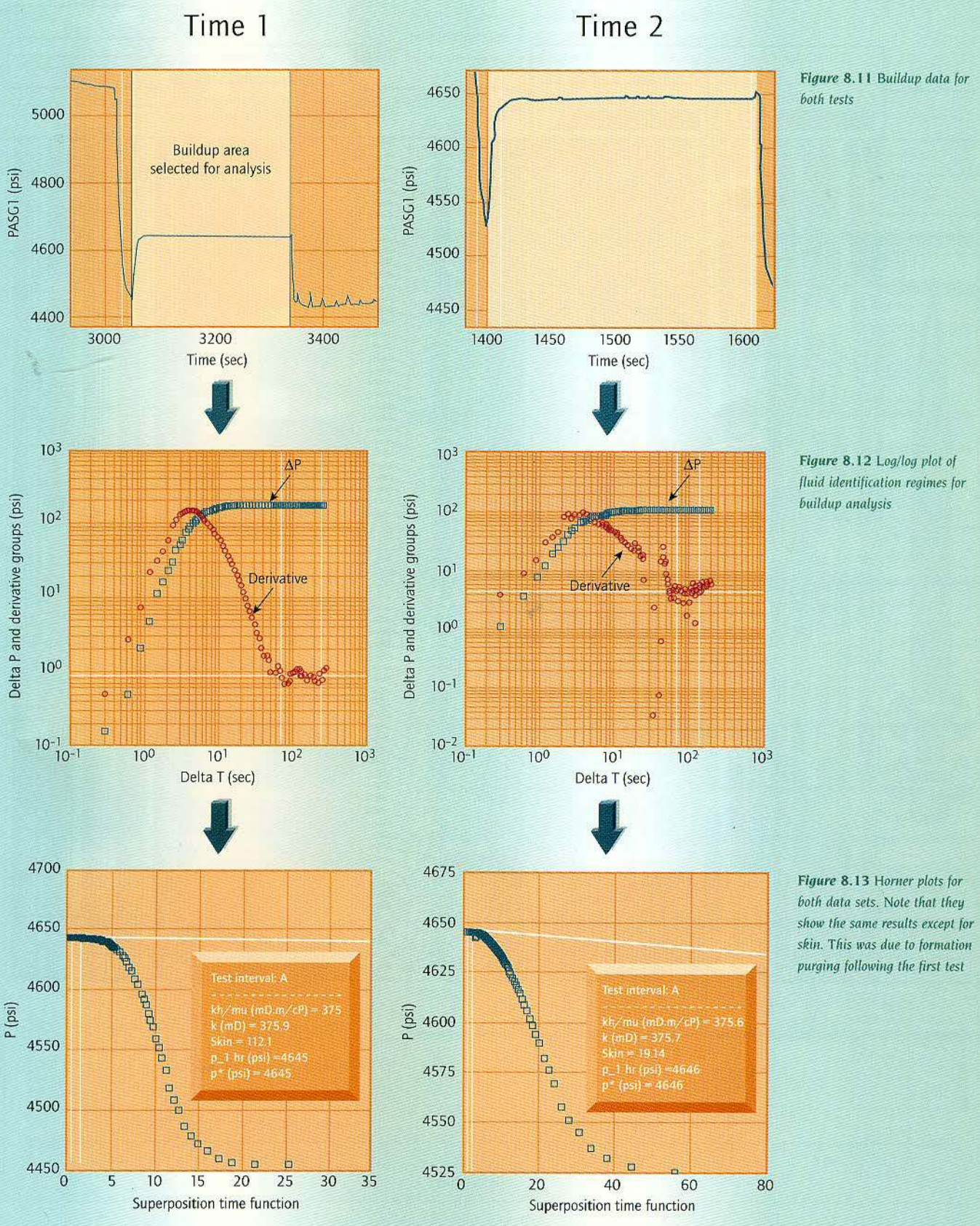

Figure 8.11 *Buildup data for both tests*

Figure 8.12 *Log/log plot of fluid identification regimes for buildup analysis*

Figure 8.13 *Horner plots for both data sets. Note that they show the same results except for skin. This was due to formation purging following the first test*

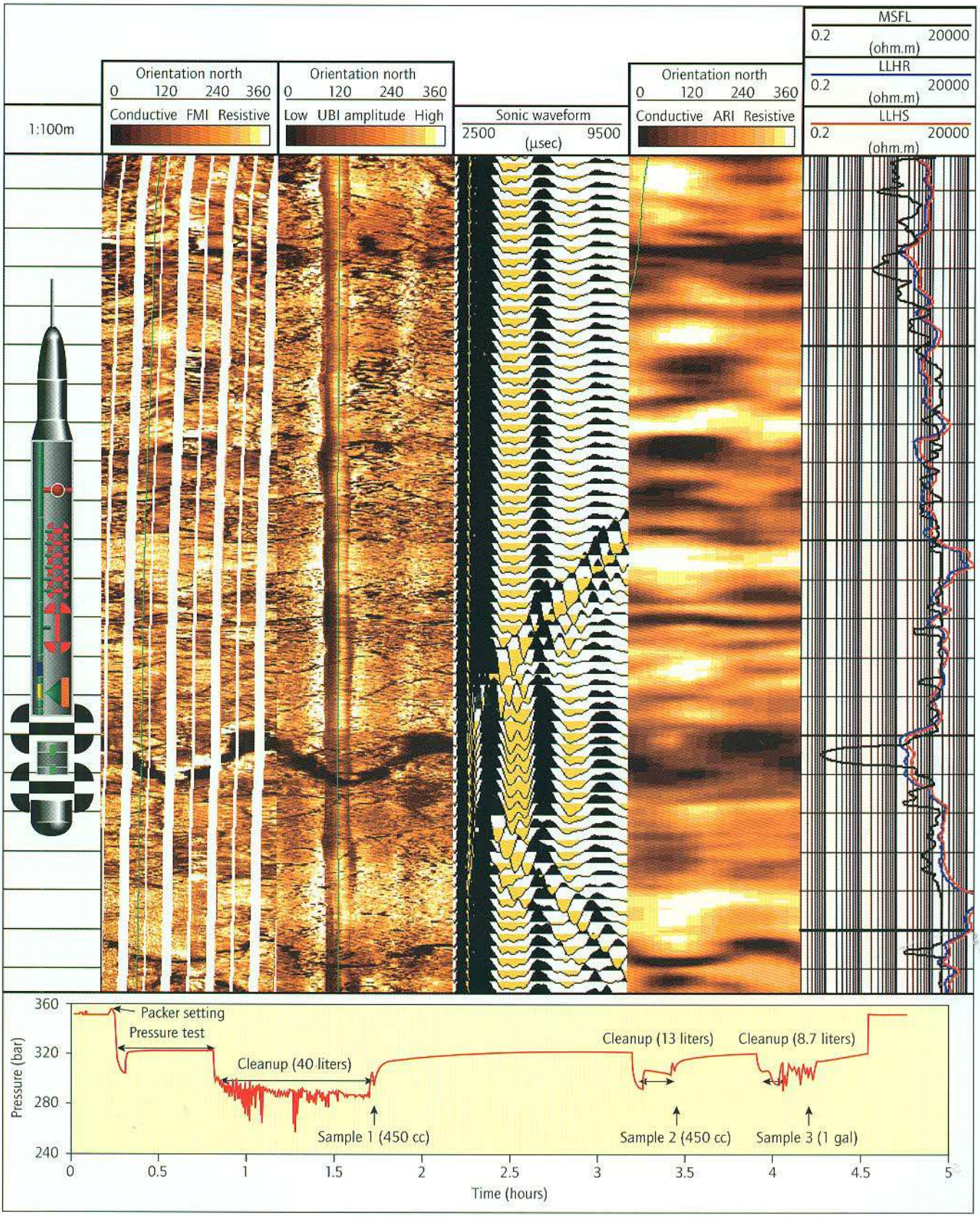

Figure 8.14 *An example of high-technology data interpretation showing how FMI/UBI/DSI and ARI (image and laterolog) data can be used for a full fracture characterization. This Italian example shows the results of a pressure test on a fracture conducted using the MDT tool. Three fluid samples were also taken (see test details at the base). The sample contents were confirmed by the production test. (The numbers in parentheses indicate the number of liters of fluid pumped out during the test)*

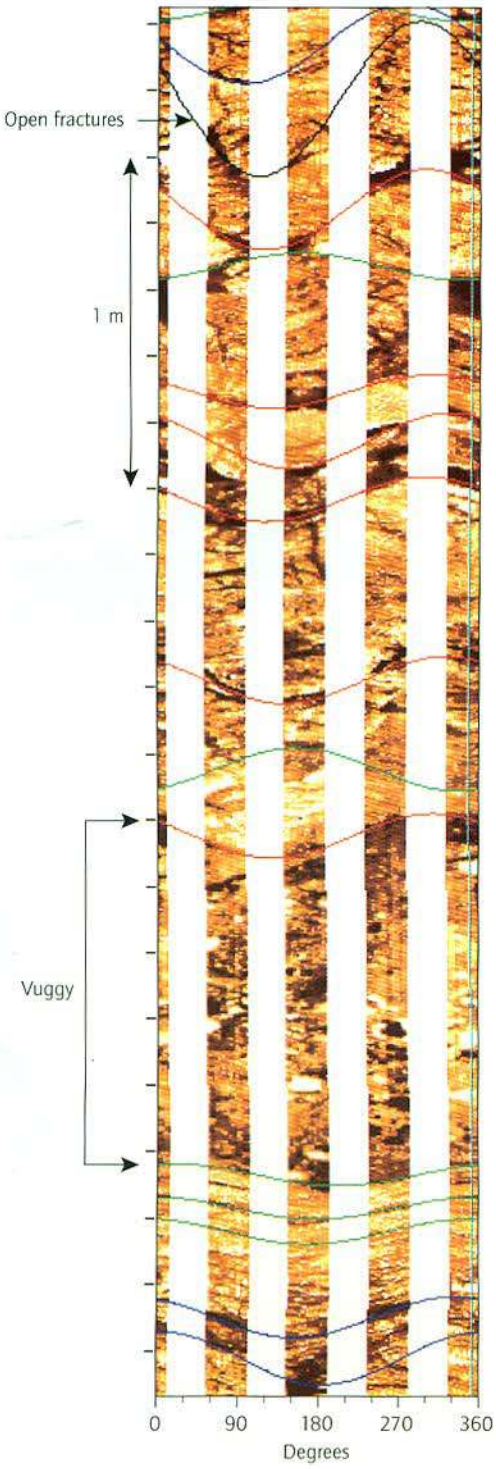

Figure 8.15 *Formation MicroScanner image from an oil zone in Well A. The imagery reveals a vuggy interval (nodular shapes), open fractures (black lines) and bedding planes (green lines). Induced fractures are indicated by both red and blue lines.*

Figure 8.16 *Cost and results comparison of MDT dual packer and openhole DST operations*

MDT					
Well	MDT cost (US$)	Time (days)	Rig cost (US$)	Total cost (US$)	Results
A February 1996	286,000	4.5	140,600	426,600	12 Pressure tests Formation pressure and fluid gradient 2 Oil samples at different depths Small-scale flow tests
B May 1996	248,000	2.5	80,600	328,000	10 Pressure tests Formation pressure and fluid gradient 2 Oil samples and 6 PVT samples at two different depths Small-scale flow tests
C July 1996	384,400	4.0	125,000	509,400	13 Pressure tests Formation pressure and fluid gradient 1 Oil sample (1 chamber failed) and 6 PVT samples at three different depths Small-scale flow tests

DST			
Well	Time (days)	Total cost (US$)	Results
D December 1995 Second DST test	12	687,500	With 32 nitrogen lifts Formation pressure, formation fluid
E February 1996 Fourth DST test	17	937,500	With 18 nitrogen lifts Formation pressure, formation fluid 2 PVT samples with bottomhole sampler

IX

Detailed reservoir characterization with DipFan†

The integration of dipmeter data with other openhole logs is now key to the exploitation of stratigraphic information contained in any logging suite. Agip and Schlumberger have worked together to make such integration possible by developing DipFan (Dipmeter Facies Analysis) – a new software package for geological interpretation. The powerful and dedicated suite of DipFan programs is now being used in field studies in Italy and around the world. This article reviews the six DipFan software modules and shows how they have been used to conduct detailed interpretation of a small gas field

L'integrazione di dati da dipmeter e di altri log in foro aperto è oggi un elemento fondamentale per sfruttare appieno le informazioni stratigrafiche derivabili da qualsiasi serie di misure in pozzo. Agip e Schlumberger hanno collaborato per rendere possibile questa integrazione, sviluppando il DipFan (Dipmeter Facies Analysis) – un nuovo pacchetto software per l'interpretazione geologica. La potente e specializzata serie di programmi DipFan viene utilizzata per studiare i giacimenti d'Italia e di tutto il mondo. Questo articolo illustra i sei moduli software del pacchetto DipFan e descrive l'uso che ne è stato fatto per ottenere un'interpretazione dettagliata di un piccolo campo a gas

Agip
P Balossino

Schlumberger
H Anxionnaz

DipFan – six steps to success

The DipFan package has six interactive modules which form a powerful data processing chain. The package can be run to suit each particular case and permits a user-oriented interpretation of the wells (Figure 9.1). Three primary modules – FasTex, SediView and Sequence – analyse the data for texture, sedimentology and vertical sequence. These three modules can be used separately. The overall results can be enhanced considerably by including three optional modules – DimQC, RockCell and StatPack.

FasTex – a question of character

FasTex uses the character of the dipmeter microresistivity curves (or fast channels) to identify zones with similar internal organization defined by layering and by texture. Electrical imaging tool data sets can be input to the module as pseudo-dipmeter curves corresponding to the dipmeter fast channels. The module proposes a zonation of the formations encountered by the well into 'morphofacies'.

The program performs a geology-driven analysis of the dipmeter curves that focuses along the apparent dip of the bedding planes. Summary curves are used to express the information contained within the dipmeter fast channels. Attributes such as thickness and contrast are used to describe the raw curve events.

Different zones are distinguished from each other by a segmentation scheme that uses a hierarchical clustering technique applied to the summary logs. The user can monitor the aggregation process through various statistical plots such as a dendrogram. The number of clusters, or 'morphofacies', is controlled via the input parameters. The clustering process is fine-tuned by using vertical logic which takes into account a minimum zone thickness.

SediView – sorting out the sediments

SediView derives accurate sedimentological information from dip and lithological results. The module helps reservoir delineation by inferring geometrical information from depositional features.

A variety of filtering techniques can be applied to focus the interpretation on meaningful dips. A typical filter would be the dip quality index output by DimQC. Lithological zonation can be used as an additional filtering technique.

Then SediView evaluates and removes the effect of post-depositional tilting or deformation. An innovative and accurate approach based on the local curvature axis technique is used to derive the structural dip that can then be removed vectorially by zone.

Previous determinations of structural dip sought zones of constant dip as being evidence of the structural tilt encasing the reservoir. The technique used in SediView makes use of the observation that the cylindrical or conical bed surface axes within each bed set are often coplanar. The current dip and orientation of this plane reflect the effect of the post-depositional deformation.

In a first automatic pass, the module computes the local curvature axis of each bed set. These axes are plotted on the stereonet and analysed interactively to define the structural dip common to a group of beds. This technique detects the subtle change in structural dip that can occur between depositional episodes.

After subtraction of the structural dip for each depositional unit, a dip dispersion analysis can be optionally performed to organize the bed sets into groups. The thickness and the azimuth of each depositional unit are then computed.

Sequence – marshalling the modules, masterminding the data

Sequence consists of a number of independent interpretation submodules. The outputs can be combined with other DipFan results to provide user-friendly stratigraphic interpretation capability. Bed boundaries, defined either by the DipFan modules or by stratigraphy and core analysis, are consolidated and ranked into an organized geological display.

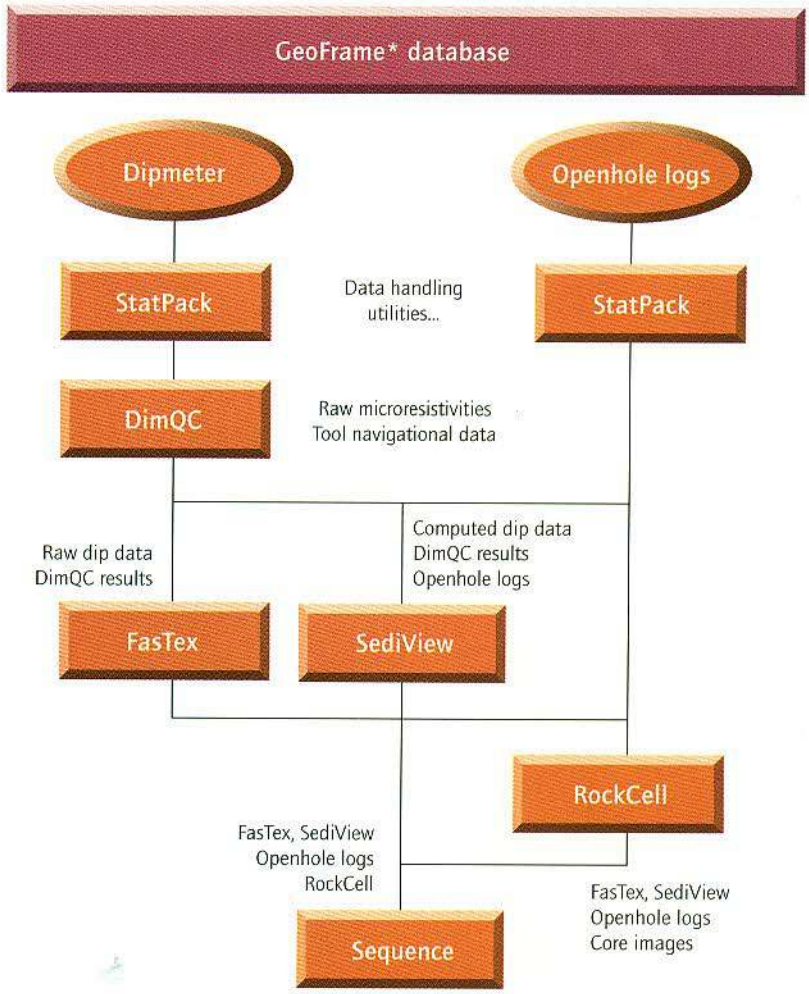

Figure 9.1 DipFan processing flow chart. The processing chain is built from six modules that can be run to suit any particular case. StatPack and RockCell can be applied to both dipmeter and other logging tool data; DimQC, FasTex and SediView analyse only raw dipmeter data and processed dip results

Sequence provides two main analyses:

- **Curve shape analysis.** Sequence performs a semi-automatic analysis of the different openhole logs for identification of bell, funnel and cylinder shapes. These are used in sand and shale sequences to describe the depositional facies in terms of their grain-size trends. The curve shape analysis is a two-stage process. Breakpoints are detected by searching for levels at which the first derivative exceeds a given threshold. Then zones defined by two breakpoints are classified in accordance with the slope of the line that approximates the input log.
- **Thickness and lithology analysis.** The thickness analysis recognizes and describes thickening or thinning upward trends in the analysed sequence. Three algorithms have been developed that enable the user to perform this analysis at different scales.

A large-scale quick-look approach over the whole sequence can be run using gravity displays. On a finer scale, regression analysis can be performed within zones defined either automatically or by the user. Alternatively, parasequence stacking pattern analysis can be inferred through interpretation of Fischer plots. Once performed in a multiwell context the Fischer plots can be used to improve well-to-well correlations.

DimQC - keeping a check on quality

DimQC performs basic quality control on the dipmeter data, detecting anomalies in the various curves, and classifies the borehole shape according to caliper values.

Quality control is performed in three phases:

- **Individual curve analysis.** Various user-defined threshold tests are applied to individual curves

such as hole azimuth, or to curves of the same family such as the sonde calipers, as well as to the dip data themselves. These tests are applied on a level-by-level or a window basis.

- **Fast channel qualification.** Any flags attached to the fast channels are crosschecked against those attached to the tension, caliper and navigation channels. This process allows degraded data to be classified as tool- or hole-related. Unqualified anomalies are classified as generic.
- **Computation of severity curves.** Two severity curves, RawQC and TadQC, are computed in the final phase. The RawQC curve, computed from the fast channel qualification results, indicates the overall quality of the acquisition. The TadQC severity curve is then computed combining RawQC values with the results of dip data and navigation curve checks. TadQC indicates the confidence of the dip processing results and whether they are related to geological features or to processing artifacts.

RockCell – in a class of its own

RockCell is a classification tool box that provides the user with different classification and estimation techniques including multidimensional regression analysis and neural network techniques.

It is used to perform multiwell facies analyses based on the assumption that facies information is known and contained in well logs. One or more wells in the set are defined as the 'key wells' and are used to define the set of facies estimators.

The RockCell module operates in three phases:

- **Key well data analysis.** This phase provides the user with a powerful working environment to display multiwell log results. Intervals representing various facies can be selected and labeled by the interpreter in both depth and crossplot views.
- **Model building and network training.** Once facies information has been defined in the key wells, the user can define a data set (a list of wells, a list of curves and a list of facies zones) and build a model. This consists of a multidimensional histogram or a neural network which after training relates the facies information to the estimator value distribution.
- **Facies estimation.** The goal of the final phase is to assign the most likely facies to each level of the target well. A number of facies will be found and these are retained in decreasing order of likelihood. In practice, only the first three facies estimated by the model are displayed.

StatPack – advanced data analysis and presentation

StatPack is designed to provide the user with data analysis techniques, statistical and mathematical functions and common graphic presentations.

StatPack can be invoked by any of the other DipFan modules as part of their processing. For example, FasTex invokes the StatPack library in order to run cluster analyses and to display the results in dendrogram, crossplot or spider plot form.

When running SediView, the StatPack library is used to provide azimuth frequency and azimuth vector plots or other statistical presentations of dip data. The library is called by Sequence to perform Markov analyses, produce Fischer plots and present other graphic displays.

StatPack can also be run as a stand-alone module by interpreters wishing to analyse and manipulate different data types.

Onshore Adriatic fields highlight the power of DipFan

The study wells are located in the onshore part of the Adriatic foredeep in central Italy. In this region the continuous interplay between sedimentation and compressional tectonics strongly influenced the internal architecture and the size of the depositional systems. A major tectonic event occurred in the Early Pliocene that folded and thrusted the sediments and generated the main traps of the area. The structures investigated by the three wells are part of a blind thrust with a NNW–SSE orientation. The reservoir is made up of deepwater siliciclastic sediments which were deposited in the foredeep during the Pliocene.

Despite a very good apparent lateral correlation of the reservoir layers from Well 1 to Well 3 the distribution of the gas-bearing reservoirs was difficult to explain at first glance. Well 1 proved to be a commercial gas discovery; wells 2 and 3 showed few gas-bearing

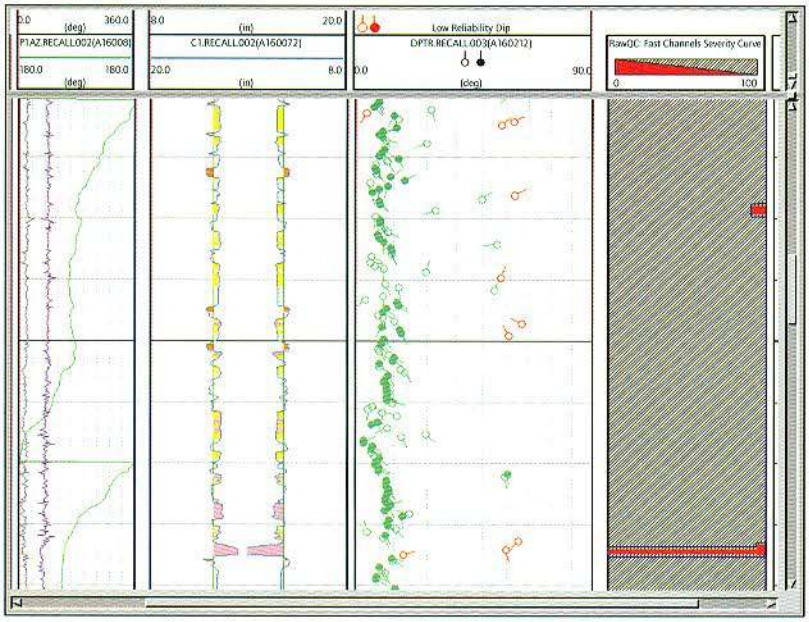

Figure **9.2** *DimQC results on Well 2*

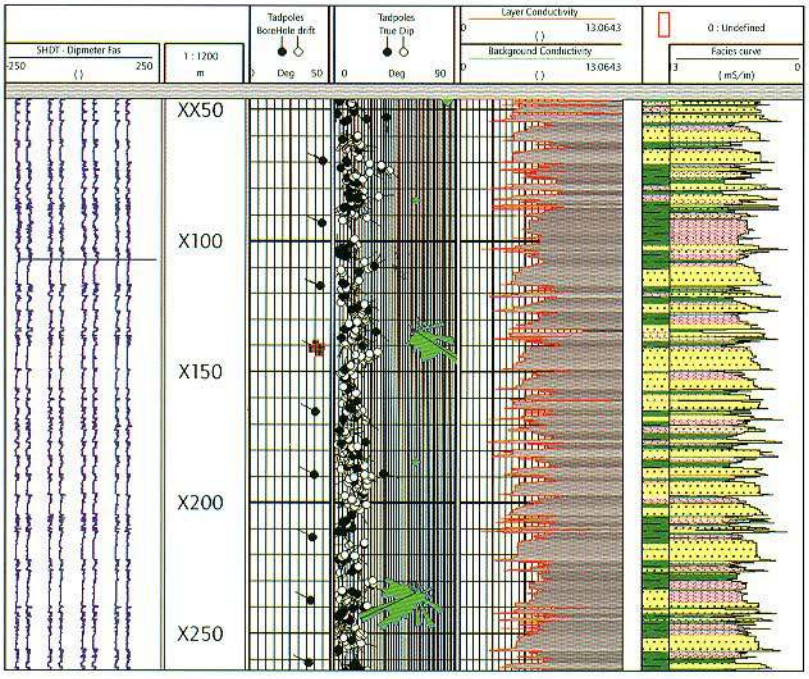

Figure **9.3** *Detailed lithological analysis produced by the FasTex program*

intervals. The main purpose of the study was to understand this anomaly .

The three wells were logged with dipmeter and the following standard openhole logs:

- Dual Dipmeter* tool (also known as SHDT stratigraphic high-resolution dipmeter tool)
- RHOB density log
- NPHI porosity log
- GR natural gamma ray log
- SP (spontaneous potential)
- EATT electromagnetic attenuation
- TPL electromagnetic propagation time

DipFan programs were deemed to be the most appropriate to highlight and interpret subtle events which very often prove to be of major importance in understanding the hydrocarbon distribution within the sequence.

The following well data were available to the interpreters:

- Well 1: SHDT raw data and processed dip results, RHOB, NPHI, GR, SP, EATT, TPL
- Well 2: SHDT raw data and processed dip results, SP
- Well 3: Processed dip results, SP, EATT

Checking data quality

As a first step, the quality and integrity of the SHDT data set from the three wells were verified using the DimQC module. The confidence factor was then used as input to the other processing steps to filter out low-confidence dip results. Figure 9.2 shows the excellent quality of the acquisition data and processed results.

The RawQC severity curve, shown on the right, indicates a high-quality data set, except in the lower part of the displayed interval where the confidence factor approaches zero due to caliper closure.

In the TadQC severity curve (third track on Figure 9.2), high-quality, reliable data are indicated by green tadpoles, and poorer quality data due to processing artifacts (false dips created by the dip processing, not related to geology) are displayed in red.

As a second step, a log-derived lithological column was computed for the three wells, using the litho_quicklook capability that is available within the SediView program or as a stand-alone utility.

The three wells cross a turbiditic sequence characterized by alternating 1 to >10 m-thick fine to very fine sandstones interbedded with shale of the same thickness. Several techniques can be used to create the lithological column:

- manual zonation
- cutoff logic on a set of openhole logs (at least one log is required)
- labeling of clustering results

Lithological columns for wells 1 and 3 have been created using a cutoff logic on the EATT and very thin layers have been identified. In Well 2, only the SP was available. Although this log was of high quality, the lack of measurement resolution meant that it was impossible to delineate the thin layers.

A different technique, available within the FasTex program, was adopted to identify these thin zones. FasTex computes a dip-compensated high-resolution conductivity by averaging along the dip the conductivity values derived from the dipmeter acquisition signal. This conductivity curve is presented in the second track from the right in Figure 9.3.

The user indicates the expected thin-bed lithologies and their respective conductivity ranges on the large-scale lithological zonation derived from the SP curve (left side of the far right track in Figure 9.3). The program uses this information to refine the large-scale zonation. The detailed lithological zonation obtained with this technique is presented in the rightmost track in Figure 9.3.

This precise lithological information is used to drive the dipmeter interpretation performed with the SediView program. The first phase of the interpretation involves filtering the dip results to remove low-confidence and out-of-sequence dips. Then, using the local curvature axis technique described above, an exact structural dip is computed and subtracted from the original data.

The different phases of the SediView computation are presented in Figure 9.4.

Track 1 on the left displays the filtered results (green tadpoles correspond to constant dips, purple tadpoles correspond to successive dips belonging to the same sequence, and blue tadpoles correspond to dips of good quality which are neither constant nor belonging to a sequence). Track 2 displays local curvature axes and track 3 displays the lithological column. The middle section displays a stereoplot that illustrates the structural dip computation technique. The first track on the right-hand side displays the structural dip zonation and the sedimentary dips.

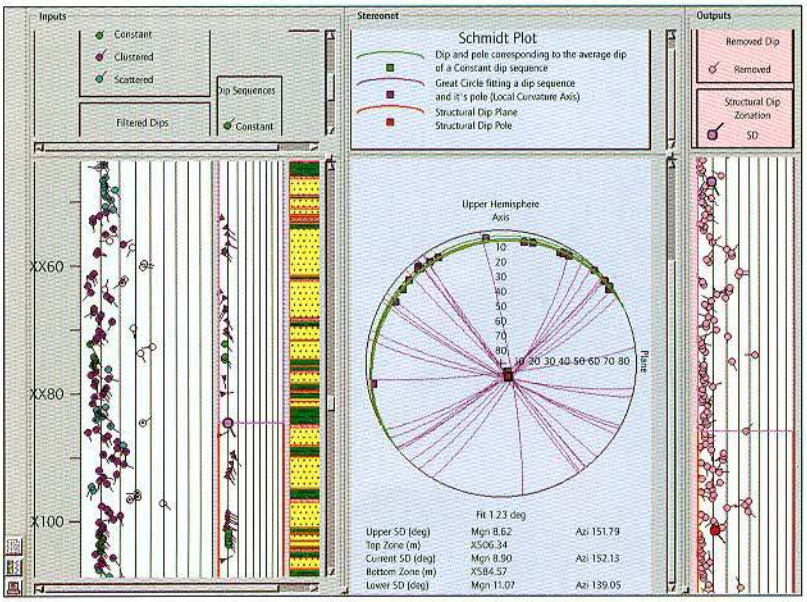

Figure 9.4 *SediView intermediate results for Well 2 with filtered dips, local curvature axes, lithological column, structural dip computation and subtraction*

Dips computed in the silt and sand layers were highly scattered, and it was decided to filter these out and use only the dips (bedding dips) computed in the shaly intervals. On each well, an azimuth vector plot was created from the filtered data. This is useful as it displays the progression of dip azimuth with depth and can be used to identify breaks in bedding attitude.

Understanding the results

The azimuth vector plot results obtained in Well 3 are presented in Figure 9.5. There is an abrupt change in azimuth at about depth X582. This confirms the structural dip computation presented in Figure 9.4. Around this depth the structural dip changes from 8° with an azimuth of 152° to 11° with an azimuth of 139°. Furthermore, this depth corresponds exactly with the top of the only gas-bearing interval recognized in this well.

WellPix* software, the GeoFrame* well-to-well correlation program, was then used to input the

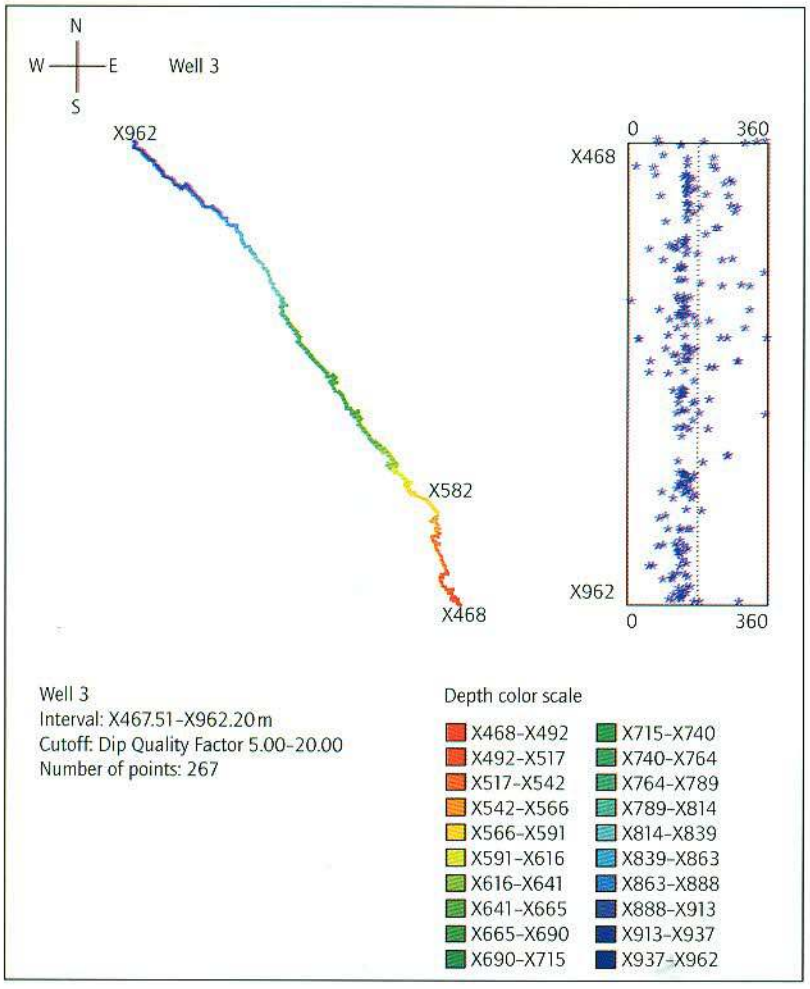

Figure **9.5** *Azimuth vector plot computed on Well 3*

known stratigraphic markers. These were correlated between the three wells across a section where the SediView processing in Well 3 had indicated a change in dip orientation. A true vertical depth and true stratigraphic thickness index were computed using the deviation survey and the structural dip output by SediView.

Figure 9.6 shows a multiwell display of the curves used to establish a correlation between the different beds. The SP and EATT attenuation curves were used for wells 1 and 3 to enable comparison between low- and high-resolution measurements. The SP curve and a high-resolution conductivity curve derived from the dipmeter data of the FasTex program were used for Well 2.

The thickness of the series located between markers D1 and C31 reduces between wells 1 and 2 (one layer is missing) and decreases drastically between wells 2 and 3 (three thick layers are missing) which are less than 500 m apart. This observation confirms the presence of an angular unconformity between sequences D and C.

A detailed interpretation of the lithological profiles of the three wells is revealed by the true stratigraphic thickness in Figure 9.7: the thickness of the series between markers C1 and C2 increases at Well 2.

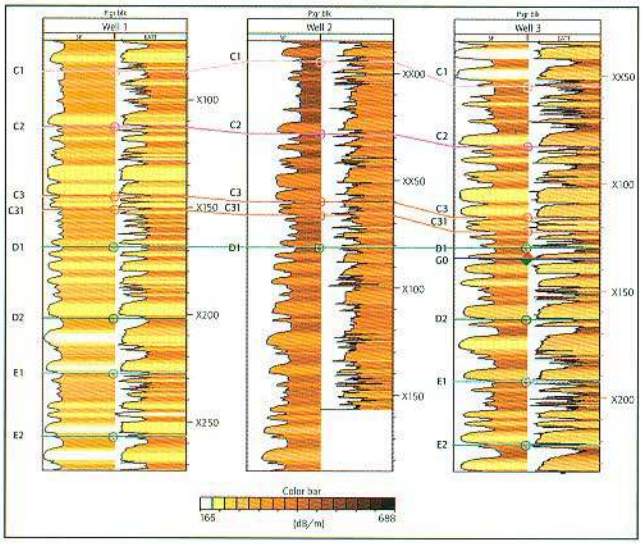

Figure **9.6** *WellPix cross section in True Stratigraphic Thickness showing the presence of a discordance above marker* D1

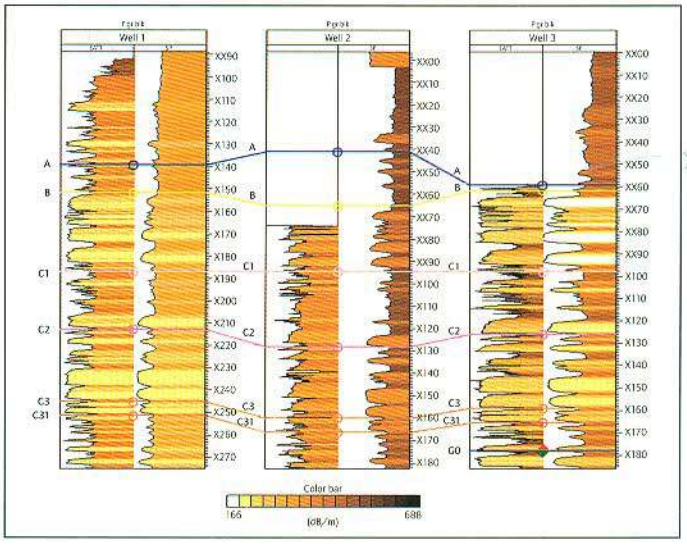

Figure **9.7** *WellPix cross section in True Stratigraphic Thickness showing the thickening of the series between markers* C2 *and* C1

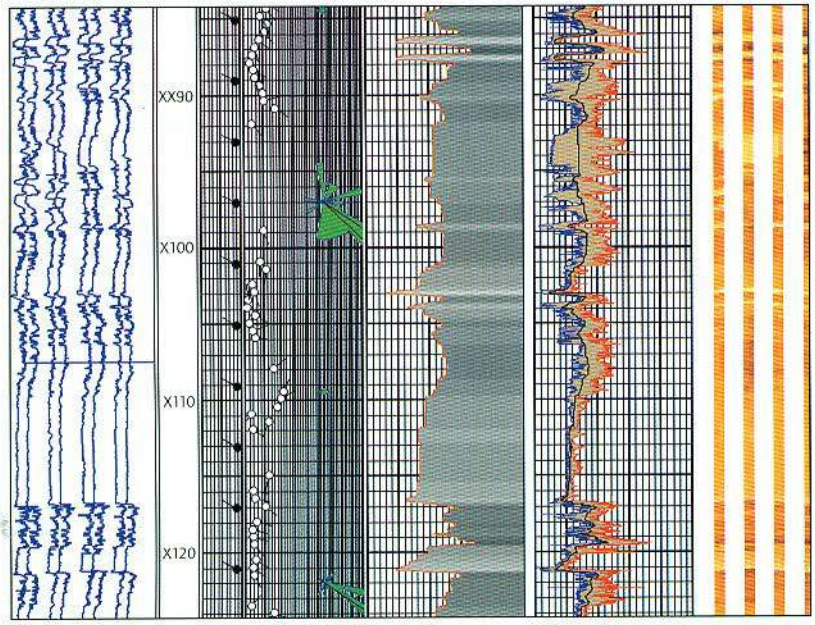

Figure 9.8 FasTex results showing the conductive anomalies around a reverse fault

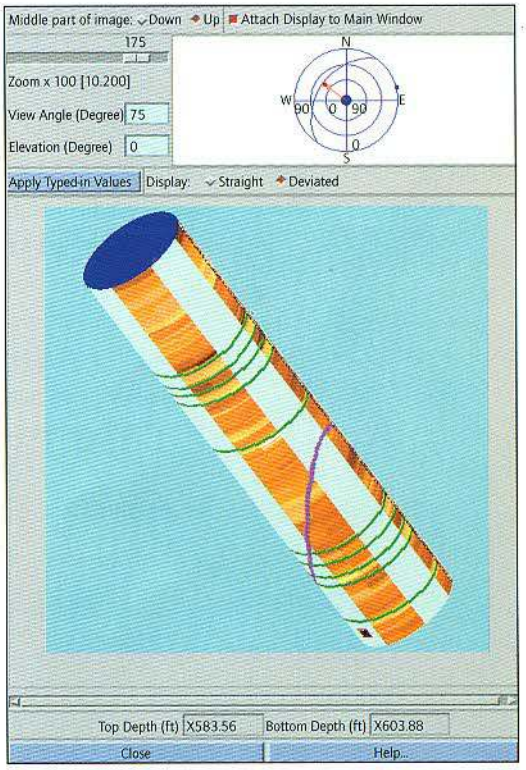

Figure 9.9 3D core-like presentation of the dipmeter pseudo-images showing the repeat section and the fault throw

The FasTex program was used to perform a detailed analysis of the microconductivity distribution over this zone and quantify the presence of non-borehole-crossing components (referred to as anomalies). Results of this analysis are displayed in Figure 9.8.

This shows a background microconductivity (emphasized by the gray-shaded area in track 3) which is constant and has high values at about depth XX95. Over the same interval the resistive anomaly values (track 4 blue curve) indicate high constant values, while the conductive anomaly values (track 4 red curve) show two clear spikes. The pseudo-images derived from the dipmeter curves (right-hand side of Figure 9.8), suggest the presence of a fault.

At about XX94 two conductive shaly beds make contact with a more resistive sandy bed and this results in the resistive and conductive anomaly profile described above. This result is even clearer on the 3D core-like image displayed in Figure 9.9.

Part of the series is duplicated by a reverse fault with a throw of about 9 m. The trace of the fault was computed by examining the interruption of the beds and found to dip 80° towards the south-east. Despite their small throw, these faults are of major importance as they compartmentalize the large structure of the reservoir and explain the different gas–water contacts in the three wells. The ability to recognize such faults is a major breakthrough in interpreting reservoir dynamics, and the DipFan capabilities played a key role in achieving this.

Conclusion

Thanks to the analysis described in this article, the poor performance of wells 2 and 3 compared with that of Well 1 could be explained, and a better reservoir characterization was achieved. These results will play a major role in optimizing the performance of future wells.

A 3D VSP case history from the Adriatic Sea

Borehole seismic acquisition and processing has become increasingly popular in recent years. It is similar to classical reflection seismics except that the receivers are located in the borehole instead of on the surface. Generally borehole seismic data have greater detail than surface seismic. That is why this technique has been upgraded to a 3D recording geometry using a multireceiver tool – ASI* Array Seismic Imager – to try to describe complex geological structures. This article shows how advances in borehole seismic may help in the description of previously overlooked features in the vicinity of the borehole

Nel corso degli ultimi anni, l'acquisizione di dati sismici di pozzo e la loro elaborazione hanno avuto sempre maggiore diffusione. Questo metodo è simile alla sismica a riflessione classica, con la differenza che le unità riceventi sono posizionate entro il foro anzichè in superficie. Poichè, in genere, i dati rilevati con questo metodo hanno un grado di dettaglio superiore rispetto a quelli ottenuti con la sismica di superficie, questa tecnica è stata ulteriormente sviluppata con una geometria di acquisizione tridimensionale, grazie all'uso di una unità ricevente multipla denominata ASI* (Array Seismic Imager), allo scopo di descrivere strutture geologiche complesse. Questo articolo spiega come i progressi compiuti nella sismica di pozzo forniscano un valido aiuto per meglio caratterizzare le formazioni che si trovano in prossimità del foro, cosa non possibile precedentemente

Agip
L Barzaghi
F Miranda

Schlumberger
R Continisio
F Ogliani

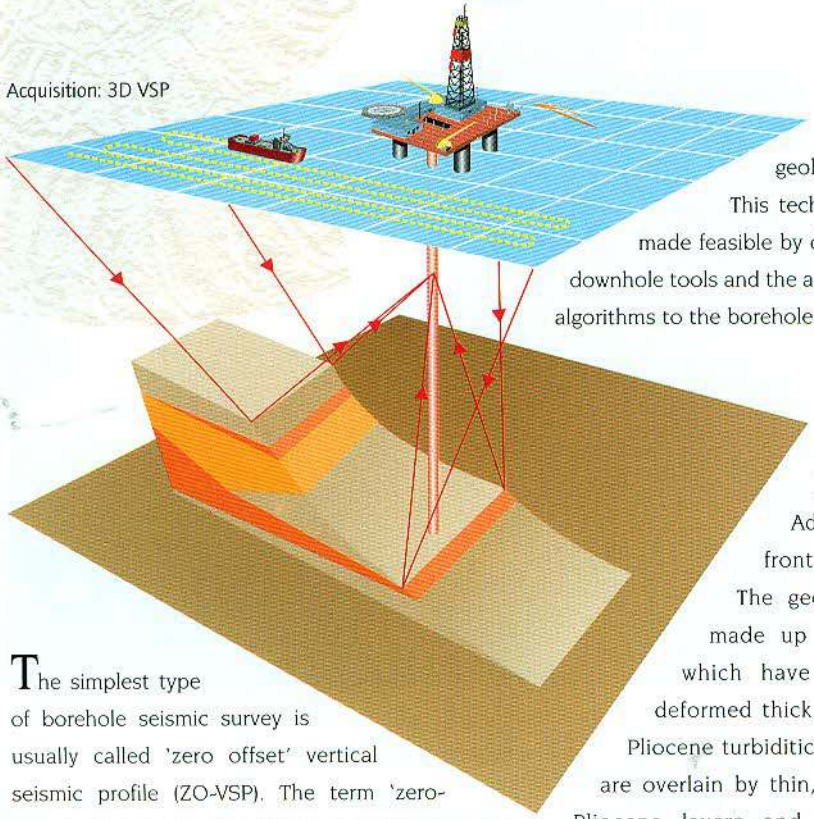

The simplest type of borehole seismic survey is usually called 'zero offset' vertical seismic profile (ZO-VSP). The term 'zero-offset' refers to the fact that the seismic source is located on the surface very close to the wellhead. Such a survey provides a one-dimensional seismic image around and below a vertical well.

When the source is positioned away from the wellhead, the 'illumination' of the subsurface becomes wider and reflectors can be interpreted several hundred meters away from the well axis. Surveys using this technique, called offset and walkaway VSPs, have become a standard practice in recent years. However, they have the same limitations as 2D surveys, such as nonuniform seismic ray paths and mispositioning of events.

Geoscientists have been keen to 'upgrade' the VSP family and describe 3D geometries in the subsurface, particularly when investigating elusive or complex traps occurring in mature exploration areas and where high resolution is needed.

In a 3D VSP survey, receivers are kept in a fixed position while the source is moved to thousands of location points at the surface (Figure 10.1). Such wide distribution of shotpoints enables a regular collection of seismic signals, even though their origin is unevenly scattered from complex geological surfaces.

This technique has recently been made feasible by development of multilevel downhole tools and the adaptation of 3D migration algorithms to the borehole geometry.

The reservoir

The study well is located offshore in the Adriatic Sea on the buried front of the Apennine chain. The geology of this region is made up of embricated thrusts which have produced a severely deformed thick series of Lower–Middle Pliocene turbiditic sediments. These rocks are overlain by thin, partially eroded Upper Pliocene layers and by thick undeformed Quaternary sediments.

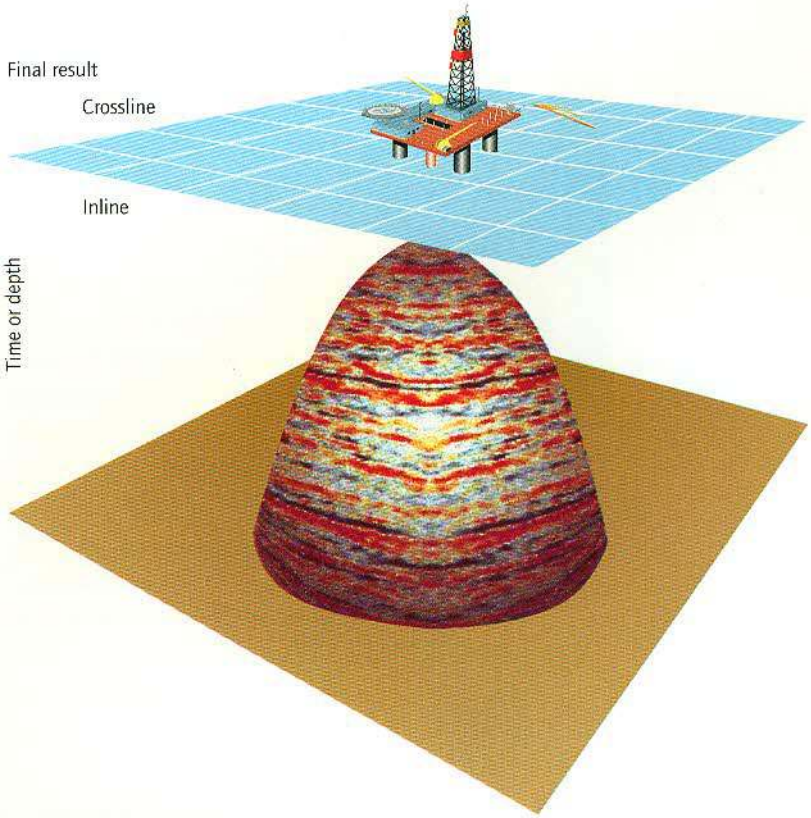

Figure 10.1 *Left. During a 3D VSP survey, a receiver string is located in the well while a ship-towed energy source is used for shooting on the surface. The receivers are kept fixed while the source moves along parallel walkaway lines*
Below. The recorded data must be processed and finally gathered in a 3D volume around the well with a typical cone geometry. The apex of the cone is located at the receiver position in the well. The optimum subsurface coverage is located at about twice this depth

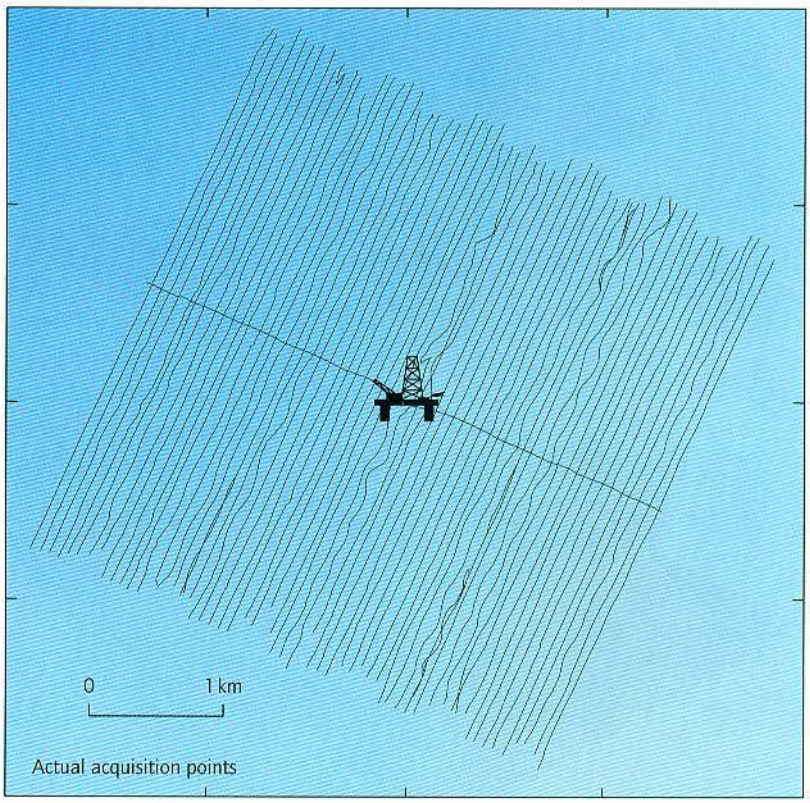

Figure 10.2 *Layout of shotpoint positions during the survey. Shotpoints are aligned in 58 inlines and 1 crossline. The well platform is located in the center of the survey*

The area has been subject to a large-scale 3D surface seismic survey and the well has been drilled to tap gas accumulations thought to be present in the sandy portion of the turbiditic layers.

Small-scale faults can play an important role in this reservoir as they may interrupt lateral sand beds and produce effective seals. The overall structure interpretation gets increasingly complicated at greater depth.

Job design and acquisition

Before acquisition commenced several tests of 3D ray-trace modeling were conducted to optimize the recording geometry. During each test a full survey was simulated with specific source and receiver locations.

These results were examined and compared, with the aim of defining the optimal subsurface coverage (with regard to uniformity and areal extent of the reflections). This helped to determine the minimum number of shotpoints for the survey, to optimize the total acquisition time.

Circular and spiral shootings were considered as they seemed to offer the shortest acquisition time. But eventually a squared geometry survey was preferred as it gave better subsurface coverage, minimized the risk of possible navigation errors, and made data processing easier. The final design of the survey comprised 58 parallel lines (inlines) and 1 crossline forming a 4 × 4 km square centered at the well (Figure 10.2). Each line consisted of about 160 shotpoints, recorded over a 4-km path.

The borehole receivers were housed in the ASI Array Seismic Imager tool – a five-level device with triaxial accelerometer sensors. The position of the ASI tool in the well was defined by presurvey modeling just above the Pliocene–Quaternary unconformity.

Data acquisition operations were performed smoothly over a 65-hour period. The recorded data were processed as individual walkaway lines, but future enhancement of the method will comprise a full 3D processing of the acquired data.

Data processing

Subsurface imaging was the main purpose of this technique, but it also provided a wealth of additional information.

The travel times from the surface source to the downhole receivers offered a means of estimating the seismic anisotropy of the reservoir sediments.

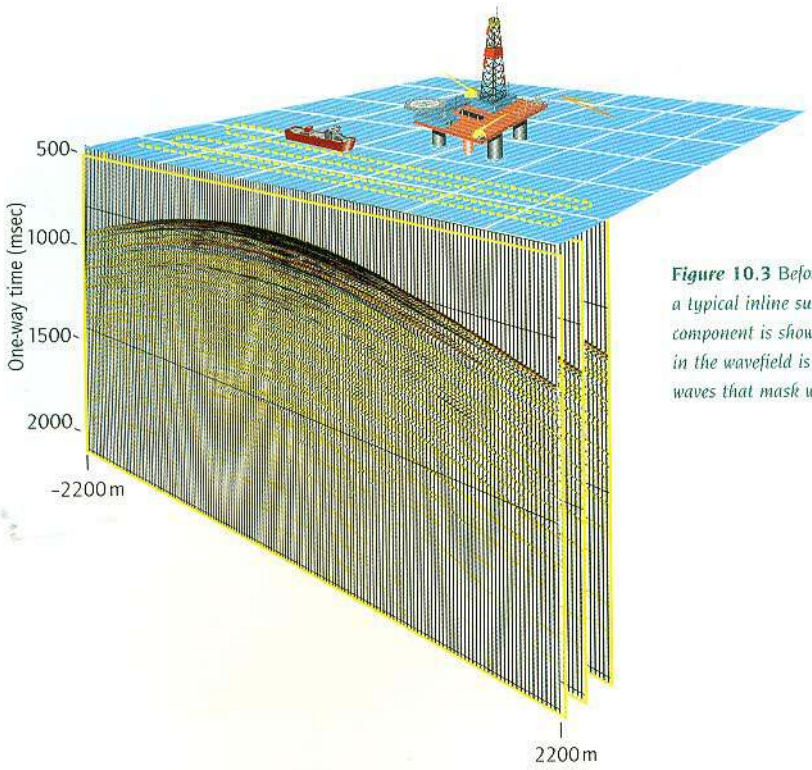

Figure 10.3 *Before data processing. Schematic of a typical inline survey. Only the vertical receiver component is shown. Most of the energy contained in the wavefield is associated with downgoing waves that mask weaker upgoing reflections*

The computed anisotropy values range from 14% in the W–E direction to 10% in the N–S direction.

The relative proportion of amplitudes recorded in the vertical and horizontal receiver components led to an understanding of the incidence angles and gave an insight into the propagation of both downgoing and upgoing waves.

The case study shows a very sharp reflector located immediately below the geophone position. The close proximity of the image and the receivers allows an 'in-situ' examination of amplitude behavior versus angle of incidence.

This additional information could be used immediately in two important data processing steps: wavefield separation and the 3D-migration.

Wavefield separation is necessary in all VSP data processing as the upgoing reflections are usually masked by more energetic downgoing waves (Figure 10.3).

Transit times and incidence angles are used to decompose the vertical and horizontal receiver components into four main wavefields: compressional downgoing, compressional upgoing, shear downgoing and shear upgoing. After subsequent deconvolution, only the compressional upgoing field is used for the final subsurface imaging.

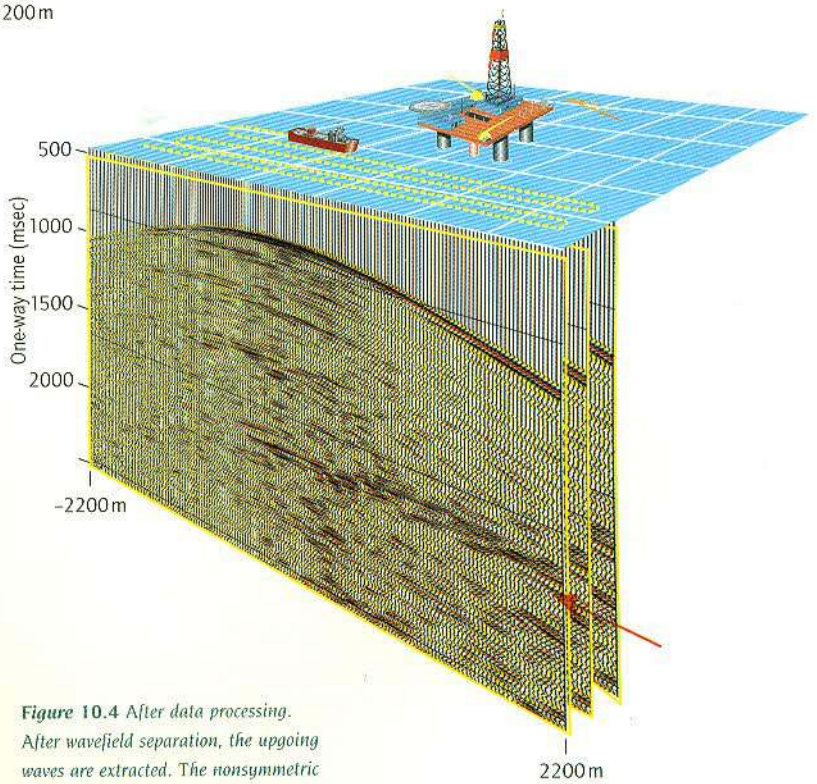

Figure 10.4 *After data processing. After wavefield separation, the upgoing waves are extracted. The nonsymmetric distribution of events confirms the complexity of the subsurface layers. The curved signal at 2000 msec on the right-hand side, indicated by the arrow, is most probably due to an isolated faulted block. The spatial position of these events is not yet defined at this stage of processing*

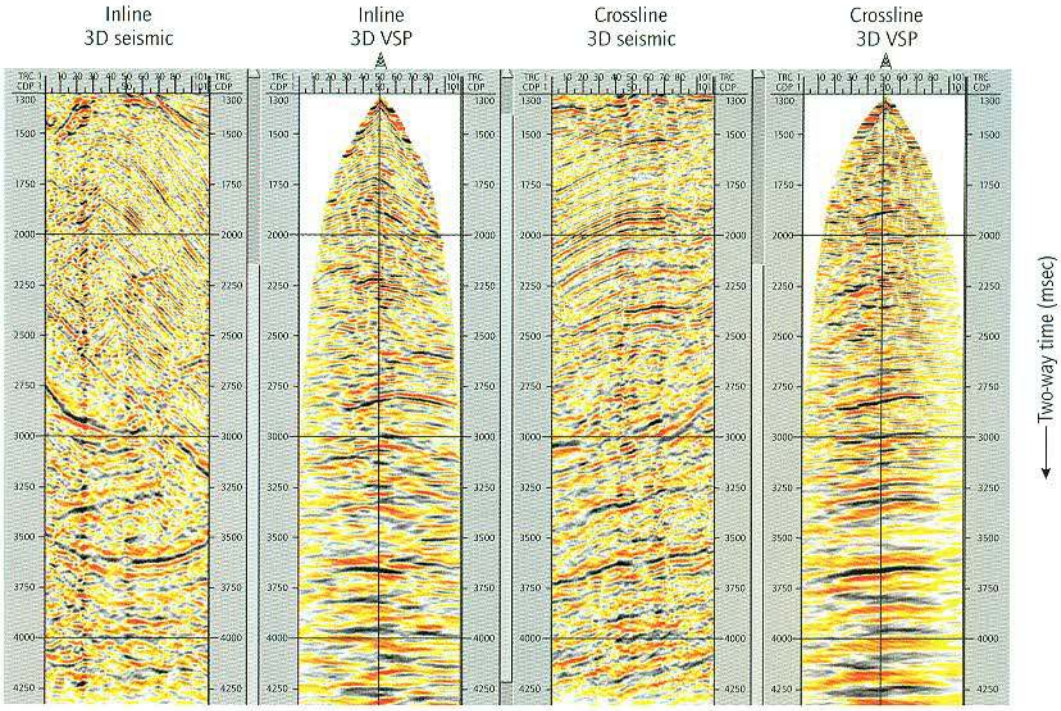

Figure 10.5 *Comparison of 3D surface seismic with 3D VSP. Each panel represents a horizontal distance of 2000 m, with the well axis located in the middle trace. The vertical distance is expressed in two-way seismic times and the well maximum depth is reached at 2200 msec*

The upgoing field of a typical line, shown in Figure 10.4, reveals a nonsymmetric distribution of events, testifying to the complex attitude of the subsurface layers.

Evidence of diffracting faulted blocks can also be found, but this information cannot be handled for the reservoir description during this processing stage.

Up to this point, only the coordinates of the source location point and the receiver location points are known, but not the position of the reflection points. Also the seismic time is related to an oblique and irregular travel path rather than a vertical path along the depth direction. Because of this, upgoing signals need to be moved (migrated) from the recording domain to a new coordinate system (x, y, z) linked to reflection points on the subsurface layers.

The adopted migration approach assumes that a specific reflected event is constantly present in all traces, and that only its amplitude varies as the source viewpoint changes from trace to trace.

The summation of all these contributions becomes a constructive process if significant reflectors are present.

The summation process is repeated at each point in the subsurface, to build up a 3D image of the rock volume around and below the well. The vertical scale is expressed in two-way seismic times, rather than depth. The process demands a considerable amount of computer processing power.

Interpreting the results

When a new migration computation is performed the results are normally compared with previous data.

Figure 10.5 shows the extracted central inline and crosslines from both the 3D surface seismics and the 3D VSP survey. The inline direction stretches from SSW to NNE and is expected to show the steepest dips of the geological structure. The crossline direction is normal to the inline survey and runs along the main strike of the structure.

Visual comparison of surface and borehole seismic data is surprising. Some similarities can be found in the shallower portion (2000 msec) and the deeper portion (3200 msec and more), but below the well maximum depth (2200 msec) the pictures show a different level of detail

The surface seismics show unrealistic crossing horizons, while a new horizon is apparent in the VSP results at 2800 msec – where the optimal VSP response is expected.

The polarity of the signal shows a decrease of the acoustic impedance with depth.

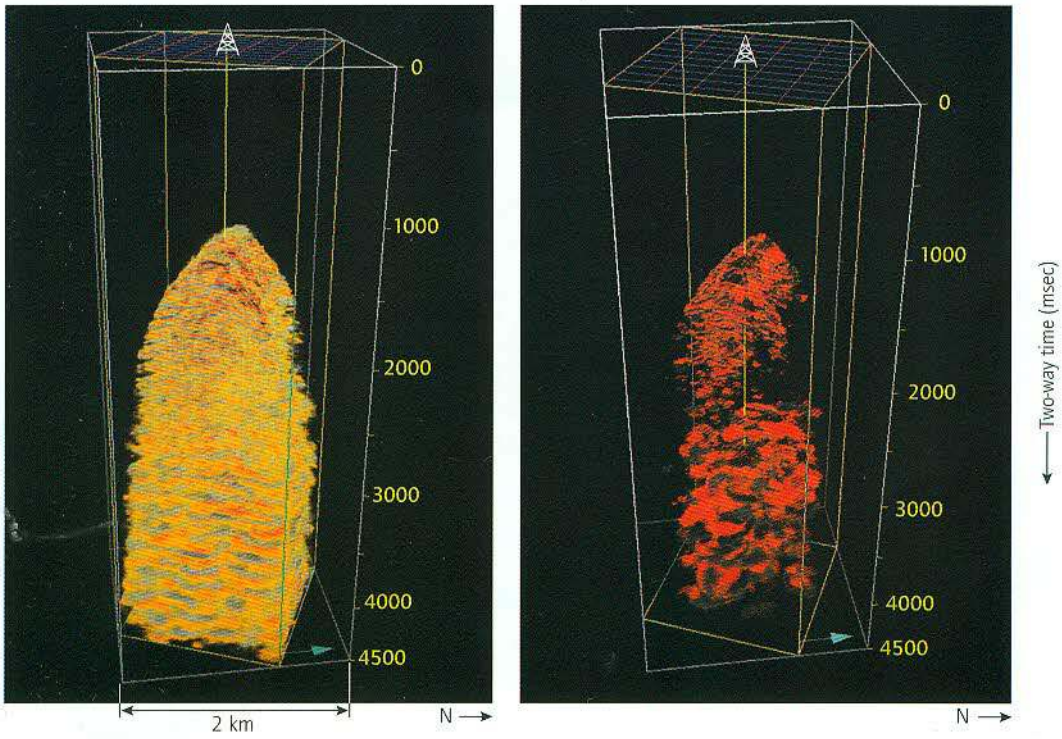

Figures **10.6** *3D view of final migrated results. Left. The full range of computed amplitudes is displayed and only the external surface of the volume is visible. Right. The volume is made transparent by muting low values. The transparent visualization shows an energetic region below 2800 msec overlain by a poor response zone. The horizontal sides are about 2 km long, and the vertical distance is expressed in vertical two-way seismic times*

A few vertical slices, however, are insufficient to evaluate the entire volume of results. A true 3D visualization highlights the major structural features.

The information for the workstation was created by storing the data results in a 3D coordinate framework created with IESX* interactive exploration software; each single amplitude value is stored as a 'voxel' (a pixel in 3D space). Only the external surface of the volume can be seen when the full range of voxel amplitudes is displayed (Figure 10.6, left).

When amplitudes close to null values are removed, during the processing, the data volume becomes transparent up to a desired degree, enabling the observer to search through it (Figure 10.6, right).

The latter type of visualization confirms that the region below 2200 msec (the well total depth) has a poor seismic response, while below 2800 msec the reflected energy becomes more relevant. In particular, the reddish peak located at 2800 msec can be traced in the vertical images extracted from the volume at any azimuthal orientation (top of Figure 10.7).

The horizon picking was started using manual picks made by the interpreter and then pursued in a semi-automatic mode using the software. The event can also be traced through horizontal slices created at constant seismic times.

The areal appearance of the reddish-black regions displays a roughly concentric zonation: when the slice is made at a greater time (ie, depth increases), the reddish-black rings expand over a wider area, revealing a convex structure.

The center of the structure is located off the well axis projection at a distance of about 500 m towards the north-east.

It is easy to pick the signal across most of the survey, except in the southern part. Here the horizon stops in a rather abrupt way – a feature also seen in nearby minor horizons. This suggests the occurrence of a fault bounding a block of sediments and continuing in the overlying low-energy zone (see Figure 10.7).

The next step is to map the interpreted horizon areally to see if the horizon corresponds to a gas-bearing layer, delimited by the natural dips of the anticline and bordered by a sealing fault.

The map view has planar geographical coordinates in x- and y-axes, similarly to previous time slices.

The mapped values, however, are not related to a constant time slice, but follow the topography of a complex buried surface (Figures 10.8 and 10.9).

The properties of interest are the time (=depth) elevation of the horizon (Figure 10.8) and seismic amplitude of the reflected signal (Figure 10.9).

Figure 10.7 *Interpreting the horizon at 2800 msec.*
Top. *The horizon is a positive-amplitude signal displayed in a reddish color. The interpreter follows this using a blue mark across the whole survey, ie, along SW–NE inlines (left) and along NW–SE crosslines (right). (Total depth of the well is at 2200 msec)*

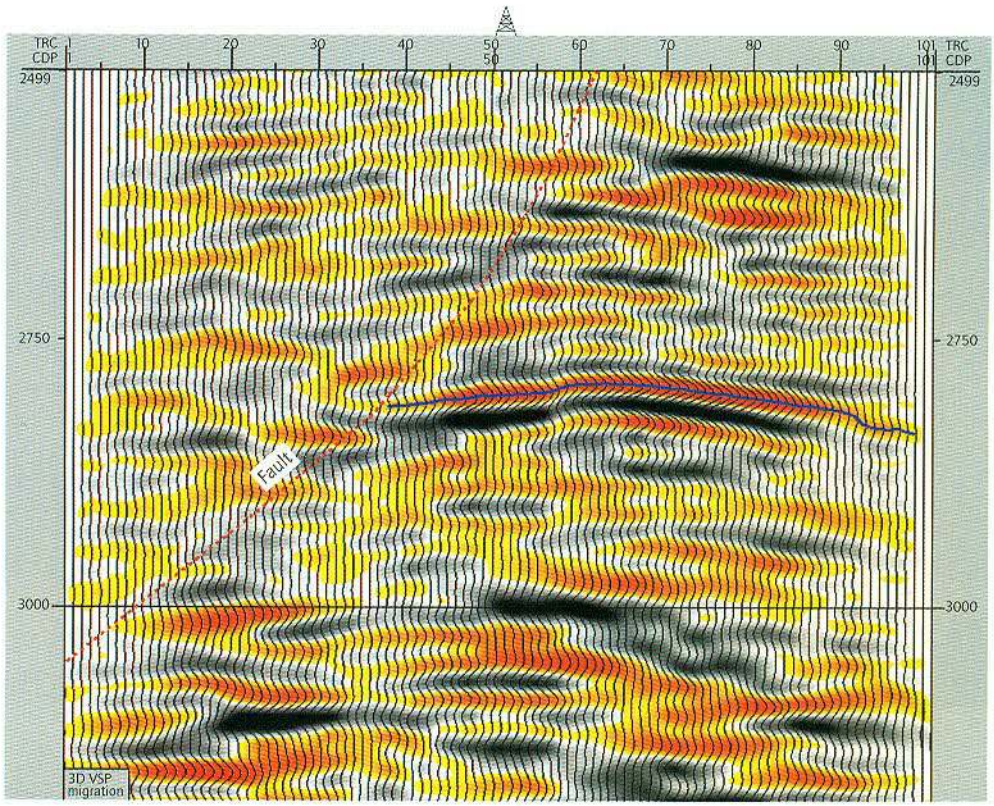

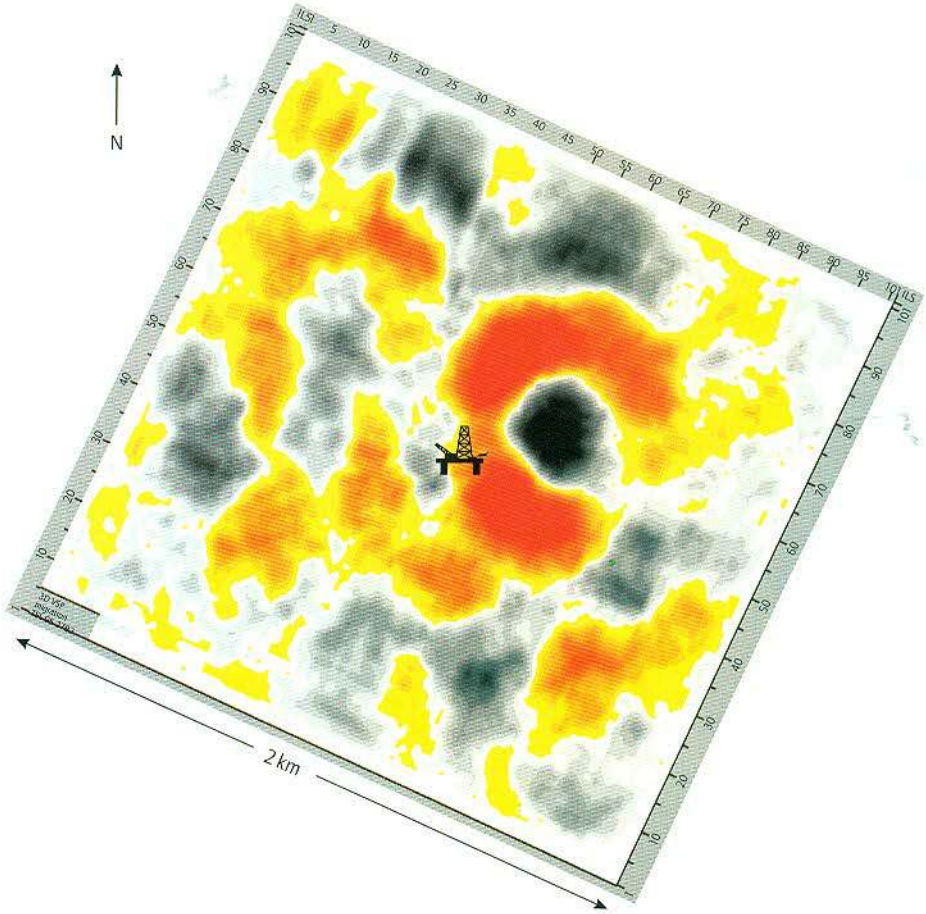

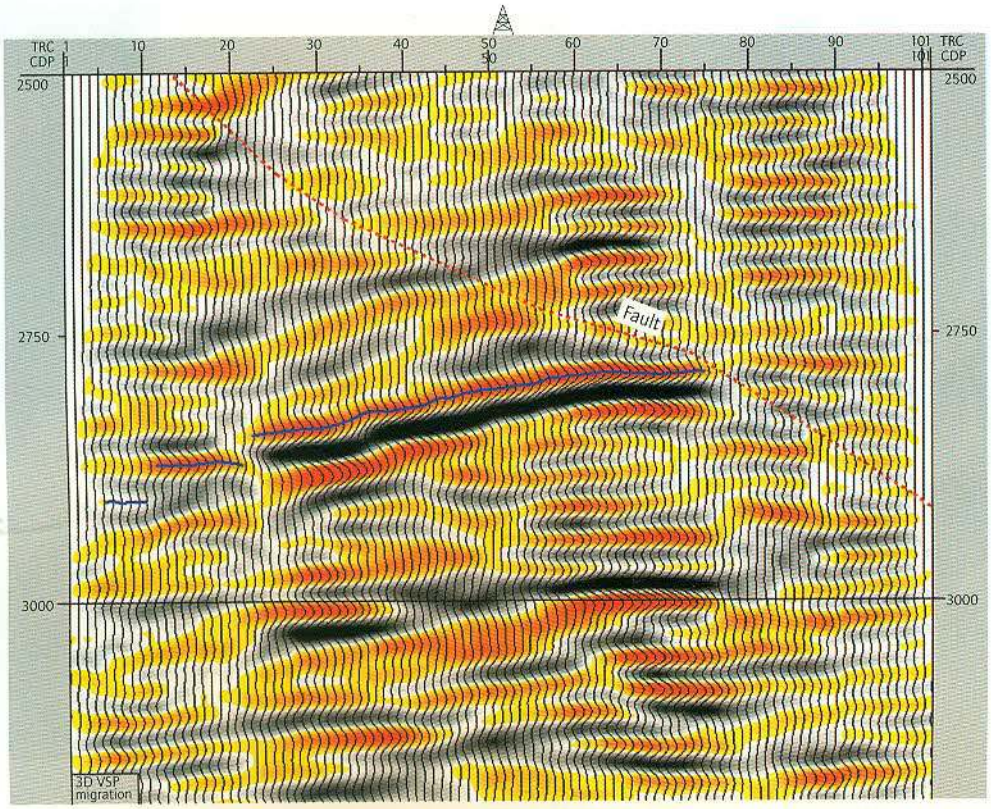

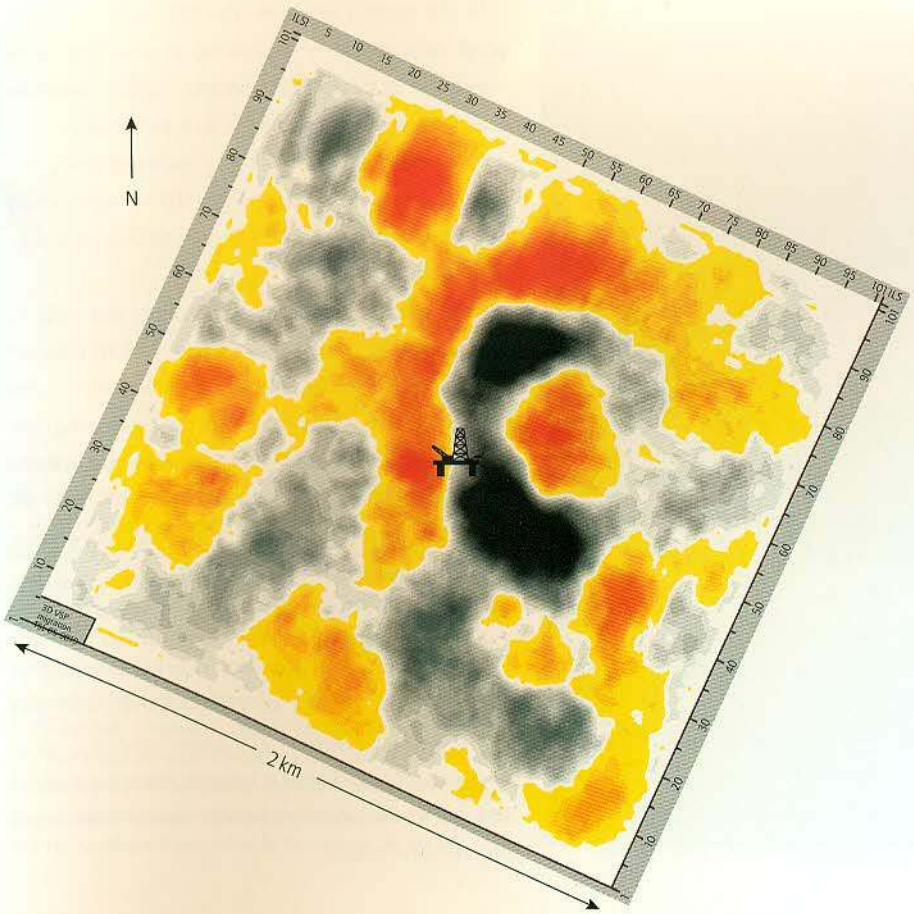

Bottom. *The areal distribution of the signal is also checked in volume slices at constant seismic times. In this areal view, the red signal and the underlying black one show a concentric distribution. The structure expands as the time (=depth) increases (slice at 2790 msec at left, slice at 2810 msec at right). This is indicative of convex folding. The center is located about 500 m from the well axis to the north-east. The horizontal continuity seems to be interrupted towards the south-east by a probable fault. The well bottom is above this depth, but the downward continuation of the well hits the center of the picture*

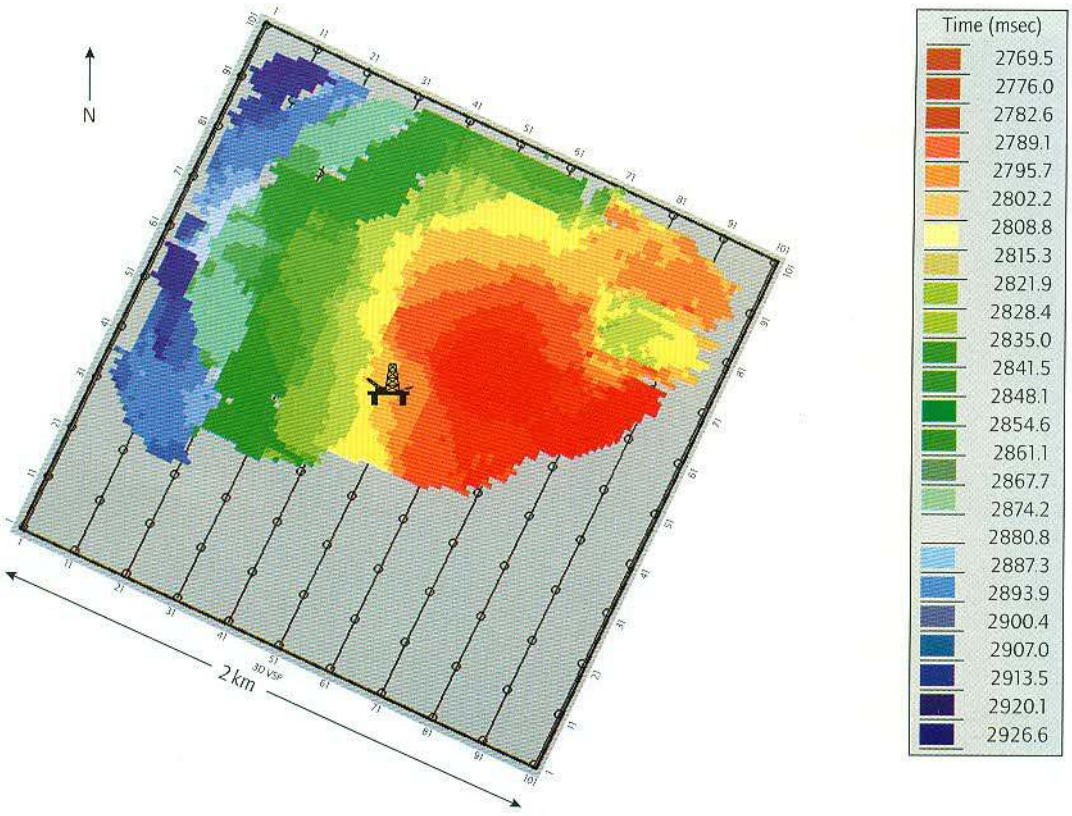

Figure 10.8 *The time map of the interpreted horizon shows its bathymetry expressed in a seismic time scale (msec). Low values (red) correspond to the culmination of the structure. The horizon gets deeper towards the west and north-west and terminates abruptly in the southern part of the survey*

Both maps converge to locate the end of the structure and reveal a positive amplitude anomaly in the same position indicated by time slices.

Figure 10.10 summarizes the 3D perspective view of the subsurface. The picture comprises both interpreted and objective features.

The fault surface is a feature drawn by the interpreter at the terminations of the reflectors, and is shown with a uniform color (blue).

A deeper horizon (4000 msec) has been tracked in negative seismic amplitudes with gray colors.

The upper horizon (2800 msec) has a convex shape that was first detected by the interpreter and then refined by the automatic volume picking software of the workstation. The color of the horizon is an objective property representing the amplitude across the surface, at the same black–yellow–red scale already used in other pictures.

The two horizons and the fault are intersected by the well axis.

The convergence of a horizon culmination with a positive-amplitude anomaly is made evident at 500 m from the well axis in the north-east direction (towards the observer in the perspective of Figure 10.10).

In the studied example, the 3D VSP has shown good capabilities in describing a new geological horizon in a structurally complex region somehow displaced and deeper than the well total depth.

The technique is in its infancy (summer 1997), but experience gained during the first 3D surveys in Italy will allow us to improve both acquisition and processing steps.

More efficient acquisition procedures will help to save rig time. At present the complexity of 3D data set handling means the technique cannot be used to give rapid answers to drilling issues. But the processing time is being reduced by ongoing software development and by increasing the computer power. Migration also will benefit by implementing quality control procedures, producing final results in a true depth scale.

Conclusions

The better resolution of 3D VSP compared with that of 3D surface seismic will allow reservoir geophysicists to make better volumetric interpretation of structures in the vicinity of a well cluster that would otherwise be missed

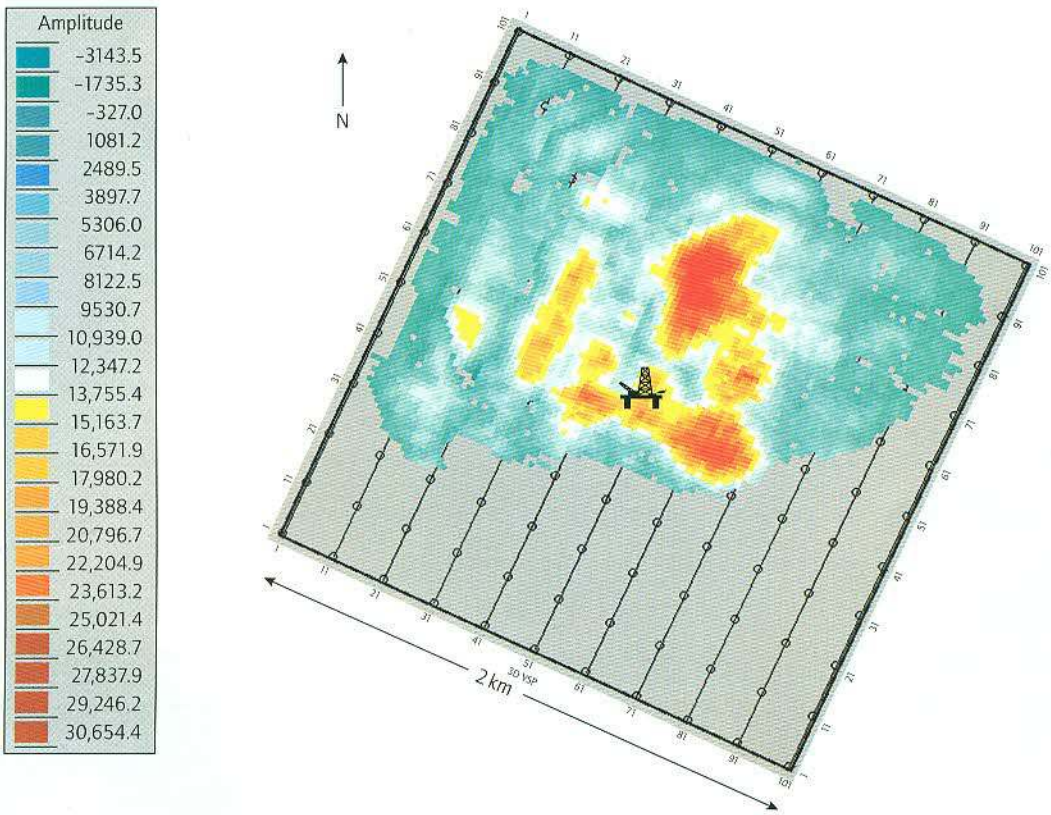

Figure 10.9 *Amplitude map of the interpreted horizon. Higher positive amplitudes are located roughly in line with the end of the horizon. A positive reflection amplitude is generated when a high-velocity layer overlies a low-velocity layer. This phenomenon is magnified when the bottom layer contains gas*

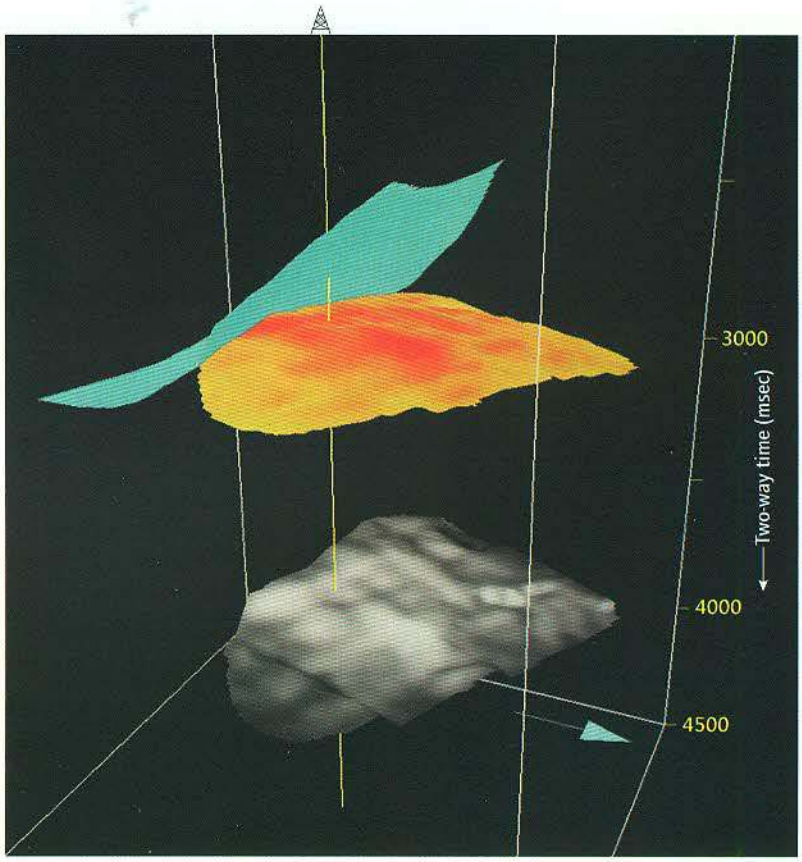

Figure 10.10 *Summarizing the results. Two interpreted results and a fault are shown in a 3D framework view. The vertical scale is in two-way seismic times expressed in msec. The arrow at the base points north. The central vertical line represents the downward continuation of the well axis. The fault is shown with a conventional color (homogeneous light blue), but the two horizons have colors indicative of their seismic amplitudes. The upper horizon (shown in Figures 10.7 and 10.9) has been tracked in yellow-to-red positive amplitudes. The strongest amplitudes occur at the horizon culmination, some 500 m away from the well axis in a north-east direction (towards the observer). The deeper horizon has a different behavior. It has been tracked in negative seismic amplitudes, with strongest values (dark gray) at the edges and the small-amplitude values in the center of the volume*

XI

Logging under tough conditions

Well logging is always a complex task, but when radioactive sources must be excluded for safety and environmental reasons, evaluation of formation characteristics such as lithology and porosity becomes even more difficult. This article tells how a new generation of nonradioactive tools, such as the APS (Accelerator Porosity Sonde), can now be used in tough logging conditions to determine these essential formation characteristics. The article also explains how an ingenious technique, LWF* logging while fishing, can enable logging to continue during retrieval of a stuck tool, resulting in major cost and time savings

Il logging è sempre un'operazione difficile; in più, quando ragioni ambientali e di sicurezza impongono di escludere le sorgenti radioattive, la valutazione delle caratteristiche di una formazione, come litologia e porosità, diventa ancora più complessa. Questo articolo descrive la possibilità di utilizzare una nuova generazione di strumenti non radioattivi, come l'APS (Accelerator Porosity Sonde), per determinare le caratteristiche essenziali di una formazione in condizioni estreme di logging. In seguito, l'articolo illustra una tecnica particolarmente ingegnosa, LWF* (logging while fishing) che consiste nella possibilità di continuare ad eseguire le misure durante il recupero di uno strumento bloccato in pozzo, con un notevole risparmio in termini di tempo e di costi

Agip
M Astorri
P A Casu
A Sartorio

Schlumberger
M Andreani
W Klopf
V Spinelli

If, for safety reasons, radioactive chemical sources need to be excluded from logging operations the conventional wisdom is to determine formation parameters using the sonic tool in stand-alone mode. This presumes that resistivity measurements in the same well are being used only to determine the mud invasion profile and hydrocarbon content of the reservoir. However, there can be a problem with this approach. The sonic measurement is lithology-dependent, especially in carbonate reservoirs containing dolomite and calcite.

The best way to overcome this is to use an epithermal neutron tool which generates neutrons using a minitron source. The APS (Accelerator Porosity Sonde), which is a key component in the IPL* Integrated Porosity Lithology tool, combines the best of both epithermal and thermal neutron techniques by using an electronic neutron source (Figure 11.1). The APS sonde contains near and far epithermal detectors and one thermal detector. Below the near epithermal detector is the array epithermal detector.

The main function of the APS sonde is to measure the formation hydrogen content with minimal influence from formation atom density which can increase neutron scattering. In conventional thermal neutron porosity tools, formation atomic density, which relates to the formation matrix density, increases scattering, resulting in fewer neutrons reaching the detector and so elevating the measured porosity readings. In clays, the presence of thermal neutron absorbers also increases the apparent porosity reading of conventional tools. The combined boost in porosity readings is called the shale effect. On the other hand, reduced or even negative porosity readings can be caused by a phenomenon known as the gas and excavation effect.

The APS eliminates these problems as it has an accelerator that emits high-yield neutrons with more energy than those emitted by a conventional logging source. This increased neutron population makes

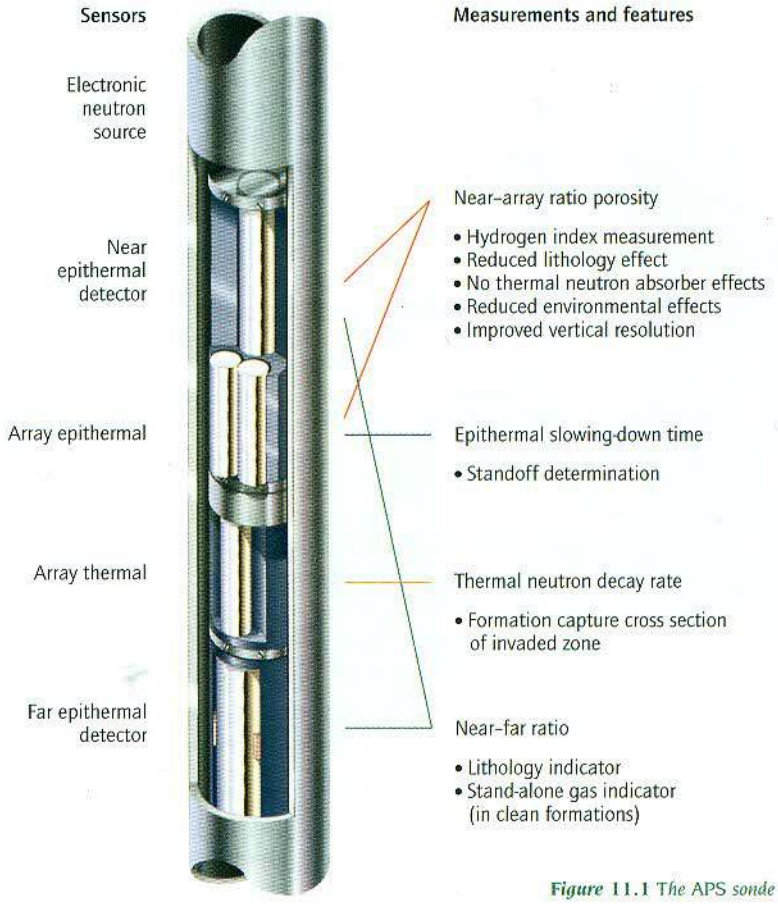

Figure 11.1 *The APS sonde*

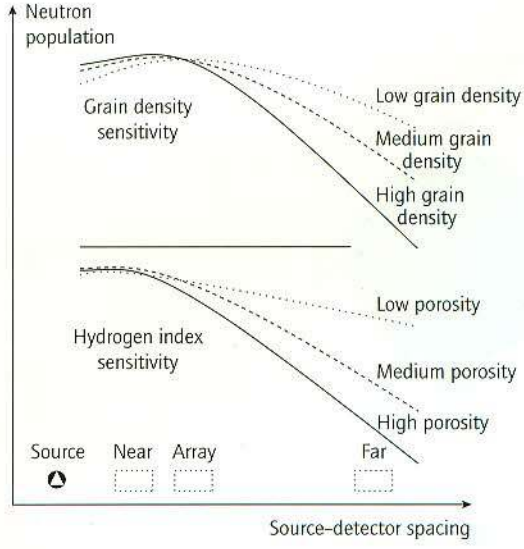

Figure 11.2 *This drawing shows how the position of the array detectors in the APS sonde has been designed to minimize the effect of lithology. The use of a minitron source makes the measurement of porosity by the array detectors possible, with a minimum of statistics. Two porosities are provided by the near array and near–far ratio with some different tool responses*

epithermal neutron detection possible without compromising counting statistics.

Figure 11.2 shows the response of the APS sonde to changes in grain density (lithology) and hydrogen index. The epithermal near-to-array measurement has a vertical resolution of 30 cm and provides an almost lithology-independent porosity log. The near-to-far ratio measurement is similar to that from a compensation thermal neutron type log but has the advantage of being taken using epithermal neutron readings and is therefore less affected by factors such as fluid salinity, temperature, pressure and borehole size.

The additional thermal neutron detector measurement provides a capture cross section Σ value which may be useful for future time-lapse comparisons or in the determination of the formation cementation factor, m.

Pipe-conveyed logging in highly deviated wells

Pipe-conveyed logging in highly deviated wells demands special operational procedures when laterolog tools are being used. A special correction is needed to correct the deep laterolog reading because the 80 ft long bridle has to be replaced by a stiff isolating string. This is because the drillpipe behaves like casing and the apparent tool reading is increased. The applied correction depends on the R_t values and is nonlinear. In addition a real-time borehole correction is needed to cope with the severe eccentralization of the tool (Figure 11.3). This becomes of greater importance when R_t values increase due to the presence of hydrocarbons in the formation.

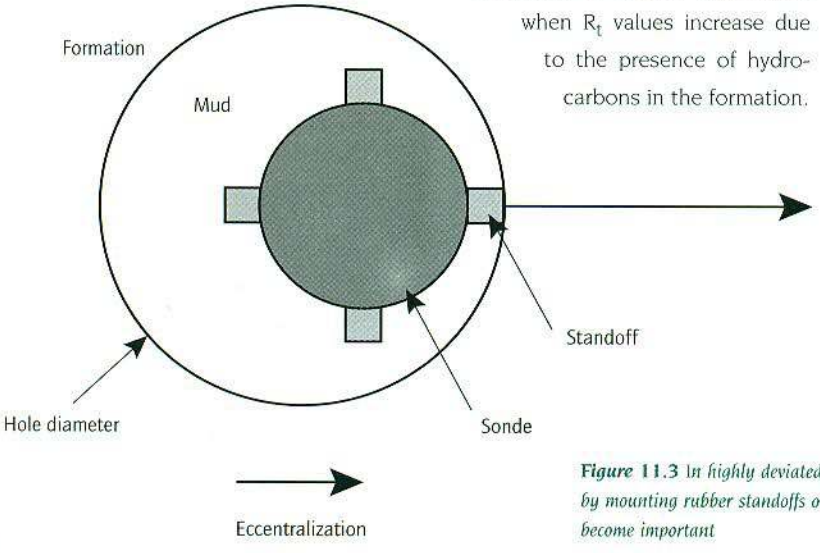

Figure 11.3 In highly deviated wells the HALS sonde is eccentralized with some standoff by mounting rubber standoffs on the tool. When R_t increases, the borehole corrections become important

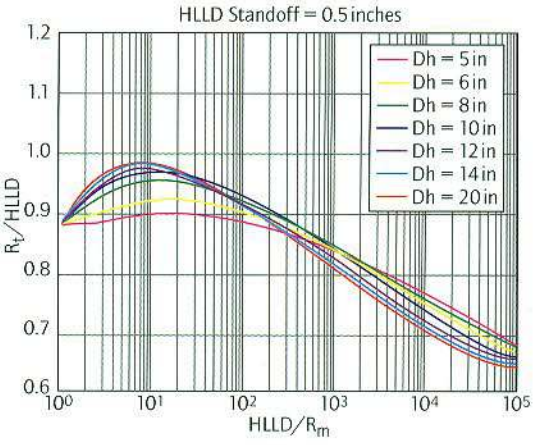

Figure 11.4a This correction chart shows that the deep laterolog on the HALS tool is very robust even in very large hole sections

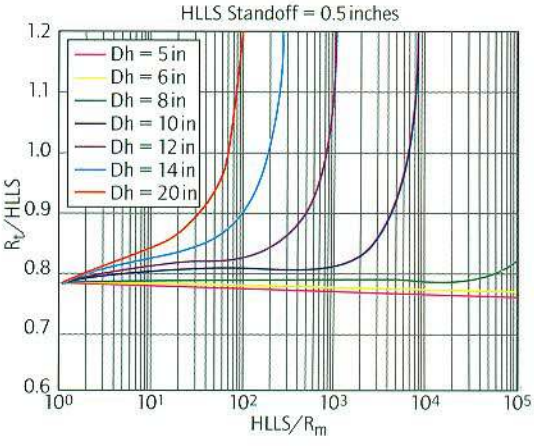

Figure 11.4b For the shallow laterolog the borehole corrections can control the signal in case of high-resistivity values if the hole is not larger than 8 inches

Figure 11.4 shows the borehole correction chart for deep and shallow laterolog readings recorded with the HALS (High-Resolution Azimuthal Laterolog Sonde) part of the PLATFORM EXPRESS* tool. The borehole corrections are applied in real time and are essential to the determination of accurate R_t values and the invasion profile.

Finally, a speed correction is needed to control the logging effects created by irregular logging speeds when tools are conveyed on pipe. The HALS tool enables R_t measurements to be aligned with other readings such as the R_{xo} and neutron porosity

measurements. This is done by selecting the azimuth reading corresponding to those from the neutron and R_{xo} measurements.

PLATFORM EXPRESS and pipe-conveyed logging

The PLATFORM EXPRESS tool string is ideal for pipe-conveyed logging in deviated holes. The tool is short, has a robust laterolog and all speed and environmental corrections are performed during acquisition. There is no doubt that the PLATFORM EXPRESS tool gives the most reliable laterolog and microresistivity readings under tough logging conditions and also provides a qualitative indicator of permeability (microlog).

Conveying the message

Figure 11.5 shows an interpreted log section taken from measurements of an ARI–MicroSFL*–APS–GPIT* inclinometry tool–GR tool string in a carbonate formation. The tools are conveyed into the horizontal well by pipe and the logging equipment is kept facing downwards by the GPIT tool.

The calcite rock is made up of 10% dolomite and has an average porosity of 10% with the presence of oil. The R_t measurement has been corrected for borehole and speed effects. In this case the sonic tool cannot be used in stand-alone mode because the presence of

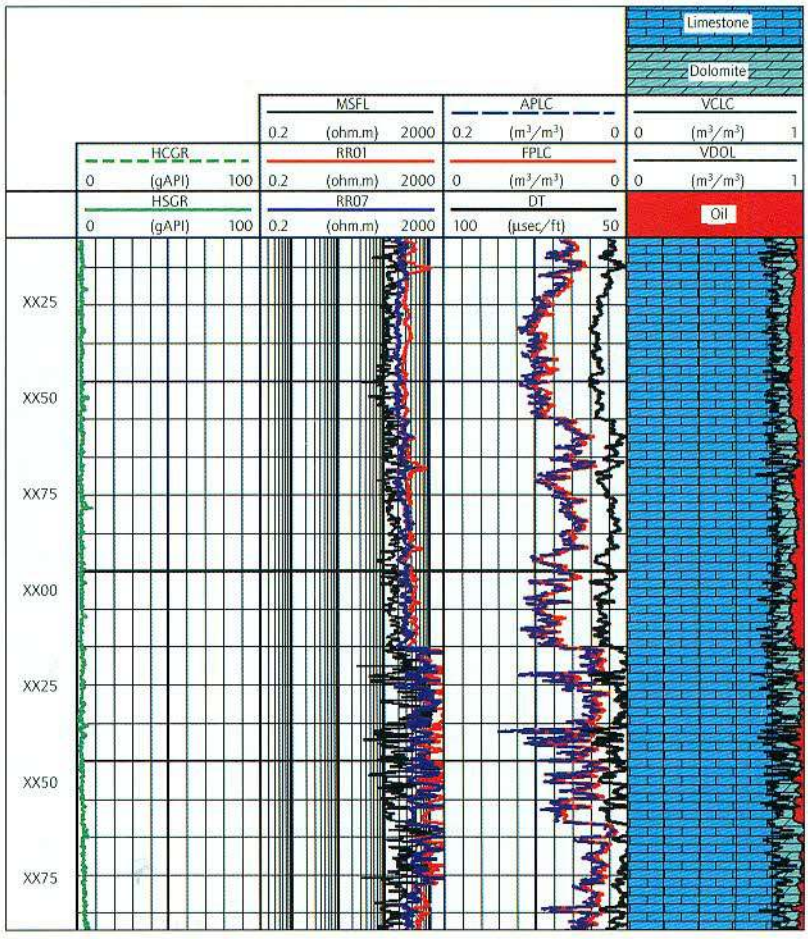

Figure 11.5 *Accurate interpretation of a calcite–dolomite reservoir from a sourceless string (ARI–APS–sonic) is possible. The top zone shows a resistivity anisotropy (difference RR01 and RR07) or borehole effect*

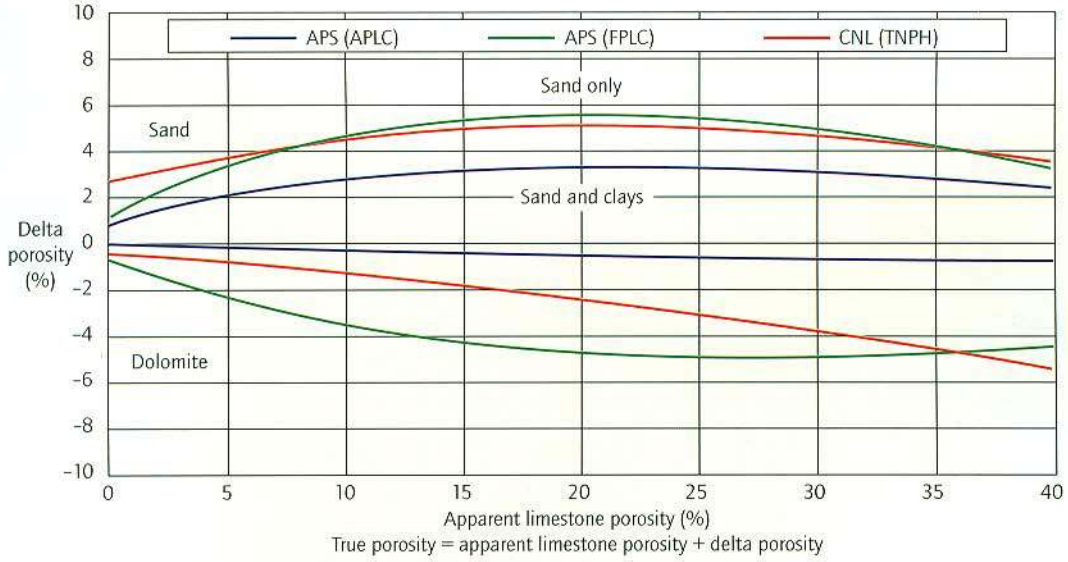

Figure 11.6 *The effect of dolomite is negligible on the APLC porosity curve. The difference between FPLC and APLC can be used to identify the presence of dolomite in this carbonate reservoir*

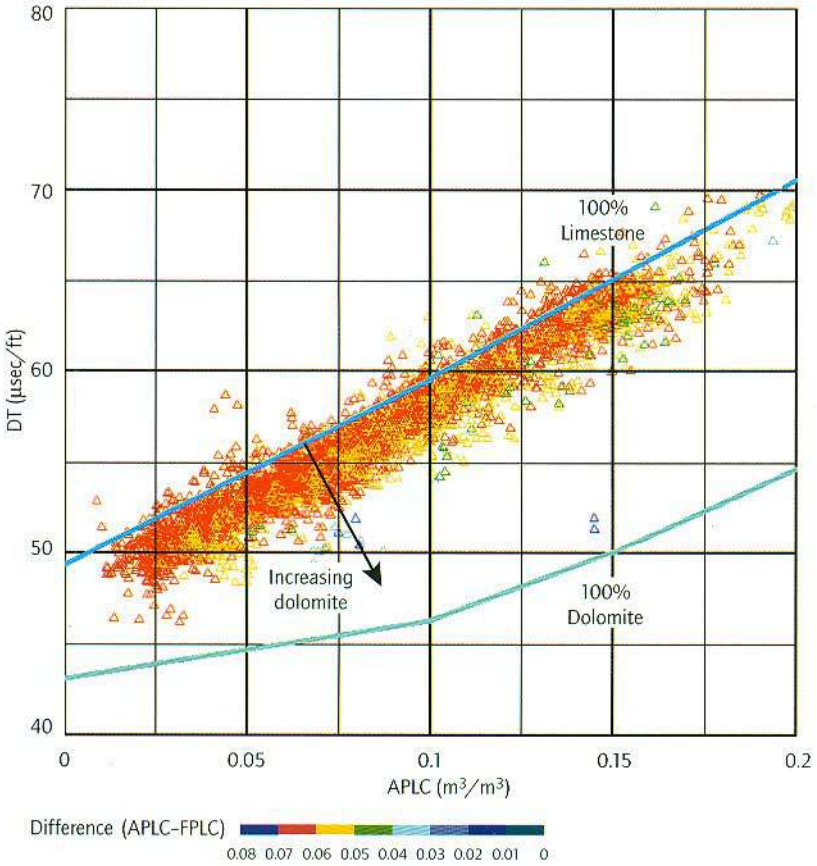

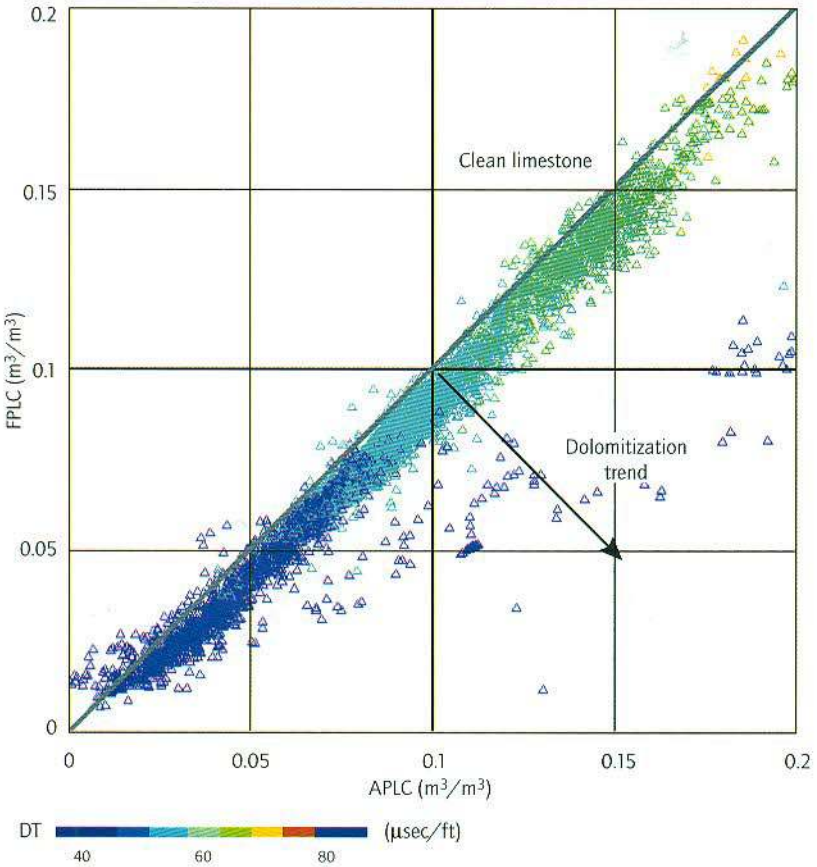

dolomite would introduce errors in the porosity determination. This is because the sonic transit time for dolomite is 43 µsec/ft compared to 49 µsec/ft for calcite. However, the APS results offer a way of determining an accurate porosity log which is not influenced by the presence of dolomite (Figure 11.6).

It has been possible to evaluate the percentage of dolomite using the APS in stand-alone mode. The percentage of dolomite has been scaled between the blue and green curves.

The crossplot in Figure 11.7 confirms the dolomite trend, and the crossplot of sonic versus APLC readings shows the effect of the dolomite on the sonic log.

The invasion profile is confirmed by the separation of the R_{xo}–R_t curves in the reservoir section and this could provide a permeability indicator. By aligning the resistivity deep laterolog and the APS and R_{xo} measurements downwards it has been possible to determine a true value of hydrocarbon content and eliminate any error on R_t due to anisotropy or borehole effects in the top side of the hole. Figure 11.5 also shows much lower values of RR07 in the pay zone and this would lead to a conventional laterolog giving a pessimistic hydrocarbon volume. The results also indicate that, in the presence of significant moldic and vuggy porosity, the capture cross section (Σ) from the APS sonde can be used in conjunction with R_{xo} to control the cementation factor, m. As yet, this evaluation has not been conducted as there are too few vugs and too low a porosity in this reservoir to validate the method.

If safety is the predominant consideration, this logging program can provide reliable results for the optimum choice of test intervals.

***Figure 11.7** The sonic–neutron crossplot (above) shows a trend to the dolomite line, which is confirmed by the APLC–FPLC difference (below)*

LWF logging while fishing, an alternative to cut and thread

New technology has been introduced to allow the completion of a wireline logging program after a tool string has become lodged in a wellbore. The costs associated with retrieving a stuck tool from a well are substantial. They are a result of the nonproductive time during a fishing trip, an associated wiper trip, and relogging the well. It is now possible to continue a logging program while retrieving the tool string from the well. The technique is already being used in Italy.

LWF logging while fishing is a hybrid of existing technologies, comprising cut-and-thread fishing (Figure 11.8), TLC* Tough Logging Conditions, and bridled tool techniques. There are several techniques of fishing a wireline tool string; however, cut-and-thread fishing is currently preferred as it allows retrieval of both keyseated and deferentially stuck tool strings. If the tool string is short or the hole extremely washed out, the cable is used to guide the overshot over the tool string. This fishing technique follows the cable to the tool and recovery is practically guaranteed, provided the correct procedures are followed.

In the case of stationary logs, formation testing and seismic, the possibility of sticking drillpipe must be taken into account. The operator should give similar consideration before electing to run any stationary log on drillpipe (TLC system). Once the LWF alternative is selected the engineer must know the casing depth and the interval remaining to be logged. This is important, as the wireline above the cable side-entry sub should never enter the openhole. If there is more openhole than casing it will be necessary to determine the zone of greatest interest and place the cable side-entry sub accordingly.

It is also necessary to know the wiring responses of various tools. When reconnecting the electrical lines a danger exists of crossing lines which could ultimately damage the downhole tools. Electric line verification for tool responses from the wireline logging unit is required.

The problem

On an Agip well, two logging descents had been completed before an RFT* Repeat Formation Tester job was run (Figure 11.9). During the RFT job the cable became stuck, and rather than performing the conventional cut-and-thread fishing operation to retrieve the tool, an LWF operation was performed. The well was 2973 m deep, $8^{1}/_{2}$-inch bit size, and the RFT was at about 2400 m in oil-base mud when the cable became stuck. The LWF technique allowed the operator to make a better informed decision whether to continue data acquisition or stop after fishing.

The solution

A safety and information meeting was held before the start of the LWF operation to explain the methodology and to decide at what depth the cable side-entry sub assembly should be placed. Placement of the sub had to be determined using the same methods as the TLC technique, but this was not needed until much later in the operation. Cut-and-thread fishing could begin while waiting for the assembly to arrive at the rig.

Standard fishing methods were followed until the side-entry sub arrived at the placement depth. The overshot was prepared and the tool power was switched off. A T-bar was used on the line, and the cable was cut. The upper sheave wheel was then lowered to the rig floor and replaced by a spade with an approved sling. The upper sheave was then rehung in the derrick, away from tripping drillpipe. A cable spear on the downhole side of the cable and a cable overshot on the uphole side were used. The fishing process continued until the desired depth was reached. As drillpipe approached the fish, tension was monitored and the tool brought into the overshot with 1000–2000 lb additional tension.

Upon reaching the predetermined depth the cable side-entry sub (CSES: see Figure 11.10) was connected into the drillstring with the T-bar on top of it. Rope sockets were built on both ends of the cable

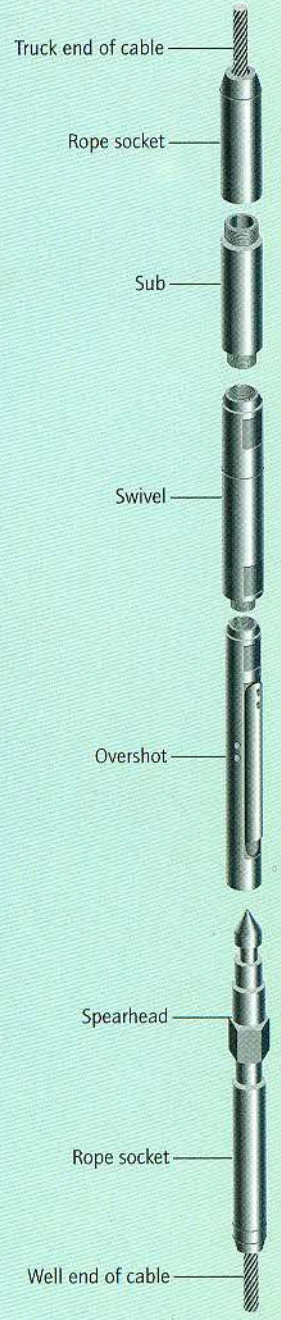

***Figure 11.8** Overshot and spearhead used for cut-and-thread fishing*

Figure **11.9** *This well sketch shows when the cable side-entry sub must be installed (in casing). The electrical connection is reinstalled to be able to log before pulling the tool out with the pipe*

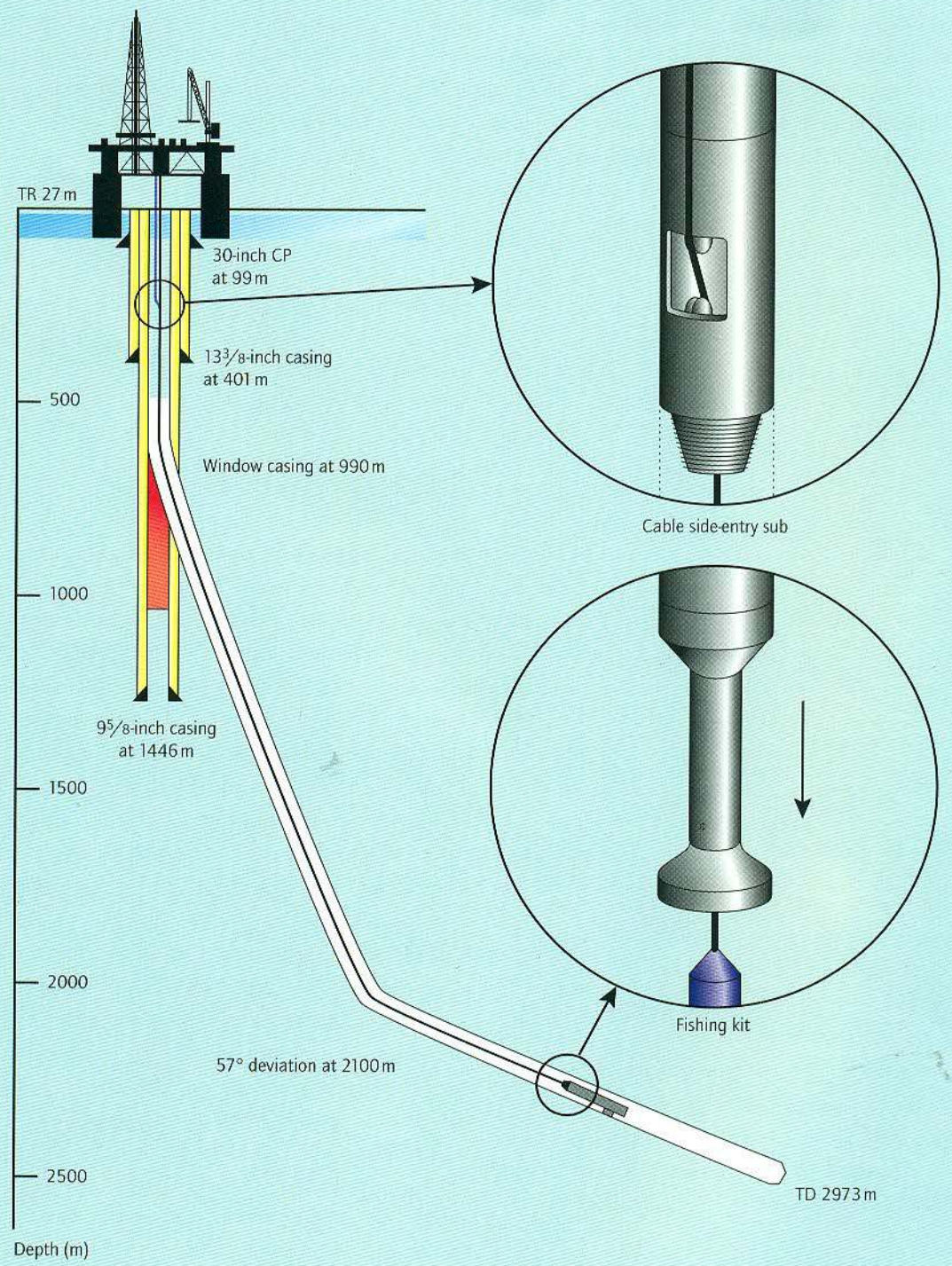

(one side male, the other female). Cable lines were clearly identified using conventional methods on the uphole side of the cable and tool response for the downhole side. The cable was reconnected and the rope sockets were placed in a double-ended torpedo. Tool power was applied. The cable was worked up and down ensuring that the double-ended torpedo held; the T-bar was then removed. On this well the cable was clamped on the CSES allowing downward logging without encountering any problems. However, this is not the case if logging up is necessary.

With the wireline on the outside of the drillpipe it is now possible to trip only drillpipe, speeding up the operation. On this well the torpedo entered the well during the downward logging. RFT acquisition was continued by spooling cable into the well as the driller lowered the tool to the depth of interest. Once acquisition was complete the drillpipe was pulled to surface; when the CSES reached the drillfloor it was removed and a T-bar was connected to the cable and the weak point in the head was broken with the blocks. The cable was then spooled onto the drum of the wireline unit. The driller then returned the RFT tool to surface.

The LWF technique offers several benefits over standard fishing operations. By reconnecting the electrical lines head tension can be monitored for drillpipe engagement on the wireline tool. Tool movement is also guaranteed over the logging interval. Drillpipe trip time is decreased after the side-entry assembly is placed, as the rig crew no longer threads cable through each stand of drillpipe. Tripping drillpipe is more than twice as fast as threading drillpipe. Safety also improves after the side-entry assembly is installed. The derrickman, Schlumberger operator and rig crew are no longer in danger of being struck by the cable overshot. The number of wiper trips is reduced due to the fact that a logging run is completed. And finally, the customer need not rely on a downlog or log with several overpulls for data.

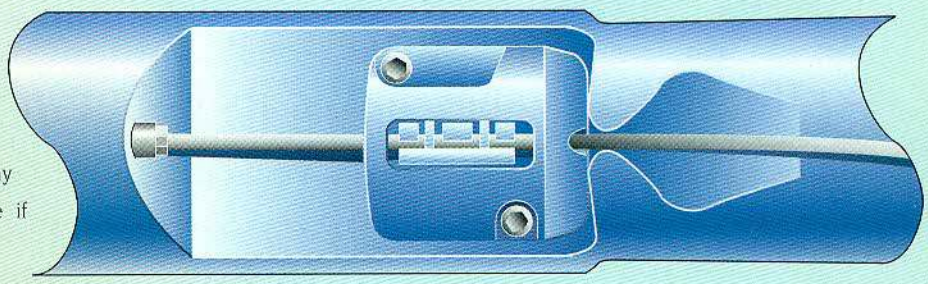

Figure 11.10 *Extended view of the cable side-entry sub with quick-release cable clamps*

Over a five year period Agip in the north of Italy has encountered 20 fishing operations due to stuck wireline tools or cables. Eleven of these were due to formation testing or stationary tools. An additional wiper trip and logging descent equates to approximately 24 hours of rig time on a 3500-m well, at an average of $50,000 per day for rig time; the annual savings to an operator can be substantial.

XII

IRIS* dual valve makes its debut in the Daria Field

During the 1995 development and completion phase of Daria Field a total of 14 gas wells had to be completed and tested in multilayered reservoirs. Underbalanced perforating using tubing-conveyed perforating (TCP) offered the best way of maximizing well performance and cleanup. However, for safety reasons, drillpipe could not be used. New technology came to the rescue: the operator introduced the newly developed IRIS* Intelligent Remote Implementation System dual valve which simplified the bottomhole assembly and increased testing efficiency by enabling 42 drillstem test (DST)–TCP jobs to be completed within 10 months

Durante la fase di sviluppo e completamento del campo di Daria, che ha avuto luogo nel 1995, si sono dovuti completare e provare 14 pozzi a gas in giacimenti multistrato. Gli intervalli sono stati aperti con spari "underbalanced" mediante un sistema "tubing-conveyed" (TCP), che rappresenta il metodo migliore per ottimizzare la produzione e lo spurgo del pozzo. Ragioni di sicurezza hanno tuttavia impedito di utilizzare le aste di perforazione, ma fortunatamente l'applicazione di una nuova tecnologia ha fornito un valido aiuto: l'operatore ha introdotto l'IRIS*(Intelligent Remote Implementation System), un sistema a doppia valvola, di recente sviluppo. Questo ha semplificato l'attrezzatura di fondo pozzo ed aumentato l'efficienza delle prove di produzione, consentendo la prova e il completamento di 42 livelli in soli 10 mesi

Agip
M Marilungo

Schlumberger
G Ciammetti

Time was of the essence during the completion and testing phase of the Daria Field wells. The operator was not only keen to ensure that the perforating phase proceeded swiftly but also wanted to conduct pressure testing to gain estimates of rock permeability and formation damage. Such a demanding schedule necessitated the use of a downhole shut-in tester valve that would minimize wellbore storage effects and so allow reservoir engineers to obtain the best results from the short pressure buildup period.

A high job efficiency was achieved by optimizing the time of flow and the shut-in period for pressure data acquisition and well cleanup, and also by simplifying the bottomhole assembly by introducing the IRIS dual valve (Figure 12.1). This eliminated the need for the older generation of circulating and test-

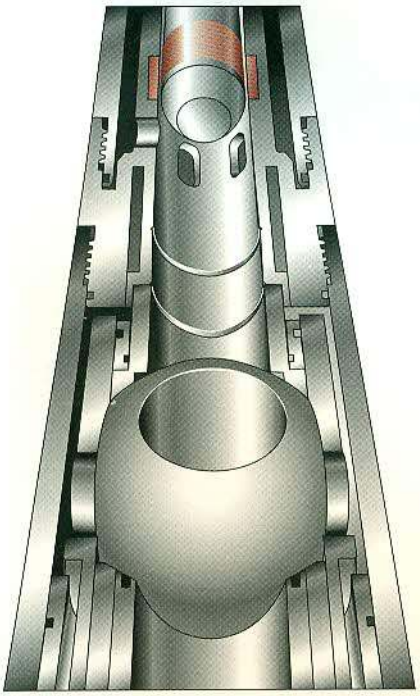

Figure 12.1 *Agip Ravenna played a major role in introducing the IRIS valve into Italy. The equipment first arrived for field test in 1993 – a program which helped to identify and resolve a few problems with the valve. Oil leaks in the hydraulic system and unexpected bursting of the rupture disk were discovered along with a minor fault in the communication software. The tool was returned to the Schlumberger engineering center where it underwent a redesign before being sent to Daria Field where it proved to be very reliable*

	Outside diameter (inches)	Inside diameter (inches)	Length (m)
Flow head 10,000 psi		3	
Tubing			
Crossover			
Drill collar	5		
Drill collar	5		
Drill collar	5		
Radioactive sub			
	5	2¼	1.07
Drill collar			
IRIS (tester valve, circulating valve and port)	5	2¼	6.22
Record carrier (2 gauges)			
Jar	5	3	1.98
Safety joint			
Positrieve packer – 9⅝-inch	8⅓	3	2.58
Tubing			
Shock absorber			
Shock absorber			
Slotted pipe			
Tubing			
Firing head			
Circulating sub			
Safety spacer			
Guns			

Figure 12.2 *Typical bottomhole string for the* DST–TCP *operation*

ing valves and enabled the operator to carry out more than one DST–TCP job every week.

An eye on the testing

Most of the cased hole wells in the Daria Field were tested with the same DST–TCP setup. Figure 12.2 shows the typical bottom testing string. A few wells required openhole gravel pack.

Each job involved underbalanced TCP perforation followed by two 6-hour flow periods and short buildups of 2–4 hours. The killing operations were conducted during buildup to improve the operational efficiency and shorten the testing time. To do this the IRIS circulating valve was opened, allowing the killing brine to be circulated back into the testing string (reverse circulation). This meant that the testing string was already filled with brine by the end of the buildup. The IRIS tester valve was then opened. Any fluid losses observed at this point were quickly stopped by pumping blocking agents into the well. In these cases of fluid losses, the operations were allowed to continue by closing the testing valve, opening the circulation valve and then pumping down the blocking agent. When the well reached stability, the testing string was removed from the hole, ready for use on the next well.

The IRIS valve proved to be remarkably reliable and maintenance free: nine consecutive jobs were run in the hole before any maintenance.

Data acquisition and interpretation

The reservoir engineers at Daria Field were concerned that they would be unable to determine reliable per-

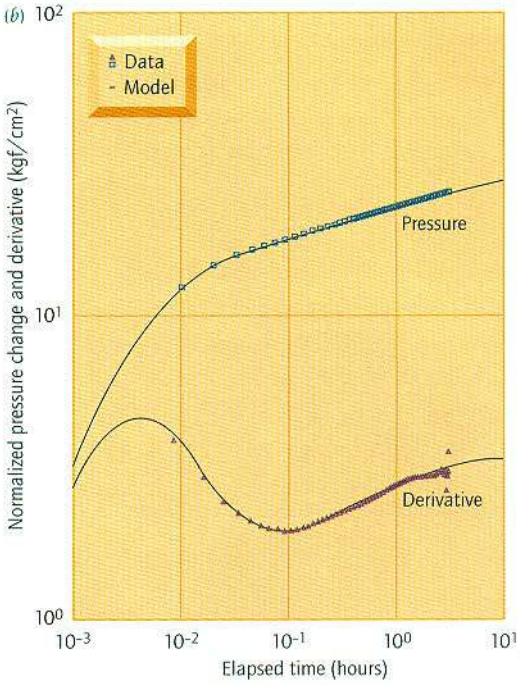

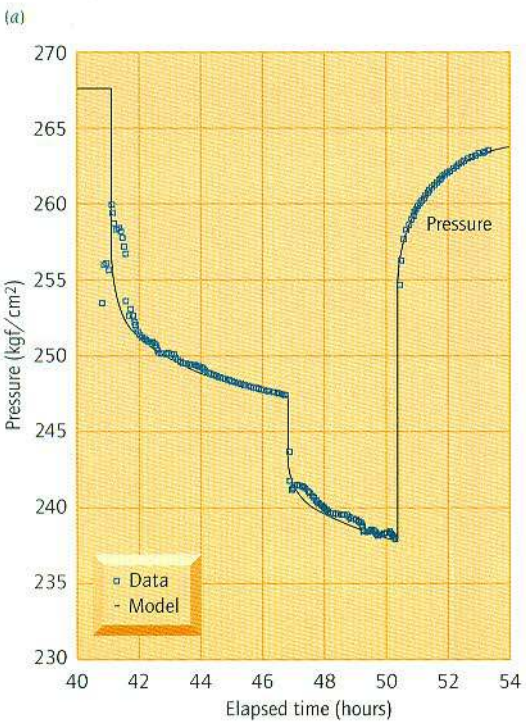

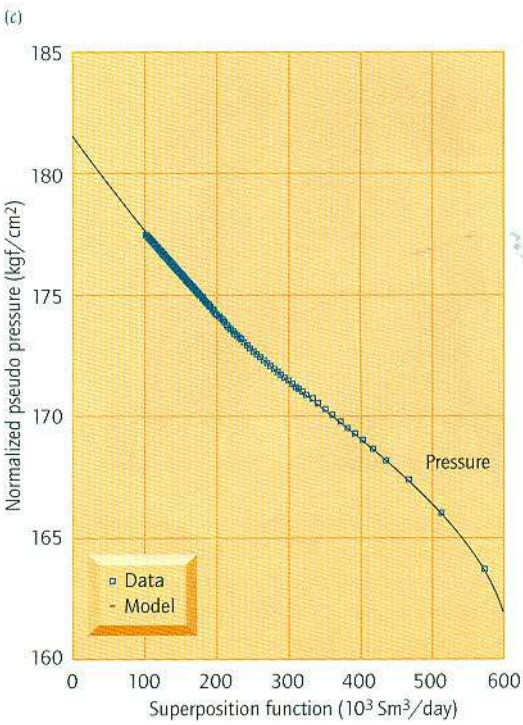

Figure 12.3 *This figure shows, for one producing level, the well test history (a), the flow regime identification plot (b) and the specialized pressure plot (c) using a $^1/_4$-inch choke and then a $^5/_{16}$-inch choke for buildup. The results obtained from this analysis are important parameters such as kh, skin and static extrapolated pressure values*

Results	
pav(i)	267.527 kgf/cm²
pwf	237.882 kgf/cm²
kh	45.29 mD.m
k	6.120 mD
C	0.006318 m³/ksc
S_1	-2.27
S_2	-1.25
Omega	0.005081
Lambda	5.879 x 10^{-5}
Kappa	0.5939
$S_{(t)}$	-1.95
ri	55 m

meability and formation damage estimates from pressure data acquired using downhole memory gauges housed in the DST string. Short tests such as these often exhibit unstable flow rates, fluid production and short buildups. However, the IRIS tool proved that their fears were unfounded. From the 42 DST–TCP jobs, 35 data sets were examined; four could not be interpreted and five had noisy data, but the remaining 26 provided accurate and useful information (Figures 12.3 and 12.4). The extrapolated pressure values agreed with those obtained using the RFT* Repeat Formation Tester tool, and permeability and skin factors proved reliable.

The advantages of IRIS valves

In the Daria Field development, there is no doubt that using the the IRIS dual valve led to considerable time savings. In particular, the assembly/disassembly of bottomhole tools was simplified considerably.

The valve also helped to maximize well performance by facilitating TCP perforation in underbalanced conditions and downhole shut-in. Both techniques bring considerable advantages in terms of pressure data acquisition and a reduction in post-perforation debris cluttering the well.

By adopting such a downhole shut-in system the operator managed to acquire reliable pressure data which in turn led to the accurate estimation of important reservoir parameters.

The ability to control the well and introduce blocking agent through the IRIS valve minimized the loss of expensive brine.

The IRIS valve is therefore a safer, more flexible and reliable downhole tool, offering direct cost savings.

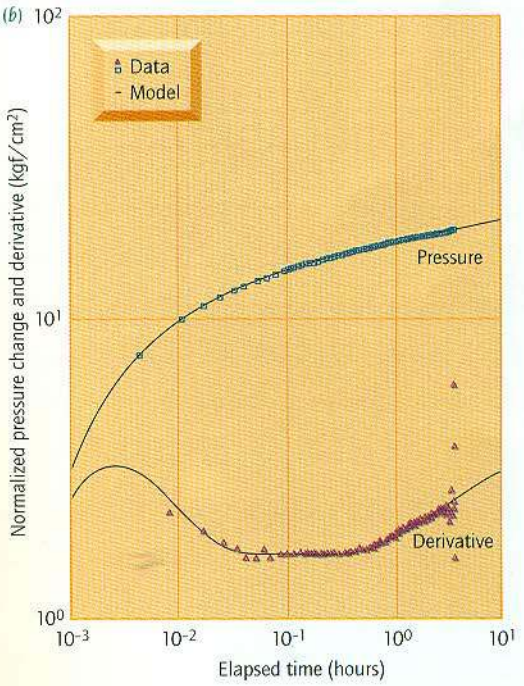

Results	
pav(i)	238.980 kgf/cm²
pwf	215.491 kgf/cm²
kh	39.49 mD.m
k	6.248 mD
C	0.005833 m³/ksc
S_1	-2.98
S_2	-2.60
Omega	4.487×10^{-4}
Lambda	2.356×10^{-5}
Kappa	0.7746
$S_{(t)}$	-2.91
ri	55 m

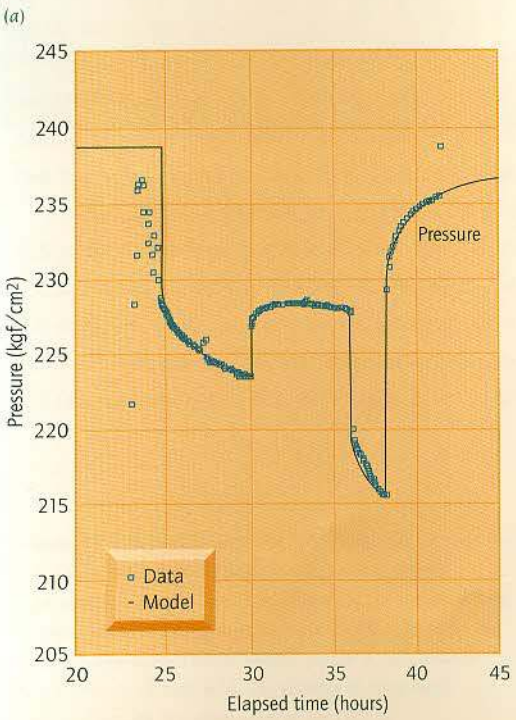

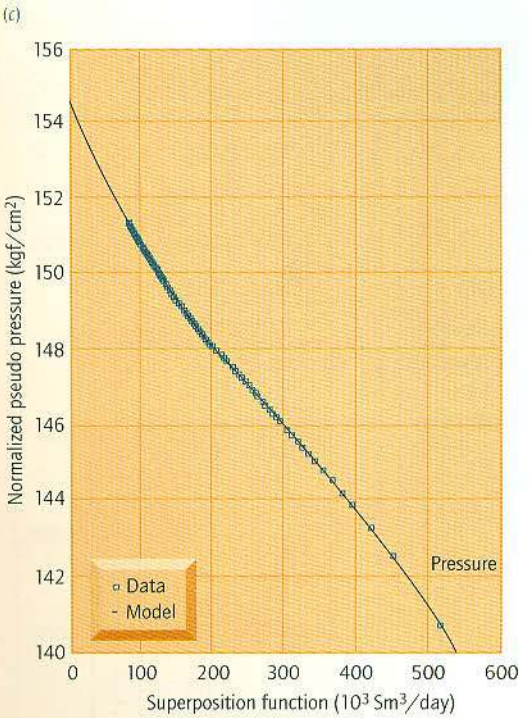

Figure 12.4 *This figure shows, the same type of plots shown in Figure 12.3, for a different producing level. In this case, to obtain a better cleanup of the well for an optimum buildup with a standard $^5/_{16}$-inch choke, a $^3/_{16}$-inch choke was used after the initial flow with a $^1/_4$-inch choke*

XIII

Nonconventional applications of logging techniques

Logging tools are normally designed to solve well-defined problems and obtain specific information. In some cases, however, it may be possible to use the same tools for different applications. This article shows several examples: the use of the TDT* Thermal Decay Time tool and the GPT (Gravel Pack Tool) to evaluate the accumulation of barite between tubing and casing of old producing wells; the use of the USI* UltraSonic Imager tool to evaluate the asphalt coating inside the casings of oil wells; and the comparison of the cement bond log (CBL) and the USI tool in concentric casings

In genere gli strumenti di logging vengono progettati per risolvere problemi ben definiti ed ottenere dati specifici. In certi casi, tuttavia, gli stessi strumenti possono essere utilizzati per applicazioni diverse. Questo articolo illustra vari esempi: l'uso del TDT* (Thermal Decay Time) e del GPT (Gravel Pack Tool) per valutare l'accumulo di barite tra il tubing ed il casing in vecchi pozzi produttivi; l'utilizzo dello strumento USI* (UltraSonic Imager), per valutare l'eventuale presenza di asfalto depositato sulla superficie interna delle colonne; ed infine il paragone del CBL log con l'USI in pozzi con doppio casing

Agip
P Giacon
A Muttoni
E Parissenti
G Toffolo

Schlumberger
M Andreani
B Godet
U Gragnani

Detecting barite in the annulus between the tubing and casing

Pulling the tubing out of some old Italian wells proved to be unexpectedly difficult. Subsequent investigations revealed that the tubing was virtually glued into the well by barite sediments originating from the completion fluid.

Dense barite mud had been used because the wells in question exhibited high formation pressures and safety considerations demanded the use of a heavy completion fluid (1.8–1.9 g/cm^3 density). Over time, the barite sediments from the mud had caused the tubing to stick. The operator faced the difficult task of identifying the areas of highest barite sedimentation in order to plan a program of tubing washover and removal.

The areas of barite sedimentation were identified by the combined use of the TDT Thermal Decay Tool and GPT (Gravel Pack Tool). Neither tool was designed for barite identification in this way, but the results provided much needed information to guide the operator.

Figure 13.1 shows a sketch of Well A prior to the scheduled workover program and curves derived from a TDT log.

Figure 13.2 shows the TDT and GPT logs recorded over a 4000-m interval. The GPT log (recorded from bottom to top) shows high-density material in at least two intervals – from bottom to level D and from level C to level B. The remaining part of the log shows lighter fluid. Readings above level A are affected by the increased tubing size and weight. The log on the left of Figure 13.2 shows two curves recorded with a TDT tool (gamma ray (GR) and inelastic far detector (INFD)); the measurement was made downwards.

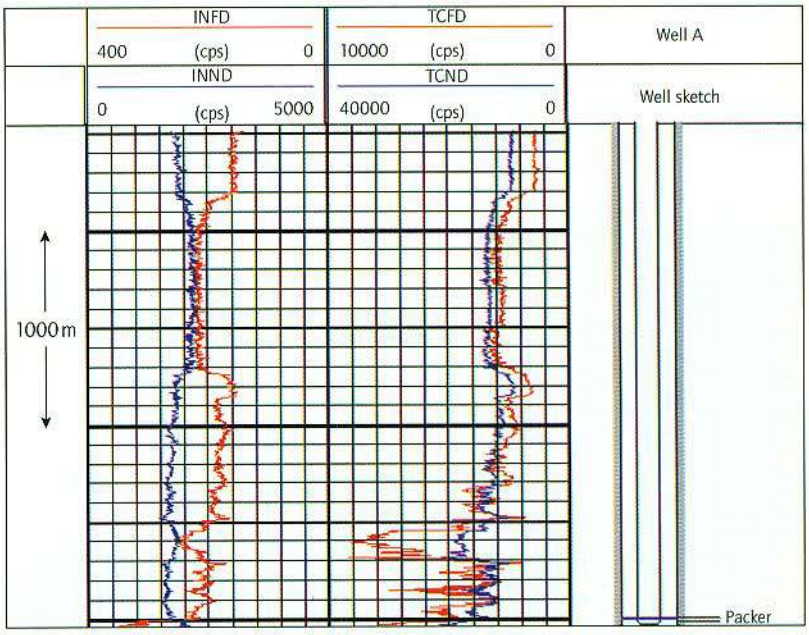

Figure 13.1 *Identification of the areas of highest barite sedimentation was made from TDT logs*

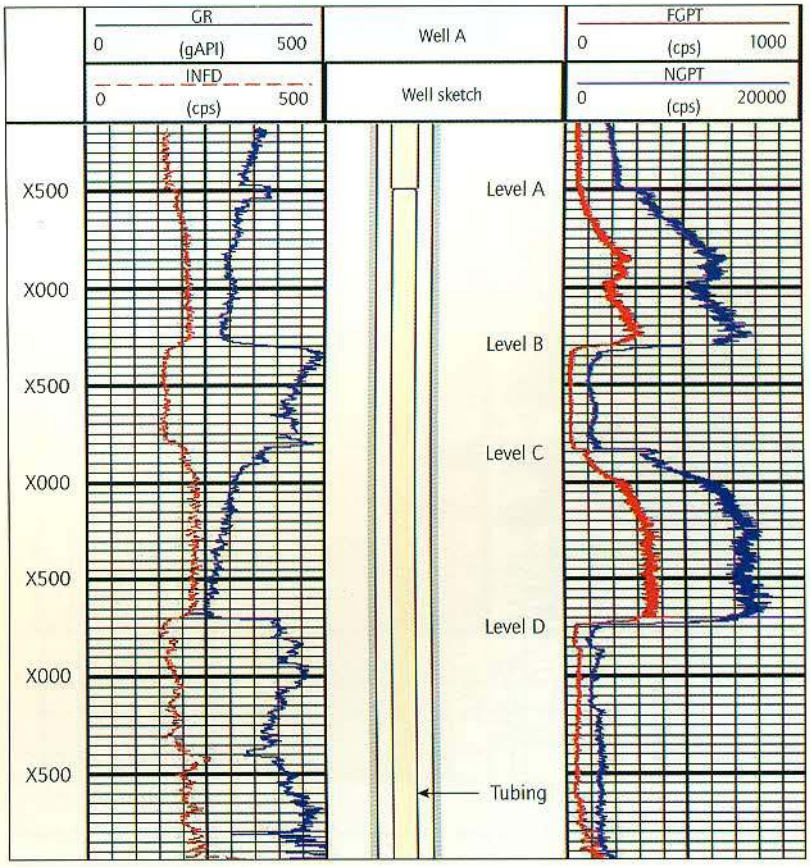

Figure 13.2 *Both TDT (left) and GPT (right) logs were run over a 4000-m interval in the problem well. There is general agreement between the logs. The gamma ray log in the left track responds mainly to oxygen activation caused by the source: this gives an indication of barite because oxygen is more abundant in barite than in oil-base mud. The presence of dense barite decreases gamma ray count rates on the GPT log*

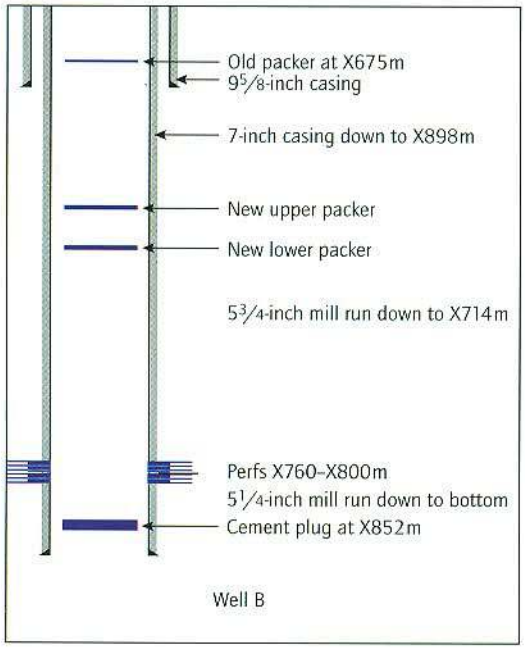

Figure 13.3 *The production packer set at X675 m had failed to seal. The operator wanted to know why*

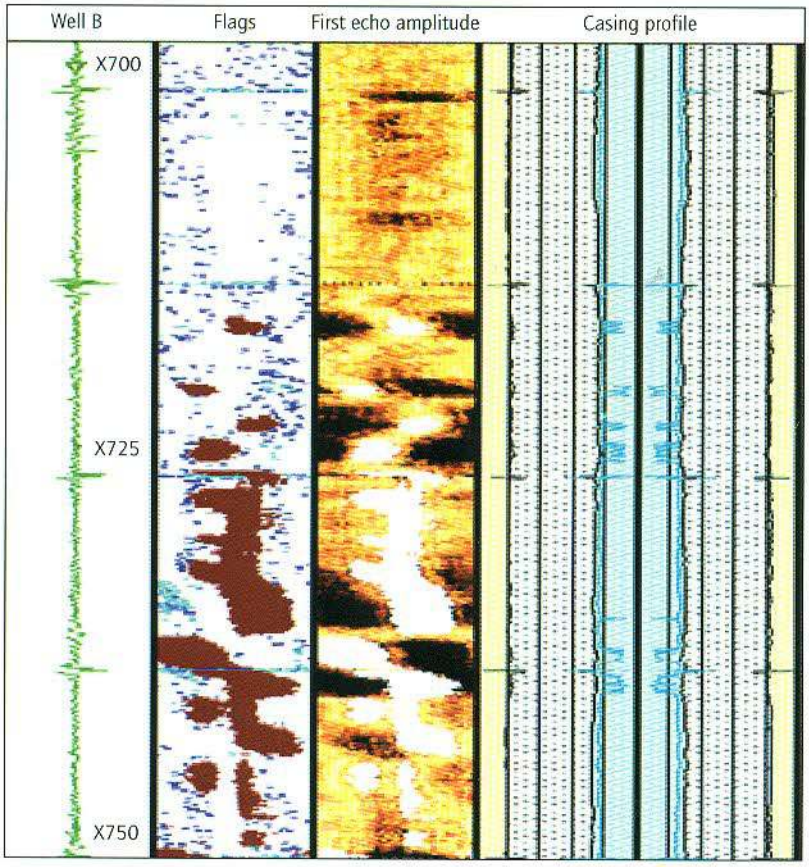

Figure 13.4 *These USI images reveal the problem. Above X714 m the images are 'clean' and more constant. Below this level they are disturbed by asphalt deposits coating the inside of the liner – the reason for the failure of the packer*

These curves are in general agreement with those of the GPT log. On the GPT log, gamma ray count rates decrease in the presence of barite on both far and near detectors due to the barite's high density.

On the TDT log, however, the GR sensor responds mainly to oxygen activated by the source. Oxygen is more abundant in the barite sediments than in the oil-base mud, so an increase in the GR count rate indicates the presence of barite.

Using this information the operator has been able to plan an efficient workover program for old wells that have been affected by barite sedimentation.

Asphalt detection

The operator of Well B had faced an unusual problem: a production packer set at X675 m had failed to seal, and there was no obvious reason why.

To shed some light on the confusion, the well was logged with a USI UltraSonic Imager tool, to check the corrosion and wear status of the 7-inch casing and to see if it contained any asphalt deposits. Before running the log, the driller cleaned the well by running a $5^1/_4$-inch mill down to the bottom and a $5^3/_4$-inch mill down to X714 m (Figure 13.3).

Figure 13.4 shows that the first echo image is cleaner and more constant from X714 m upwards. Below X714 m the first echo is disturbed by asphalt deposits coating the inside of the casing. This proved that the $5^1/_4$-inch mill was not able to remove all the asphalt efficiently and indicated that it was inadvisable to set production packers below X714 m.

Unreliable results of cement logging tools in concentric casings

The operator of the workover program for Well C decided to run a cement squeeze between the $9^5/_8$-inch and $13^3/_8$-inch casings (Figure 13.5).

The cement bond log (CBL) recorded previously indicated poor cementation between the casings above X920 m. The client decided to cut the $9^5/_8$-inch casing at X910 m and to remove the casing above the cut, but after the cut the casing was still stuck, so two further cuts were made at X900 m and X820 m. Still it was not possible to remove the casing or to circulate cement in the annulus.

At this point it was decided to use a combined USI and CBL tool string to investigate the problem.

The CBL log in Figure 13.6 shows a very poor bond but the USI log shows good cement up to about X700 m. The different answers given by the two tools are thought to be caused by either microannulus or concentric casing effect.

Seven casing punchers were shot at X687 m and through these holes it was possible to establish circulation to the surface. The cement could then be squeezed from this depth.

CBL log response in concentric casings

A section of CBL log recorded inside the 7-inch casing of Well D is shown on the left of Figure 13.7. Later, a 5-inch casing was set in the same well and another CBL log was recorded. A section of the second log is shown on the right side of Figure 13.7.

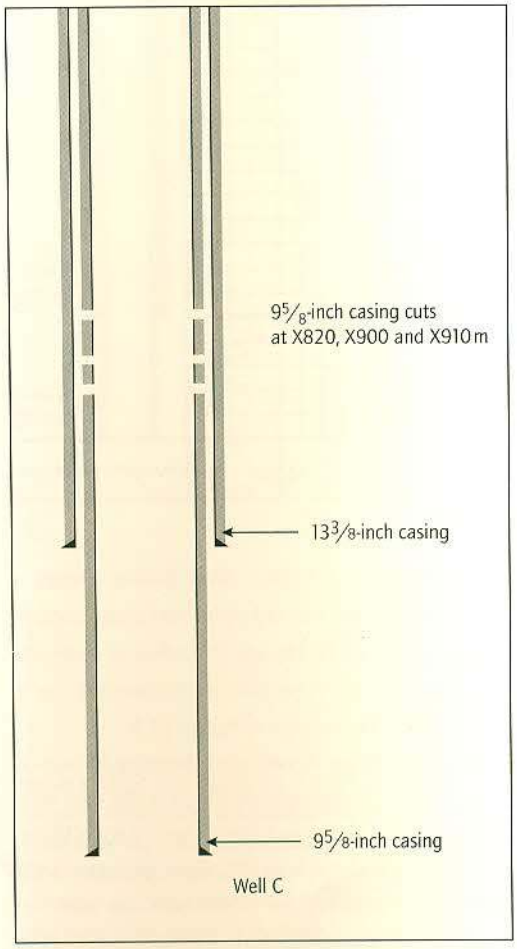

Figure 13.5 *The operator of this well wanted to cut and remove the upper section of the 9⅝-inch casing or to run a cement squeeze between the casings, but circulation of cement was proving to be a problem*

The marked correlation between the logs is evident, mainly in the interval X520–X490 m (indicated by the red box). The CBL log inside the 5-inch casing may be picking up the signal from the 7-inch casing, thus repeating the cement bond status of the 7-inch casing. The stretching of the transit time (TT) log recorded over the same interval supports this theory. It seems that a

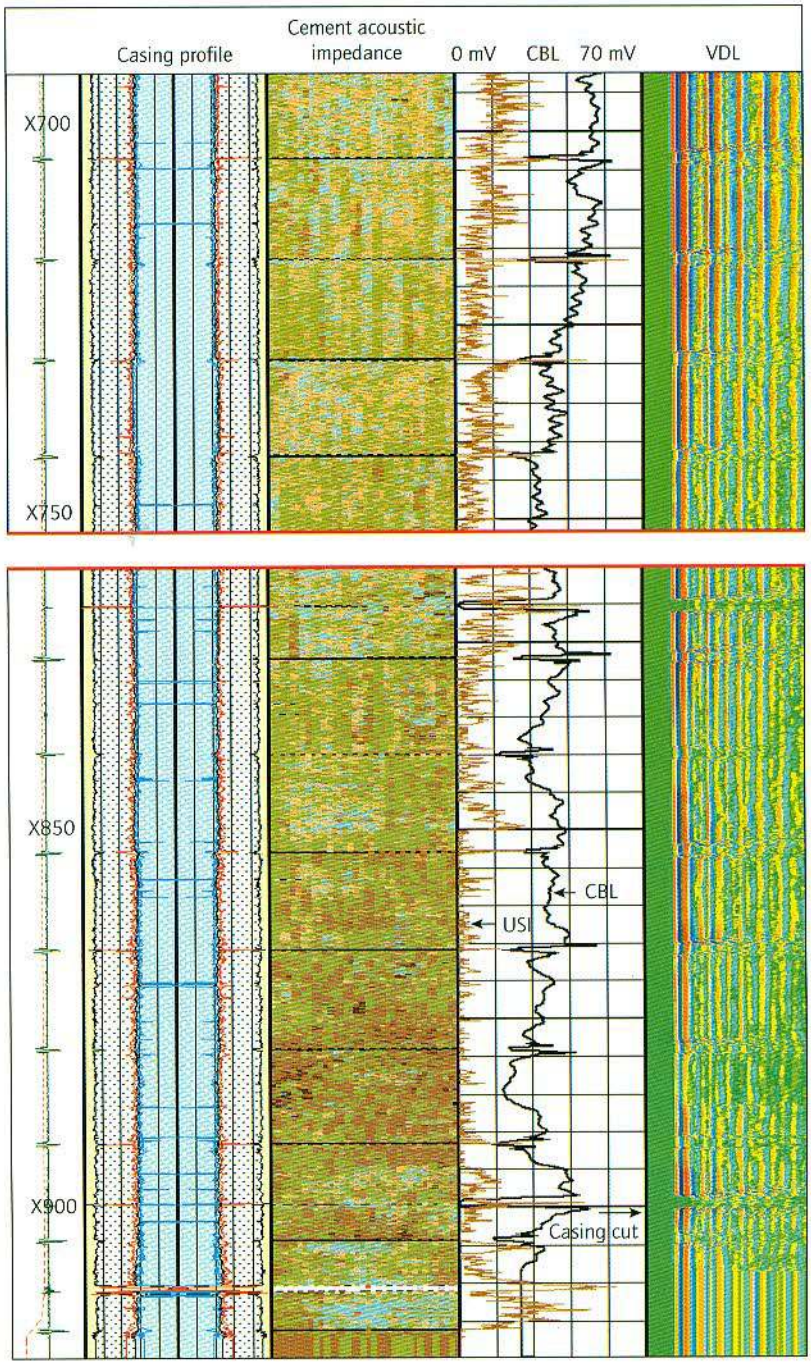

Figure 13.6 *In this interval the* CBL *log revealed poor cement bond but the* USI *log showed good cement up to about* X700 *m*

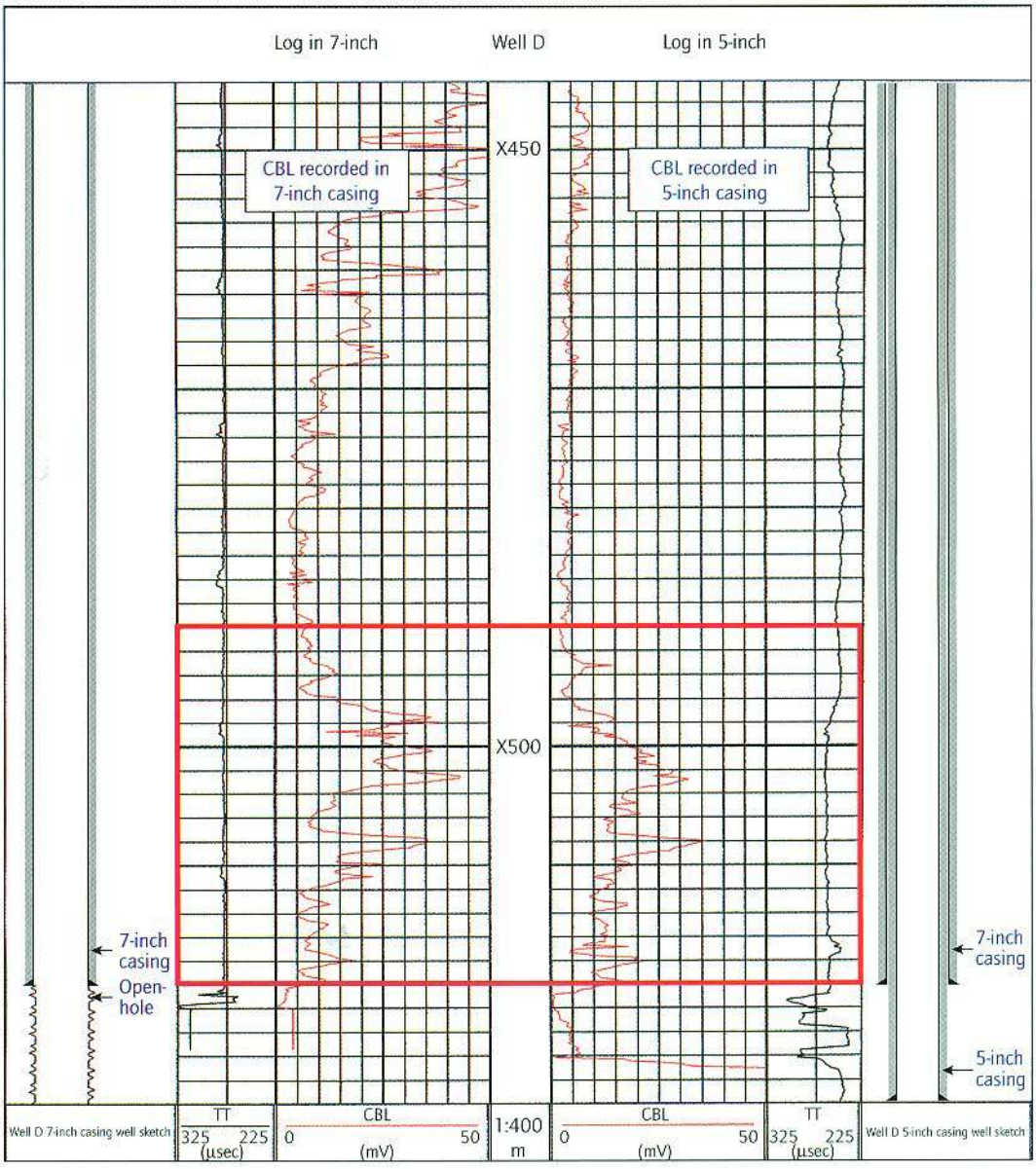

Figure 13.7 *The CBL log was recorded inside the 7-inch casing and later in the 5-inch casing. Both logs show poor cement in the interval X520–X490 m (indicated by the red box), but in reality the cement between the 7-inch and 5-inch casings is good. In the latter case the poor cement between the 7-inch casing and the formation may be causing interference on the log. The transit time (TT) increase supports this theory*

strong 'concentric casing' effect is responsible for a signal of very poor cement quality, as shown by the CBL log in the 5-inch casing, while, in reality, the cementation between the 5-inch and 7-inch casings should be very good. The conclusion is that, in this specific case, CBL-type logs cannot give the correct answer. The USI tool can be used to solve the problem.

Comparing CBL and USI tools

The cement evaluation logs recorded in Well E provided an opportunity to compare the CBL/Variable Density* logs with logs from the USI tool.

Figure 13.8 shows, on the left, a section of CBL log recorded in $9^5/_8$-inch casing. There is very poor cementation up to X320 m. After drilling deeper, a 7-inch casing was set and cemented from bottom to surface. The CBL log was recorded to evaluate the cement bond. A section of this second log is shown in the center part of Figure 13.8.

Because this log showed poor bonding in several places, the operator decided to run a USI tool over the same interval. Comparison of the USI and CBL results reveals that the high CBL signal between X397 and X368 m is mainly due to microannulus effect or concentric casing effect. The USI log displayed to the right of Figure 13.8 shows good bonding almost all over, especially from X397 to X368 m, proving that this tool is not affected by either microannulus or concentric casing effect.

Conclusions

It can be shown that workover in wells with extreme conditions (such as depth, temperature, high density mud) is very costly. Good interpretation of proper measurements, made prior to the workover, can lead to a better understanding of the actual well condition, which in turn can lead to a reduction in workover costs.

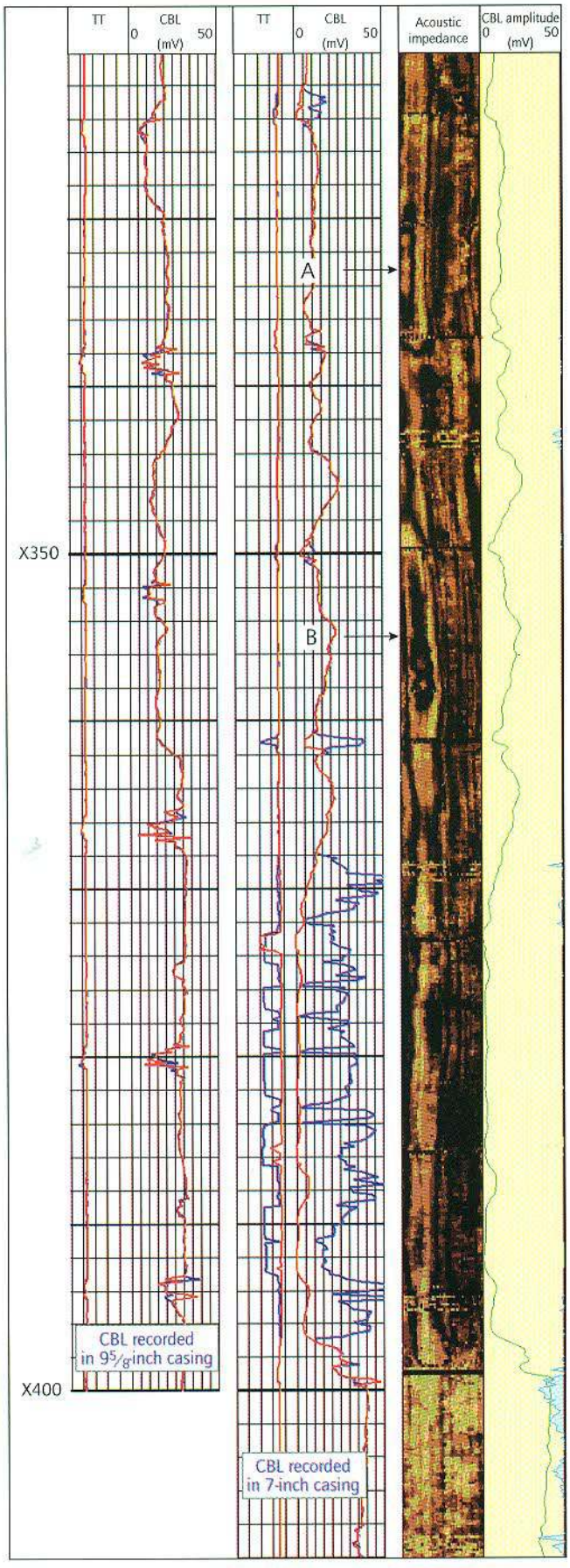

Figure 13.8 *The CBL log recorded in the 9⅝-inch casing (interval X410–X320 m) showed a poor bond. After the well was drilled deeper the 7-inch casing was installed and cemented. A second CBL log was recorded in the 7-inch casing; this showed a poor bond, especially below X368 m. The USI log confirms a good bond in the entire interval for the 7-inch casing, except below X400 m. The difference between the CBL log (blue curve) and the USI log (brown curve) is explained by the signal arriving from the 9⅝-inch casing which disturbs only the CBL log. Note also some 'galaxy patterns' visible on the USI acoustic impedance image (left side of the image), indicated by the arrows at A and B*

Further reading

I Combining complementary seismic and dip data

Etchecopar A and Bonnetain JL. "Cross sections from dipmeter data." AAPG bulletin, 1992

Etchecopar A and Dubas MO. "Methods for geological interpretation of dips." SPWLA 33rd ALS, June 1992, paper J

II Log interpreters tune in at the correct volume

Kenyon WE. "Petrophysical principles of applications of NMR logging." The Log Analyst, March–April 1997, Vol 38, #2

III CMR* tool brings new insight into reservoir properties

Flaum C, Kleinberg RL and Hurliman MD. "Identification of gas with the Combinable Magnetic Resonance tool CMR." SPWLA 37th ALS, June 1996, paper L

Gossenberg P, Galli G, Andreani M and Klopf W. "A new petrophysical interpretation model for clastic rocks based on NMR, epithermal neutron and electromagnetic logs." SPWLA 37th ALS, June 1996, paper M

Kleinberg R and Vinegar HJ. "NMR properties of reservoir fluids." The Log Analyst, November–December 1996, Vol 37, #6

Kenyon WE, Kleinberg R, Straley C, Gubelin G and Morriss C. "Nuclear magnetic resonance imaging: Technology for the 21st century." Oilfield Review, Vol 7, No 3, pp 19–33, 1995

Gossenberg P, Casu PA, Andreani M and Klopf W. "A complete fluid analysis method using nuclear magnetic resonance in wells drilled with oil based mud." OMC97, Offshore Mediterranean Conference, Ravenna, Italy, 1997

IV Unraveling the secrets of thin-bedded reservoirs

Eisenmann P, Gounot MT, Juchereau B and Whittaker SJ. "Improved R_{XO} measurements through semi-active focusing." SPE 69th ATC, New Orleans, September 1994, SPE-28437

Eyl KA, Chapellat H, Chevalier P, Flaum C, Whittaker SJ, Becker AJ and Groves J. "High-resolution density logging using a three detector device." SPE 69th ATC, New Orleans, September 1994, SPE-28407

V Sorting out the Adriatic's silty sediments

Barber TD and Rosthal RA. "Using a multiarray induction tool to achieve high-resolution logs with minimum environmental effects." SPE 66th ATC, Dallas, October 1991, SPE-22725

Cannon D and La Vigne J. "Shaly sands. Field data compared to theory." SPWLA 29th ALS, June 1988, paper CC

Case CR, Flaum C, Wraight PD and DasGupta T. "Improved porosity estimation in invaded gas reservoirs using a pulsed neutron porosity device." SPWLA 36th ALS, June 1995, paper X

Cheruvier E and Suau J. "Applications of microwave dielectric measurements in various logging environments." SPWLA 27th ALS, June 1986, paper MMM

Scott HD, Wraight PD, Thornton JL, Olesen J-R, Hertzog RC, McKeon DC, DasGupta T and Albertin JJ. "Response of a multidetector pulsed neutron porosity tool." SPWLA 35th ALS, June 1994, paper J

Morris CE, MacInnis J, Freedman R and Smaardyk J. "Field test of an experimental pulsed nuclear magnetism tool." SPWLA 34th ALS, June 1993, paper GGG

VI Fracture analysis of carbonates in Val d'Agri

Cestari R and Sartorio D. "Rudists and facies of the periadriatic domain." Agip, Milan, Italy

VII Shaping up to stress in the Apennines

Bell JS and Gough DJ. "The use of borehole breakouts in the study of crustal stress." National Academic Press, Washington, pp 201–209, 1983

Bott MHP. "The mechanics of oblique slip faulting." Geological Magazine, Cambridge, pp 109–117, 1959

Etchecopar A, Vasseur G and Daigniere M. "An inverse problem in microtectonics for determination of stress tensor from fault striation analysis." Journal of Structural Geology, 3,1, pp 51–65, 1981

Cheung PS and Etchecopar A. "Estimation of the in-situ stress using breakout orientation measured in deviated wells". Schlumberger Wireline and Testing Interpretation Symposium, 1995 (internal document)

Mastin L. "Effect of borehole deviation on breakout orientations." JGR Vol 93, No B8, pp 9187–9195, 1988

Vaseur G, Etchecopar A and Philip H. "Stress state inferred from multiple focal mechanisms." Annales Geophysicae 1, 4–5, pp 291–298, 1983

VIII Enhancing the image of the southern Apennines

Gaz I, Santi S and Ciammetti G. "Exploring new methodologies to acquire DST type data." OMC97, Offshore Mediterranean Conference, Ravenna, Italy, 1997

Joseph J, Ireland T, Colley N, Richardson S and Reignier P. "The MDT tool: A wireline testing breakthrough." Oilfield Review Vol 4, No 2, pp 58–65, 1992

Zimmerman T, MacInnis J, Pop J and Long T. "Application of emerging wireline formation testing technologies." Eighth Offshore South East Asia Conference, Singapore, December 1990, OSEA-90081

IX Detailed reservoir characterization with DipFan†

Balossino P and Anxionnaz H. "Deriving textural and geometrical information from dip meter data as a help to define subsurface geological models." EAGE, 1996

Delhomme JP, Pilenko T, Cheruvier E and Cull R. "Reservoir applications of dipmeter logs." SPE 61st ATC, February 1988, SPE-15485

Delhomme JP and Serra O. "Dipmeter derived logs for sedimentological analysis." SPWLA 9th Europ. Intern. Eval. Trans. paper 50

X A 3D VSP case history from the Adriatic Sea

Dangerfield JA. "Shallow 3D seismic and a 3D borehole profile at Ekofisk Field." In: Brown AR (ed), Interpretation of three-dimensional seismic data. 3rd edition. AAPG Memoir 42, pp 271–279, 1991

Miranda F, Barzaghi L, Ogliani F, Belaud D and Godet B. "The 3D VSP technique: a case history from the Adriatic Sea." OMC97, Offshore Mediterranean Conference, Ravenna, Italy, 1997

van der Pal R, Bacon M and Pronk D. "3D walkaway VSP, enhancing seismic resolution for development optimization of the Brent Field." First Break, Vol 14 (12), pp 463–469, 1996

XI Logging under tough conditions

Scott HD, Wraight PD, Thornton JL, Olesen J-R, Hertzog RC, McKeon DC, DasGupta T and Albertin IJ. "Response of a multidetector pulsed neutron porosity tool." SPWLA 35th ALS, June 1994, paper J

Smits JW, Benimeli D, Dubourg I, Faivre O, Hoyle D, Tourillon V, Trouiller JC and Anderson BI. "High resolution from a new laterolog with azimuthal imaging." SPE ATC, Dallas, October 1995, SPE-30584

XII IRIS* dual valve makes its debut in the Daria Field

Vella M, Veneruso T, Le Foll P, McEvoy T and Reiss A. "The nuts and bolts of well testing." Oilfield Review Vol 4, No 2, pp 14–27, 1992

XIII Nonconventional applications of logging techniques

Hayman AJ, Hutin R and Wright PV. "High-resolution cementation and corrosion imaging by ultrasound." SPWLA 32nd ALS, June 1991, paper KK

Hayman AJ, Gai H and Toma I. "A comparison of cementation logging tools in a full-scale simulator." SPE 66th ATC, Dallas, October 1991, SPE-22779

Acknowledgements

The authors wish to express their gratitude to the oil companies who gave permission to use the log, core, production and well data presented in this book.
Special thanks go also to all colleagues who helped to review the articles.
All the core pictures and thin sections were kindly made available by the Agip Laboratories.

Agip

British Gas International

Chevron

EDISON GAS

elf

Enterprise Oil

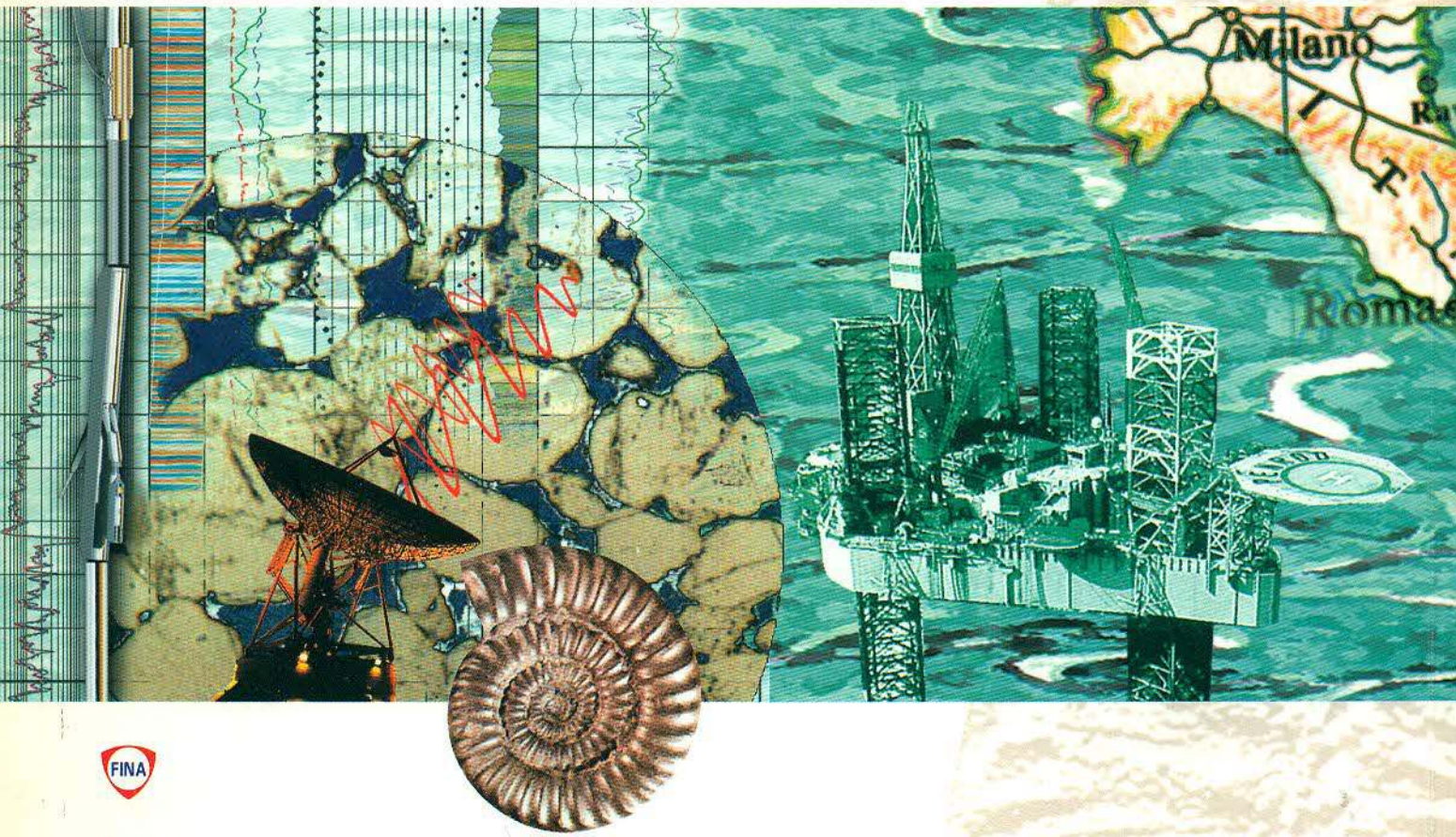

FINA

LASMO

PHILLIPS 66

Spi

TRITON